ACTA UNIVERSITATIS SZEGEDIENSIS

ACTA

MINERALOGICA-PETROGRAPHICA

Tomus XLVIII

Szeged, 2008

Published by the Department of Mineralogy, Geochemistry and Petrology, University of Szeged

ACTA MINERALOGICA-PETROGRAPHICA
established in 1922
HU ISSN 0365-8066

Abbreviated title:

Acta Mineral. Petrogr., Szeged

The Acta Mineralogica-Petrographica is published by the
Department of Mineralogy, Geochemistry and Petrology, University of Szeged

---

On the cover: Well-developed zircon, apatite, biotite and alkali feldspar in magmatic microgranular enclaves. (Hassen et al., Fig. 4E, p. 7)

Designed by: Elemér Pál-Molnár & György Sipos

*Acta Mineralogica-Petrographica, Szeged 2008, Vol. **48**, pp. 1-15.*

ACTA Mineralogica Petrographica

GEOCHEMISTRY OF THE MAGMATIC MICROGRANULAR ENCLAVES OF WADI RAHABA AREA, SOUTHERN SINAI, EGYPT

IMBARAK SAYED HASSEN[1], RASMY ISMAIL EL-GHARBAWY[2], NABIL NASR EL-MASRY[1], GYÖRGY BUDA[3]

[1]Department of Geology, Faculty of Science, Suez Canal University, 41522 Ismailia, Egypt.
[2]Department of Geology, Faculty of Science, Ain Shams University, Cairo, Egypt.
[3]Department of Mineralogy, Eötvös Loránd University of Sciences, H-1117, Pázmány sétány 1/C, Budapest, Hungary
e-mail: buda@ludens.elte.hu

ABSTRACT

The study of the magmatic microgranular enclaves (MMEs) as relics of mafic magmas gives important information on the origin of parent magmas and their evolution. In the study area, MMEs are either concentrated at the margins of the I-type granodiorite pluton or within some parts of its interior. Most of the enclaves are either ellipsoidal or ovoid in shape and tend to have sharp contacts with the enclosing host rock. Sizeable enclaves, however, are less ellipsoidal and are characterized by curved boundaries. The contact is sometimes marked by a chilled margin with no sign of solid state deformation.

MMEs exhibit classical features of mafic melts globules trapped in granitic magma. Swarms of MMEs are either related to convection currents in magma chamber or to gravitational sorting of heterogeneous magmas.

The enclaves contain the same mineral assemblages as the host rock though their proportions are different. They contain megacrysts of plagioclase similar in composition to that of the host rock. The enclaves are composed mainly of plagioclase, K-feldspar, and hornblende in addition to minor amounts of clinopyroxene and orthopyroxene.

The MMEs are rather basic to intermediate in composition as their SiO_2 content ranges between 46% and 58%. The composition of most MMEs clusters near the granodiorite trend line. Many trace elements do not show clear linear correlation with the SiO_2 content and are scattered off the trends defined by related granodiorite.

The petrographic and geochemical characteristics of the enclaves and their hosting granodiorite indicate that granodiorite is a product of partial melting and fractional crystallization of a basic magma, and that the enclaves are trapped blobs of basic to intermediate parental magma. Both major and trace elements contents of the investigated enclaves indicate that they were formed as a result of mingling and mixing during magma evolution.

Key words: granodiorite, I-type magmatic enclaves, chilled margin, Southern Sinai.

INTRODUCTION

Saint Katherine Complex is situated in the high mountainous area of southern Sinai. The country rock includes Solaf gneisses, a volcanoclastic suite (Rutig volcanics), a calc-alkaline plutonic series represented by metagabbro-diorite complex, quartz monzonite, quartz diorite, and other granitoid rocks (Hassen 1997).

The quartz monzonite, granodiorite, and quartz syenite at Wadi Rahaba-Gebel Sheikh El-Arab area contain rounded microgranular enclaves oriented locally by the magmatic flow of the host-rocks. Large composite enclaves occur in quartz syenite, whereas very small enclaves are found in the porphyritic quartz monzonite. Granodiorite is the most prevailing magmatic phase in the study area.

The magmatic microgranular enclaves (MMEs) are common components in the I-type granitic rocks. Didier (1973), White and Chappell (1977), and Barbarin and Didier (1991) indicated that mafic enclaves provide important information about the nature of their source rocks as well as the genesis of granitic melt . The study of enclaves is of great importance because it could shed some light on the mode of emplacement of granitoid magmas, the dynamics of magma chambers, their cooling processes, and the origin and evolution of the granitoid melts.

The MMEs constitute trapped mafic fragments of fine-grained igneous products, generally with ovoid shape and sharp contacts, representing blobs of coeval magmas. Didier and Barbarin (1991) and Vernon (1983) defined and reviewed the French term "enclave". It is clearly known that xenoliths refer to foreign rock fragments, while inclusions refer to mineral grains enclosed in another. Consequently, there is a close relationship between enclaves and their host rock. Therefore, the term enclave but not xenolith is the most suitable term for the present study.

The MMEs are widespread in the granitic rocks of calc-alkaline, shoshonitic, or alkaline nature. Their characterization, geochemical affinity, genesis, and evolution have been extensively investigated by several authors. Some of them suggested that they are products of the coexistence of two contrasting magmas. Vernon (1984, 1990) and Barbarin and Didier (1992) suggested that the majority of enclaves represent the mafic end members of a more or less hybridized or mixed two magmas. The mingling, according to those authors, should be restricted to systems with mechanical interactions. The authors recognized the following three interaction processes in the coexisting magmas: thermal, mechanical, and chemical exchanges. The specific textural and compositional characteristics of an enclave will vary with the relative intensity of these three factors. For example, when the mechanical exchange predominates, megacrysts of the host magma are abundant in the enclaves. Chemical and mechanical exchanges cause the

hybridization of the microgranular mafic enclaves, producing compositions closer to the host rock. These exchanges frequently precede the basic magma batch dispersion by magma flow, producing the microgranular mafic enclaves (Hibbard, 1995).

Magma mingling as a mechanism for the genesis of MMEs attracted the attention of many authors (Didier 1987, Vernon et al. 1988, Dodge and Kistler 1990, Barbarin and Didier 1991, Castro et al. 1990, 1991, Tobisch et al. 1997, Sinha et al. 2001, Dahlquist 2002). The typical igneous textures described by many researchers (Didier 1984 and Vernon 1991) stated that the fine-grained chilled margins surrounding many MMEs favor their formation from the crystallization of silicate melt.

Some authors used numerical simulations of a chaotic dynamic system involving stretching and folding processes (Perugini et al. 2002, 2003). Others have modelled the process using whole-rock compositions (Wei et al. 1997, Moyen et al. 2001). They focused their studies on the textures, trace element patterns and isotope geology of the zoned minerals, (Bussy 1990, Ginibre et al. 2002, 2004, Barbarin 2005, Gagnevin et al. 2005ab; and Słaby et al. 2007a).

In many granitic intrusions, microgranular magmatic enclaves provide strong evidence of interaction between coeval mafic and felsic magmas (Vernon 1990, 1991, Barbarin and Didier 1992, Barbarin 2005). The mechanical migration of crystals, back and forth, from one magma to another causes zonal growth (Vernon 1986, Waight et al. 2000ab, Barbarin 2005, Słaby et al. 2007ab).

Feldspars are sensitive indicators of thermal and chemical heterogeneities in their crystallization environment (Knesel et al. 1999, Ginibre et al. 2002, 2004, Troll and Schmincke 2002, Perugini et al. 2005, and Słaby et al. 2007ab). Primary melt compositions may be well reflected in the trace and major elements compositions of the growth zones if the feldspar crystals grow close to the crystal-melt equilibrium boundary. Slowly diffusing compatible trace elements, for example Ba, which is commonly chosen as an index of magma mixing, can be used to track the process step by step (Cherniak 2002) and is often used to examine growth histories of K-feldspar crystals (Long and Luth 1986, Cox et al. 1996, Ginibre et al. 2004, Gagnevin et al. 2005a and Słaby et al. 2007a).

The origin of the microgranular enclaves is interpreted as being related to one of the followings: (1) fragments of wall rock facies closely related to the host magma; (2) globules of mafic melt injected into resident felsic host melt; and (3) fragments of recrystallized refractory metamorphic rocks co-mingled with resident granitic melt (Maas et al. 1997). So the origin of the microgranular enclaves is controversial.

The enclaves of the Egyptian Precambrian granitoids have been studied by several researchers. For example, Ammar et al. (2003) studied the enclaves of El-Delihimmi-Nusla granite pluton, central Eastern Desert of Egypt, and concluded that they were formed as restite in a granite source. Several granitoid masses are also widely exposed in southern Sinai; many of them contain microgranular enclaves and granodiorite represents one of these examples. El-Metwally (1993) studied the microgranular enclaves of the granitoid rocks in southwestern Sinai and suggested a mingling model of mafic globules of different compositions. Surour and Kabesh (1998) described swarms of mafic microgranular enclaves in Wadi Risasa area southeastern Sinai. They reported that the opaque mineralogy and geochemistry of the enclaves and their host rocks are almost identical.

The main objective of this paper is to test the magmatic processes that might have been involved in the genesis of the microgranular enclaves hosted by the granodiorite of Wadi Rahaba. Therefore, the geologic setting, petrology, and geochemistry of the microgranular enclaves and their host rock are thoroughly studied to present a workable model for their petrogenetic evolution.

Geologic Setting

Saint Katherine area is composed of late-Precambrian rocks including metagabbro-diorite complex, granodiorite, quartz-monzonite, quartz diorite, and other varieties of granitoid rocks (Fig. 1).

Granitic intrusions in southern Sinai are classified into three groups according to their geological, geochemical, and petrological characteristics (Hassen 1997). These three groups are:

(1) Calc-alkaline granitoids *(Phase I)*: (quartz diorite, quartz monzodiorite, quartz monzonite, granodiorite, and hornblende-biotite granite).

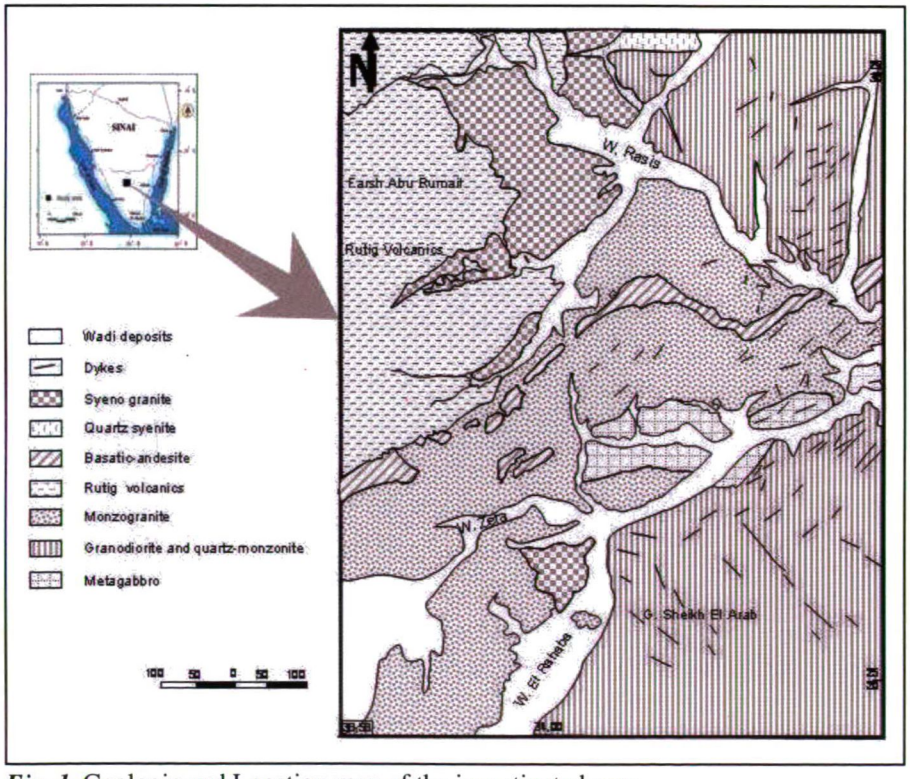

Fig. 1. Geologic and Location map of the investigated area.

(2) Subcalc-alkaline granitoids *(Phase II)*: (porphyritic biotite monzogranite, coarse-grained biotite monzogranite, and pegmatitic monzogranite).

(3) Syenogranite *(Phase III)*: (Alkali feldspar granite, syenogranite, microsyenogranite, and granophyric granite).

Metagabbro is represented by small homogenous weathered outcrops (2 x 5 km) of brown to greenish-brown color, medium- to coarse-grained texture, and are massive to weakly-foliated. It also occurs as an E-W-trending belt located to the southeast of Gebel Nakhla. It is intruded by monzogranite, quartz monzonite, and the ring dyke of Saint Katherine. Some metagabbroid sheets were locally intruded by diorite and syenogranite.

The two largest occurrences of quartz diorite intrude the metagabbro-metadiorite complex at Gebel Sheikh El-Arab. They are homogeneous, weathered, greenish-grey colored rocks, and generally have medium- to coarse-grained granular to weakly-foliated texture. The fine-grained diorite, on the other hand, is recorded in the northeastern and northwestern parts of the study area. In the southeastern parts, small masses of medium- to fine-grained quartz monzodiorite are observed showing gradational contacts with quartz monzonite. There are also large elliptical monzodioritic blocks making sharp contacts with quartz monzonite.

Quartz monzodiorite is massive to weakly-foliated and heterogeneous, with subangular psammitic and gabbroic xenoliths. Foliation in the xenoliths predates the emplacement of quartz monzodiorite, which is also cut by monzogranitic dykes.

Granodiorite intrudes into mafic magmatic rocks. It has sharp contacts with the country rocks which comprise metagabbroic and dioritic rocks. The effect of contact metamorphism was observed in the surrounding country rock. Facies of contact metamorphism formed around the granodiorite porphyry dikes range from K-feldspar-cordierite-hornfels facies, and hornblende-hornfels facies down to albite-epidote-hornfels facies. Both the intrusive rock and the country rock are intruded by Katherina ring dyke. The volcanic rocks comprise andesite, latite-andesite, dacite, rhyodacite.

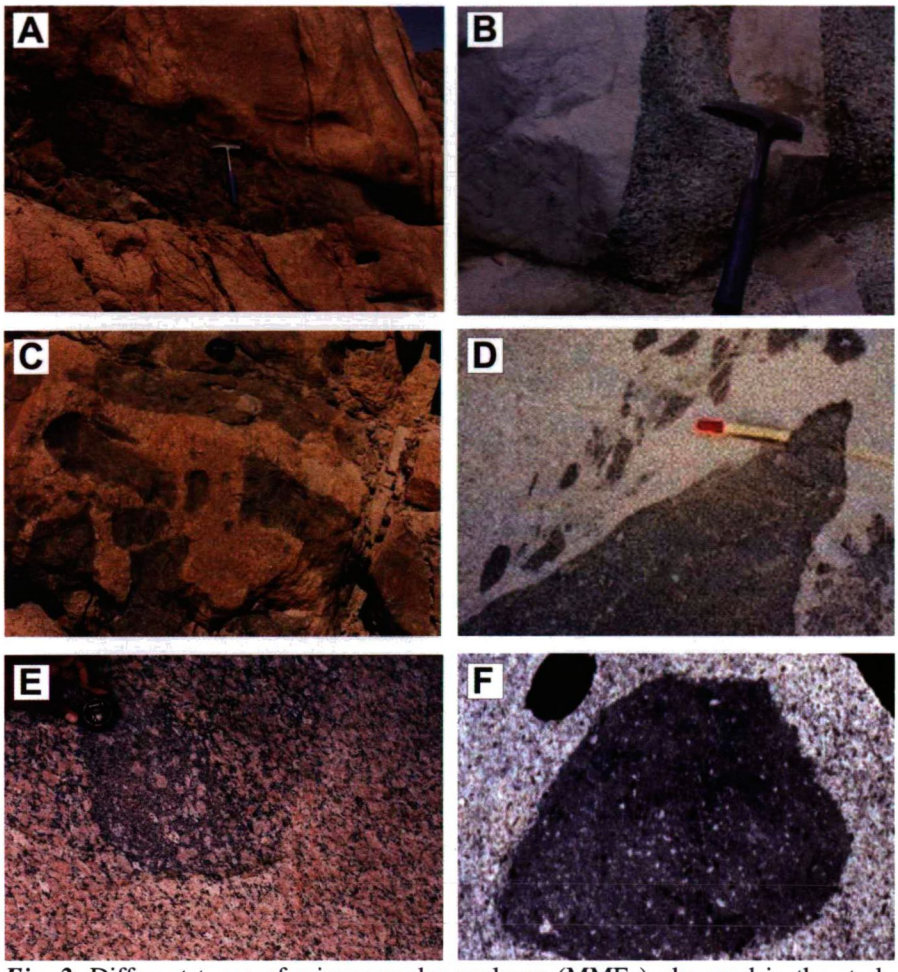

Fig. 2. Different types of microgranular enclaves (MMEs) observed in the study area. ***(A)*** Pillow-like mafic enclave formed as an offshoot of basic magma. ***(B)*** Dyke-like enclave showing curved boundary and sharp contact with the host rock. ***(C)*** Different types of microgranular enclaves. ***(D)*** A swarm of enclaves showing interaction with the host rock. Note whitish colored alkali feldspar megacrysts in the largest enclave. ***(E)*** A microgranular enclave showing gradational contacts with the host rock. Alkali feldspar crystals enclosed in the enclave are indicative of magma mingling. A hybrid zone is also observed in the upper part of the photo. ***(F)*** A microgranular mafic enclave showing a sharp contact with the host rock and enclosing prominent crystals of plagioclase feldspars.

Granodiorite has a medium- to coarse-grained hypidiomorphic granular texture. The marginal zones of the intrusion were commonly injected with aplitic veins, which have various orientations and thicknesses. Small pegmatitic as well as minor composite dikes are also observed near the margin of the intrusion. Large pegmatitic veins consisting of K-feldspar, biotite, quartz, epidote, topaz, and pyrite usually occur at the contacts between aplites and granodiorite or within the aplitic vein itself. Nodular pegmatites, which have the same mineralogical composition as the pegmatitic veins, are present around Rahaba Village.

Hornblende monzogranite pluton is either equigranular or porphyritic with a medium- to coarse-grained matrix containing K-feldspar megacrysts attaining 5 cm in length. Monzogranite intrudes granodiorite, quartz monzonite, and the metagabbroid rocks of Wadi Rahaba. Large granodiorite enclaves within monzogranite were also observed.

Pillow-like enclaves, formed as an offshoot of basic magma, are recorded near the contact between the ring complex and monzogranite (Fig. 2A). They are angular to oval in shape and locally occur as dyke-like enclaves, which become progressively thinner towards their termination with the host granitoid. They show curved boundary as well as sharp contact with the host rock (Fig. 2B).

Quartz monzonite occurs northwest of the study area at Wadi Isbaiya mainly in the central part of both the eastern and northern borders of the pluton. It is greyish-pink colored and has a massive, non-foliated, coarse- to medium-grained hypidiomorphic granular texture, in which up to 1 cm long K-feldspar megacrysts are frequently observed.

The contact between quartz monzonite and syenogranite is commonly sharp or locally grades to a fine- to medium-grained quartz syenite, which contains some dioritic enclaves and gneissose xenoliths. Other quartz monzonitic to monzodioritic masses in the investigated area have also been assigned to the quartz monzonitic intrusive suite of Wadi Isbaiya (Hassen 1997).

There are two intrusive masses which show compositional and textural affinity. The largest one is a quartz-poor, K-feldspar porphyritic hornblend-biotite monzogranite. The other monzogranitic mass has an equigranular texture and contain lesser amounts of hornblende. The contact between monzogranite and metagabbro is sharp and is interleaved with gabbro. Alignments of K-feldspar megacrysts in the central part of the mass refers to primary foliation that developed during the early stages of crystallization.

K-feldspar porphyritic hornblend-biotite monzogranite is widespread in the Rahaba area. The rock grades from porphyritic monzonite to equigranular monzogranite. The rock is pink in color, slightly weathered, massive to weakly-foliated, and ranges in texture from medium- to coarse-grained granular to strongly porphyritic. Megacrysts of K-feldspar, up to 5 cm long, account for 10 to 20% of the rock, whereas those of plagioclase feldspars are quite rare.

Syenite and quartz syenite of the ring dyke are typically massive. Most of them have a coarse- to medium-grained granular texture and a dark brown to deep purple color. They may, however, contain K-feldspar megacrysts, where K-feldspar/plagioclase ratios vary considerably. Biotite is the main mafic mineral, often associated with pyroxene and magnetite. A coarse-grained greyish variety of syenite was also observed and is characterized by well-developed laths of feldspars. Some outcrops form sheet-like bodies, up to two kilometers long, interleaved with country rocks; their margins are commonly intensively sheared.

Augite-bearing porphyritic basaltic-andesite occupies a small area of Gebel Nakhla. The rock is medium- to fine-grained, grey to black in color with some amygdales filled with epidote and K-feldspar.

Orange-pink to brick red colored syenogranite is among the most widespread rock types in Saint Katherine area. It forms roughly an oval-shaped pluton taking a NE-SW direction. The contact of syenogranite with the country rock is sharp showing no evidence of metasomatic alteration. These rocks, however, are cut by veins and pockets of pegmatite as well as microgranite dikes. Basic enclaves are occasionally observed. Miarolitic cavities are locally common and often contain orthoclase and smoky quartz crystals up to 3 cm long. In many localities, syenogranite is cut by pink to pinkish-buff colored, fine-grained aplite dikes that are mineralogically similar to granite. Aplite dikes are usually less then 5 cm wide.

Syenogranite contains 5% biotite with lesser amounts of hornblende, epidote, titanite and/or magnetite. Locally, however, it may contain up to 15% mafic minerals. It is therefore identified as biotite syenogranite that varies in texture from medium- to coarse-grained granular to fine- to medium-grained sub-porphyritic. It is composed of quartz, alkali feldspar, minor plagioclase, biotite, and minor amphibole. In the syenogranite showing sub-porphyritic texture, graphic texture is frequently recorded in the fine-grained variety and biotite is often altered to chlorite. Fluorite-bearing syenogranite was also observed in Wadi Rasis area.

Magmatic Microgranular Enclaves

Magmatic microgranular enclaves (MMEs) are fine-grained and darker in color than the host-rock (Fig. 2C). They are basic, dioritic, monzonitic, tonalitic, and granodioritic in composition. The enclaves are not only restricted to the margins of the hosting granodiorite pluton but they were also recorded in other parts as well. They may appear closely spaced but they do not commonly form swarms (Fig. 2D). Some mafic enclaves (basic in composition) may also contain smaller monzogranite enclaves indicating that mafic and felsic magmas were coeval.

The enclaves range from 1 to 70 cm in diameter. Most of the enclaves, however, may cluster around either the 2-5 cm or the 20 cm across size range. The largest enclaves are commonly observed along the margins of the granodiorite pluton. Although they vary widely in size, most of the enclaves are elliptical. They have crenulated surfaces, chilled margins, and sharp to partly diffuse contacts with their host rock. Some of these features are indicative of plastic behavior. Sharp contacts, however, are frequently observed among the smallest enclaves, which tend to show a finer grained texture and a more mafic content at their margins compared to their core. Biotite enrichment is rarely observed along the margins of the enclaves.

The enclaves have porphyritic to hypidiomorphic granular fine-grained textures (0.05-0.5 mm). Grain size varies from the chilled margin to the core of the enclave. This is largely attributed to different cooling rates, which variably affects the nucleation rates and the growth rates of the crystallizing mineral phases.

It was observed that mafic enclaves may also enclose alkali feldspar megacrysts related to the granite host rock (Fig. 2E). In this case, their margins tend to display a gradational contact with the host rock and a hybrid zone may develop. Other enclaves, enclosing host-related plagioclase crystals, have margins displaying a rather sharp contact with the granodioritic host rock (Fig. 2F). Megacrysts of amphiboles are also recorded in both the enclaves and the surrounding host rock.

These aforementioned observations suggest that two contrasting magmas were involved in the evolution of the magmatic rocks of the study area and that the MMEs represent quenched globules of a mafic magma caused by magma mixing/mingling processes (Hibbard 1991, Vernon 1991, Kim et al. 1998).

Hybrid Zone

A well-preserved outcrop of a hybrid zone shows gradational contacts with granodiorite. It is comparable, both mineralogically and texturally, to the MMEs and is composed of mesocratic to melanocratic quartz diorite and

granodiorite. The dark color is attributed to the presence of microgranular enclaves where markedly higher proportions of hornblende and biotite occur. It is believed that these rocks are products of mafic-felsic magma mixing, where mafic magma is relatively more abundant.

PETROGRAPHY

The host rocks of the MMEs are as follows:

(1) Quartz Diorite:

Quartz diorite has a medium-grained granular texture and is mainly composed of oligoclase, quartz, hornblende (10%), biotite, and K-feldspar in addition to minor amounts of magnetite and epidote.

The textural characteristics of quartz diorite reflect slow cooling and the presence of volatiles, which facilitated mineral growth. Similarly, biotite and hornblende indicate the availability of water and thence high-vapor pressure during crystallization. Some of the amphibole crystals are considered as products of primary magmatic crystallization, but many others may represent late- to post-magmatic crystallization. Reactions involving water-rich fluids are also responsible for the replacement of hornblende by late-magmatic overgrowths of biotite.

(2) Granodiorite:

Granodiorite shows variation in both texture and mineral composition. It varies from medium- to coarse-grained equigranular to porphyritic in texture. Its essential mineral constituents include plagioclase, quartz, K-feldspar, hornblende, and biotite, whereas accessory mineral phases comprise zircon, apatite, titanite, allanite, and opaque minerals. Plagioclase, hornblende, and biotite tend to form euhedral to subhedral crystals, whereas quartz and K-feldspar occur as string microperthite and containing fine-grained quartz inclusions (Fig. 3A).and occurs as interstitial minerals. Zoned crystals of plagioclase may also display spongy cellular texture. Hornblende commonly displays simple twinning. Biotite is subordinate, fresh, or scarcely altered to chlorite with epidote and/or sphene. Both biotite and hornblende often have small inclusions of euhedral plagioclase, particularly near their crystal margins.

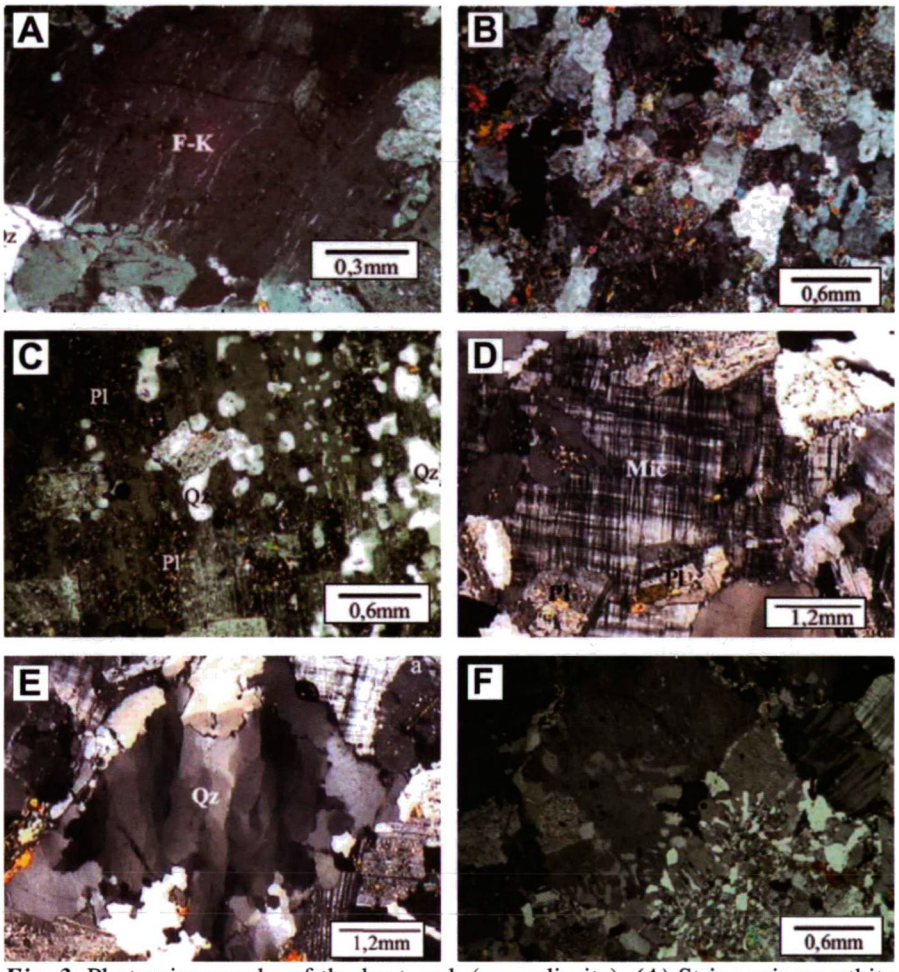

Fig. 3. Photomicrographs of the host rock (granodiorite). ***(A)*** String microperthite and fine-grained quartz inclusions in the host rock. ***(B)*** Xenomorphic plagioclase and quartz. ***(C)*** Xenomorphic aggregates of quartz grains within plagioclase phenocryst. ***(D)*** Microcline crystal showing cross-hatched twinning with plagioclase and quartz inclusions. ***(E)*** Strained quartz grain showing wavy extinction. Biotite and cross-hatched microcline are present. ***(F)*** Micrographic intergrowth in Quartz syenite.

Some samples, however, are partially replaced by secondary minerals such as sericite, clay minerals, and epidote.

Partly resorbed early-formed crystals of plagioclase are mantled with marginal overgrowths of alkali feldspar and xenomorphic plagioclase and quartz (Fig. 3B).

(3) Monzogranite:

Monzogranite consists essentially of plagioclase, quartz, and microperthitic alkali feldspar in addition to biotite and hornblende. Apatite, magnetite, zircon, allanite, and tourmaline are accessories. Sphene also is present, but the lack of idiomorphism and its disposition between biotite cleavages, indicates that it as a secondary mineral. Plagioclase predominates as an early-formed mineral phases. It appears as tabular crystals with zoning (oscillatory zoning). Monzogranite has two varieties inequigranular hornblende monzogranite and equigranular monzogranite.

(a) Plagioclse megacryst-bearing hornblende monzogranite:

This hornblende monzogranite has a light grey color and a coarse-grained porphyritic texture. It is distinguished by well-developed megacrysts of plagioclase (up to 1 cm long). Plagioclase, orthoclase microperthite, quartz, hornblende, and biotite are the essential minerals. Xenomorphic aggregates of quartz grains occur within plagioclase phenocryst (Fig. 3C). Tourmaline, allanite, and zircon are the predominant accessories in addition to smaller proportions of opaque minerals, apatite and monazite. Chlorite and opaque minerals represent the alteration products of primary mafic minerals. Alteration minerals tend to coexist with secondary biotite and tourmaline.

(b) Equigranular monzogranite:

It has a medium- to coarse-grained texture and is rich in mafic enclaves. It is composed of microperthitic K-feldspar, plagioclase, and quartz, in addition to the mafic and accessory minerals commonly observed in inequigranular monzogranite. Microcline crystal showing cross-hatched twinning with plagioclase and quartz inclusions (Fig. 3D). Strained quartz grain showing wavy extinction. Biotite and cross-hatched microcline are present (Fig. 3E). Well-developed crystals of epidote, which are ascribed to hydrothermal alteration, are accompanied by pervasive sericitization and chloritization. Some quartz grains may display weak wavy extinction.

Reaction between mafic enclaves and monzogranite is indicated by the presence of rims of biotite around the enclaves.

(4) Porphyritic quartz syenite:

Porphyritic quartz syenite has a grey color with porphyritic texture, in which phenocrysts of microperthitic alkali feldspar and partially resorbed quartz are set in a fine- to medium-grained groundmass. Essential minerals comprise alkali feldspar, quartz, biotite, and hornblende. Magnetite, ilmenite, apatite, and zircon are accessory minerals. Micrographic intergrowth is predominate at quartz syenite (Fig. 3F).

(5) Syenogranite:

Syenogranite has a greyish-pink color and a medium- to coarse-grained equigranular to mildly porphyritic texture. Essential mineral constituents include alkali feldspar, quartz, and plagioclase. Microperthitic orthoclase and plagioclase tend to form tabular subhedral crystals. Zoning in plagioclase feldspars are not frequently observed. Individual crystals of alkali feldspar may display both pristine and brownish-colored turbid areas. The proportion of turbid areas to pristine ones is highly variable, but averages about 15–30%. Perthitic texture is common. Quartz occurs as anhedral grains. Minor brown biotite occurs as euhedral to subhedral flakes, which contains inclusions of zircon, apatite, ilmenite, and monazite. Biotite is also partly altered to chlorite. Accessory minerals, in general, include Mn-rich titanomagnetite, titanite, fluorite, zircon, and apatite.

Hybrid Rocks

The mineral assemblage of the hybrid rocks, namely mesocratic to melanocratic quartz diorite and granodiorite, includes plagioclase, quartz, K-feldspar, hornblende, and biotite with subordinate amounts of apatite, zircon, titanite, magnetite and ilmenite. Prominent textural features include rapakivi texture, where well-developed K-feldspar crystals are surrounded by rims of plagioclase, and ocellar texture, where aggregates of hornblende and biotite mantle quartz crystals.

Microgranular Enclaves

The MMEs and the host rocks show different types of textural relationship. The observed textural differences are resulted from local variations in physical conditions during crystallization. The texture of the MMEs, however, is not considered a cumulate fabric. As products of early crystallization from a parental magma, the MMEs have the same geochemical role as cumulates *sensu stricto* in basic magmatic systems, especially with regard to the development of the fractional crystallization process (Vernon 1991).

Some MMEs are equigranular, whereas others form porphyritic subhedral seriate texture and contain oligoclase-andesine phenocrysts in tonalitic enclaves, and andesine-labradorite in dioritic ones. In this case the plagioclase forms the phenocrysts and the matrix consists of fine-grained quartz, plagioclase, hornblende, and rarely biotite. The MMEs contain the same mineral phases as the granitoid host but with different proportions. They are mainly composed of Ca-plagioclase and mafic minerals, such as pyroxene, hornblende, and biotite, whereas the host granitoids tend to contain lower modal proportions of Ca-plagioclase and mafic minerals but much higher modal proportions of quartz and alkali feldspars. Plagioclase and hornblende, however, are invariably the dominant minerals in the enclaves.

The microgranular enclaves are classified modally as tonalites, granodiorites, and monzogranites. The MMEs commonly show porphyritic hypidiomorphic granular texture with phenocrysts of plagioclase, quartz, and minor biotite and alkali feldspar. The phenocrysts are thought to be petrogenetically related to the host granitic magma because they are similar to those of the surrounding granite both in size and in texture.

The groundmass is largely composed of elongated laths of zoned plagioclase feldspars, biotite, hornblende, and interstitial quartz. The grain size of the groundmass material ranges from 0.05 to 0.3 mm. Biotite and hornblende are mostly less than 0.1 mm in length. Plagioclase occurs as lath-shaped euhedral grains that may display zoning. Large desorbed plagioclase crystals with albite rims coexisting with idiomorphic plagioclase (Fig. 4A).

Phenocrysts of plagioclase occurs as euhedral to subhedral with polysynthetic twins, tabular crystals that tend to have markedly altered cores, some of which may represent isolated patches or skeletal relics of early-formed plagioclase feldspars Partial melting of enclave and its reaction with the host rock (Fig. 4B). Fine-grained plagioclase, hornblende, biotite, and accessory minerals, particularly acicular apatite may occur as inclusions in plagioclase phenocrysts. Some phenocrysts may also exhibit different types of zoning textures, such as oscillatory zoning. Others, however, do not display any chemical zoning and are plausibly derived from the host granite as they are frequently associated with primary magmatic crystals of quartz and biotite. This type of phenocrysts usually displays cellular texture. Coarse-grained zoned plagioclase with inclusions of mafic minerals (Fig. 4C) are common.. Small laths of plagioclase feldspars are clearly discernable in the groundmass material.

Alkali feldspars occur as phenocrysts and as interstitial fine-grained crystals in the groundmass. Phenocrysts comprise orthoclase and microcline microperthite. The groundmass, however, is apparently dominated by cross-hatched microcline. Many alkali feldspar phenocrysts display poikilitic textures, which are quite similar to those observed in the hosting granodiorite. Alkali feldspars may also contain minute inclusions of apatite and opaque minerals. Myrmekitic and micrographic intergrowths are frequently observed at the mutual contacts of alkali feldspars and plagioclase .

Quartz is distinguished into three main types. The first one defines markedly-developed anhedral crystals surrounded by

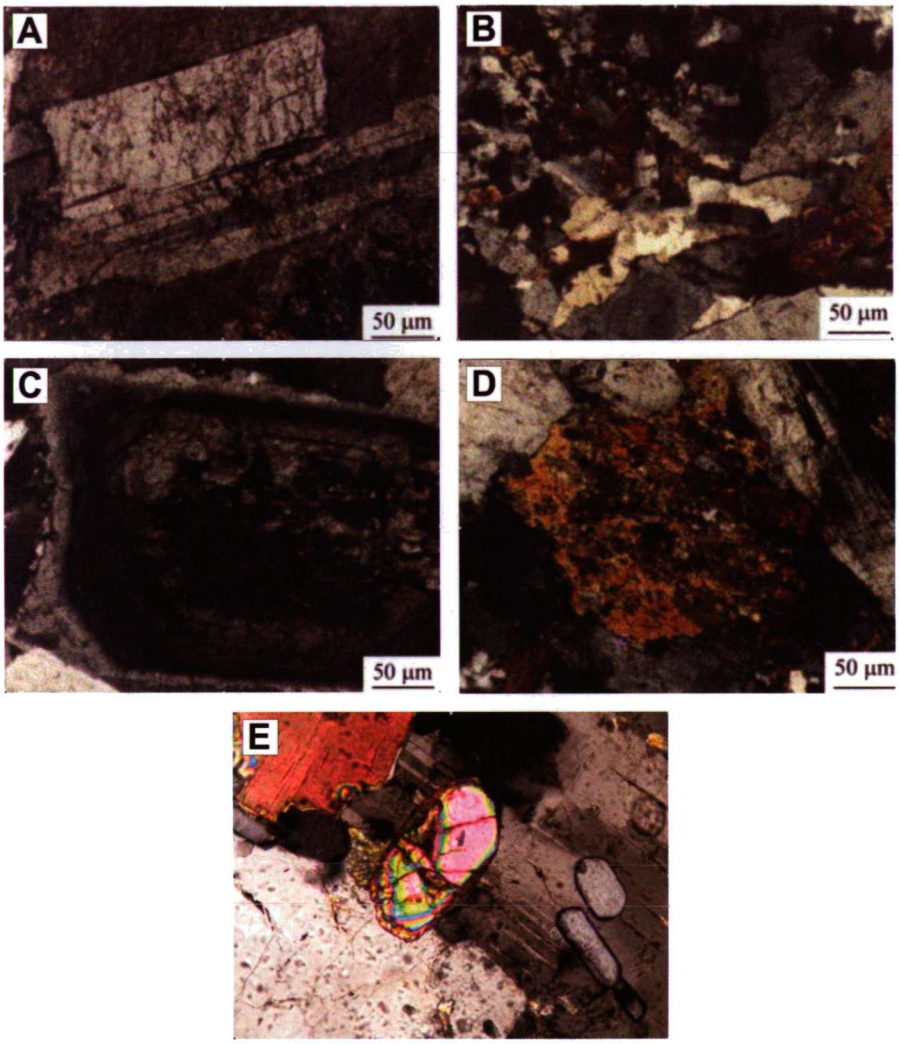

Fig. 4. Photomicrographs of the Microgranular. ***(A)*** Large resorbed plagioclase crystals with albite rims coexisting with idio-morphic plagioclase. ***(B)*** Partial melting of enclave and its reaction with the host rock. ***(C)*** Coarse-grained zoned plagioclase with inclusions of mafic minerals. ***(D)*** Amphibole rim and Fe-oxides developed along crystal cleavage. ***(E)*** Well-developed zircon, apatite, biotite and alkali feldspar in MME. Apatite shows quenched morphologies.

rims of hornblende and biotite. These large quartz ocelli, however, could be considered as xenocrysts of granitic origin. The second type is the poikilitic quartz, which is characterized by small inclusions of lath-shaped plagioclase, hornblende, biotite, Fe-Ti oxides, and acicular apatite. The third type is represented by the interstitial quartz of the groundmass material.

Biotite may attain 2 mm in length, but it is mostly less than 1 mm. It occurs either as subhedral flakes or as irregular crystals with ragged ends. Some enclaves contain blade-shaped biotite, which is usually located near the crystal margins of plagioclase. Prominent flakes of biotite may contain inclusions of plagioclase, hornblende, and zircon. Greenish-colored biotite is partly replaced with chlorite, particularly along grain boundaries and cleavage planes. Biotite, and also hornblende, may partly enclose early-formed crystals of plagioclase.

Hornblende occurs as medium-grained or fine-grained stubby prismatic crystals. It also occurs in aggregate with biotite and Fe-Ti oxides and as pseudomorphs after decomposed pyroxene. In the groundmass, hornblende evidently concentrates in the inner parts of MME. Large poikilitic crystals of hornblende enclose fine-grained biotite, plagioclase feldspars, titanite, zircon, and opaque minerals. Pyroxene crystals, which represent relics of the initial mafic magma, occur in minor amounts. They are partly or completely altered to hornblende Amphibole rim and Fe-oxides developed along crystal cleavage (Fig. 4D).

Apatite is the most common accessory mineral. It occurs mainly as acicular crystals that range from 0.1 to 1 mm in length but average less than 0.4 mm. These crystals are either arranged in radial or parallel patterns or are randomly scattered. They are enclosed in quartz, plagioclase, and K-feldspar, but they are more commonly concentrated in K-feldspar and quartz than in plagioclase. Wyllie et al. (1962) suggested that acicular apatite crystals are characteristic of rapidly cooling magmas.

Other accessory and secondary minerals include epidote, allanite, sphene, and zircon. Epidote may occur in aggregate with hornblende and biotite or as secondary alteration product that extensively replaces the Ca-rich core of the plagioclase. Allanite forms fine-grained subhedral crystals, whereas sphene occurs either as early-formed perfect wedge-shaped crystals or as interstitial crystals (<0.5 mm) in the groundmass. Zircon forms fine-grained rounded grains. Some prismatic and stubby zircon crystals, however, are enclosed alkali feldspars.

In summary, criteria shown by plagioclase indicates that crystallization took place under disequilibrium magmatic conditions and that poikilitic quartz and alkali feldspars define late stage crystallization from infiltrating granite melt. Quartz ocellars observed in the groundmass suggest mechanical transfer of quartz into the mafic microgranular enclaves during the crystallization stage of both mafic and felsic magmas. The presence of large poikilitic crystals of hornblende and blade-shaped biotite flakes indicate that they were formed during late magmatic stages. Acicular crystals of apatite are rather suggestive of a rapid growth from a mafic magma undergoing high rates of under-cooling. Pyroxene crystals, however, represent relicts of the initial mafic magma.

GEOCHEMISTRY

Method: Major-element whole-rock analyses were carried out in the laboratories of the Egyptian Geological Survey, Cairo. Most of the trace elements were determined by XRF Philips PW 1450/20. Rare earth elements were carried out in Instrumental neutron

Table 1. Whole-rock chemical analyses of the granodiorite of Wadi Rahaba, southern Sinai, Egypt.

	HR3	HR6A	HR7	HR8	HR9	HR11	HR12A	HR13	HR14A	HR15A	HR17	HR18	HR19	HR25	HR26	HR27A	HR28	HR29	HR33	HR34	HR35
SiO_2	65.5	66.25	66.8	65.5	65.5	64.82	68.71	67.67	66.85	64.11	64.95	63.94	65.36	61.26	61.86	72.94	73.47	65.76	66.96	66.15	72.81
TiO_2	0.51	0.51	0.54	0.56	0.56	0.59	0.46	0.48	0.51	0.59	0.59	0.6	0.26	0.59	0.56	0.35	0.31	0.53	0.54	0.56	0.39
Al_2O_3	15.3	14.86	14.9	14.9	14.7	15.46	14.66	14.26	15.06	15.86	15.46	15.77	15.73	16.06	15.86	13.25	12.94	15.38	14.66	15.06	13.36
$Fe_2O_3^T$	4.25	4.25	4.25	4.6	4.6	4.66	3.44	3.85	3.95	4.66	5.12	4.87	4.27	5.06	4.67	2.03	1.86	4.01	3.96	4.87	2.04
MnO	0.07	0.07	0.07	0.08	0.08	0.08	0.06	0.08	0.07	0.07	0.08	0.07	0.06	0.08	0.07	0.04	0.04	0.07	0.07	0.07	0.04
MgO	2.02	1.96	1.95	2.23	2.23	2.32	1.47	1.8	1.96	2.18	2.23	2.22	2.08	2.5	2.22	0.5	0.5	1.82	1.8	1.85	0.79
CaO	4.07	4.3	3.46	4.07	3.84	4.22	3.08	3.15	3.46	3.99	3.61	4.07	4.03	6.13	5.96	1.96	2.05	4.22	3.84	3.81	1.97
Na_2O	3.4	3.32	3.35	3.32	3.4	3.32	3.16	3.32	3.32	3.48	3.4	3.39	3.34	3.48	3.44	3.53	3.55	3.45	3.48	3.48	3.59
K_2O	3.63	3.6	3.68	3.77	3.74	3.53	3.96	3.87	3.85	3.69	3.59	3.58	4.07	3.47	3.68	4.28	4.44	3.48	3.5	3.57	4.19
LOI	0.58	0.74	0.66	0.55	0.76	0.97	0.69	0.59	0.85	0.59	0.48	0.61	0.56	0.72	0.87	0.47	0.54	0.65	0.64	0.55	0.5
Total	99.3	99.86	99.6	99.6	99.4	99.97	99.69	99.07	99.88	99.22	99.51	99.12	99.76	99.35	99.19	99.35	99.7	99.37	99.45	99.97	99.68
Ga	13.4	16.6	16.5	17.9	12.2	18.1	16.2	16.2	13.1	15.0	20.0	14.6	15.5	15.7	18.0	11.1	13.7	16.6	12.4	16.7	12.5
Rb	107.2	121.6	127.7	116.0	116.1	109.5	135.6	137.9	139.4	113.6	118.5	114.0	115.4	103.5	112.9	139.3	146.9	110.6	119.5	119.1	139.8
Sr	623.6	599.1	621.1	610.5	618.2	631.2	631.9	447.7	502.1	574.8	623.3	633.4	632.8	601.9	635.0	191.5	202.0	532.6	508.2	493.0	181.9
Y	24.9	26.6	31.0	31.6	29.3	29.7	32.7	26.0	25.8	29.0	31.3	28.2	24.0	30.6	33.0	53.6	36.1	22.7	24.0	24.3	50.8
Zr	151.0	151.0	123.7	141.8	160.6	158.1	126.6	115.5	124.6	149.6	141.1	144.7	135.1	142.7	135.9	199.4	150.9	124.4	112.4	123.3	203.1
Nb	6.0	11.7	8.4	10.9	11.2	6.7	13.9	13.8	4.7	9.9	6.0	4.0	11.3	10.5	9.4	9.5	12.3	12.1	10.7	5.5	16.0
Ba	622.5	538.6	607.1	685.1	713.1	648.0	537.7	586.3	655.4	644.9	575.2	632.1	636.0	606.4	674.6	524.5	387.3	573.1	602.3	563.9	472.2
Th	1.3	3.5	19.0	0.0	6.4	0.0	0.0	28.9	14.1	11.1	16.6	4.1	12.6	8.0	16.9	31.9	16.9	0.0	12.5	16.0	2.1
U	4.0	0.0	21.3	2.2	0.0	0.0	0.0	4.7	5.0	0.0	3.7	6.1	13.9	0.0	5.6	16.7	12.9	0.0	14.2	11.9	0.2

Table 2. Whole-rock chemical analyses of the microgranular enclaves of Wadi Rahaba, southern Sinai, Egypt.

	E1-1	E1-2	E1-3	E1-4	E1-5	E1-6	E1-7	E1-10	E1-D	E1-E	E1-F	E15-C	E16-B	E19-B	E19-D	E20-B	E40-1
SiO_2	56.14	55.02	58.46	57.46	54.58	55.82	53.23	53.30	56.45	59.15	53.10	52.47	56.80	57.76	58.46	57.25	58.44
TiO_2	0.85	0.78	0.70	0.83	0.82	0.68	0.97	1.03	0.86	0.66	1.23	1.14	0.57	0.69	0.91	0.69	0.57
Al_2O_3	17.24	14.54	17.17	17.13	16.90	17.72	14.91	18.45	17.26	15.61	15.20	18.50	15.31	14.90	17.43	16.29	14.91
$Fe_2O_3^T$	6.61	7.83	6.02	6.10	6.95	5.99	8.50	7.81	6.87	5.08	8.72	6.07	5.10	5.82	4.28	5.96	6.33
MnO	0.16	0.28	0.13	0.14	0.17	0.16	0.28	0.15	0.16	0.18	0.18	0.18	0.15	0.18	0.14	0.17	0.18
MgO	4.98	7.02	3.77	3.85	5.26	4.70	7.62	4.56	4.67	5.08	8.76	6.02	5.10	5.83	4.28	5.49	6.06
CaO	6.53	7.90	6.03	6.15	7.18	7.37	8.70	6.65	5.95	7.42	6.64	7.53	5.82	6.43	5.78	6.66	7.10
Na_2O	3.85	3.34	4.06	4.13	3.98	4.13	3.31	4.62	4.28	4.10	2.54	4.52	3.04	3.29	4.27	3.70	3.71
K_2O	3.56	3.17	3.55	4.06	3.02	3.32	2.31	3.58	3.34	2.63	3.54	3.42	7.99	4.88	4.35	3.04	2.56
Total	99.93	99.87	99.90	99.85	99.14	99.87	99.83	100.15	99.84	99.90	99.91	99.85	99.88	99.88	99.90	99.33	99.86
Ni	21.6	111.0	16.9	17.3	37.1	28.0	89.8	20.9	23.6	27.6	159.4	24.3	67.4	55.6	22.0	37.8	41.7
Cu	44.7	24.9	46.8	28.2	8.7	32.5	13.4	0.0	38.5	16.4	50.9	14.1	11.5	39.6	33.1	23.0	13.0
Zn	76.1	83.3	68.0	76.7	78.8	67.3	110.9	80.2	75.8	71.4	129.5	82.0	59.4	82.3	77.8	71.8	74.5
Ga	16.9	15.4	17.1	16.9	17.1	19.6	18.7	20.4	15.5	15.6	14.9	18.5	11.9	15.2	18.2	14.9	16.5
Rb	128.1	97.4	110.0	148.2	112.0	98.0	97.4	146.4	131.5	79.2	145.7	126.8	162.7	136.1	172.6	72.2	66.1
Sr	405.4	388.9	614.5	477.4	450.9	559.5	468.1	474.1	409.6	491.8	412.8	529.7	567.1	448.8	542.9	485.1	429.8
Y	41.6	44.3	43.4	34.6	45.2	42.4	33.7	47.9	36.7	54.3	34.1	36.2	39.4	42.2	46.2	32.1	26.1
Zr	147.7	150.4	154.8	172.6	204.7	128.5	243.5	196.2	175.0	179.8	160.4	188.1	155.2	152.6	176.3	73.5	91.7
Nb	14.2	13.6	14.1	12.3	16.8	12.3	11.8	19.4	17.8	13.6	16.1	14.7	11.7	14.3	20.8	10.9	9.0
Ba	799.0	485.0	905.1	844.8	614.5	843.5	482.4	756.4	641.6	418.9	590.2	590.6	2470.7	1522.9	696.2	694.3	601.2
Th	0.0	0.0	0.0	0.0	0.0	0.0	0.0	0.0	5.7	11.4	1.7	1.7	10.0	0.0	0.0	2.4	0.0
U	8.0	0.0	2.7	0.0	0.0	6.9	0.0	8.4	0.0	25.9	0.0	0.0	7.2	3.8	2.4	0.0	0.0

activation analysis (INAA) technique (Atomic Reactor of the Technical University, Budapest).

*Result:*Seventeen rock samples from mafic microgranular enclaves and twenty one samples from the host country rocks have been analyzed for major and minor elements (Table 1 and 2). The mafic microgranular enclaves are chemically distinct from the host granodiorite. It is observed that the chemical composition of the granodiorite is rather homogeneous.

The SiO_2 contents of the enclaves range from about 46% to 57 % and lower than the SiO_2 contents of the host rock. Al_2O_3, CaO and Na_2O of the enclaves are higher and K_2O content is generally lower than the similar components of the granodiorite host. The higher Al_2O_3 and Na_2O in the mafic microgranular enclaves are related to the higher plagioclase content and higher CaO is effect of higher plagioclase and hornblende contents.

On the diagrams of silica vs. major oxides (Fig. 5), correlations are good for apparent for all these major oxides of the enclaves and host granodiorite with the exception of Na_2O, K_2O and Al_2O_3 which show scatter plot for the sample of enclaves. Na_2O in the granodiorite shows no clear trend relative to SiO_2, but Na_2O variation fall within a narrow interval between about 3% and 3.5%. All samples of granodiorite show linear negative correlation with SiO_2 except for K_2O. The femic oxides ($Fe_2O_3^T$, MgO, CaO and MnO) show well–defined, continuous negative correlation relative to the SiO_2.

Many trace elements do not show clear correlation with SiO_2 (Fig. 6). They are scattered off the trends defined by related granodiorite. The Rb plot displays notable scatter. Although a vague trend of increasing Rb with increasing SiO_2 is apparent for the granodiorite, while Rb abundances in the enclaves, show notable scatter plot. Nb abundances roughly increase relative to decreasing SiO_2, though in view of the scatter, the trend probably has little significance. Ga abundances in both enclaves and granodiorite are characterized by their scatter plot. Usually Th and U abundances of the enclaves are lower than the host granodiorite. The Y and Zr abundances

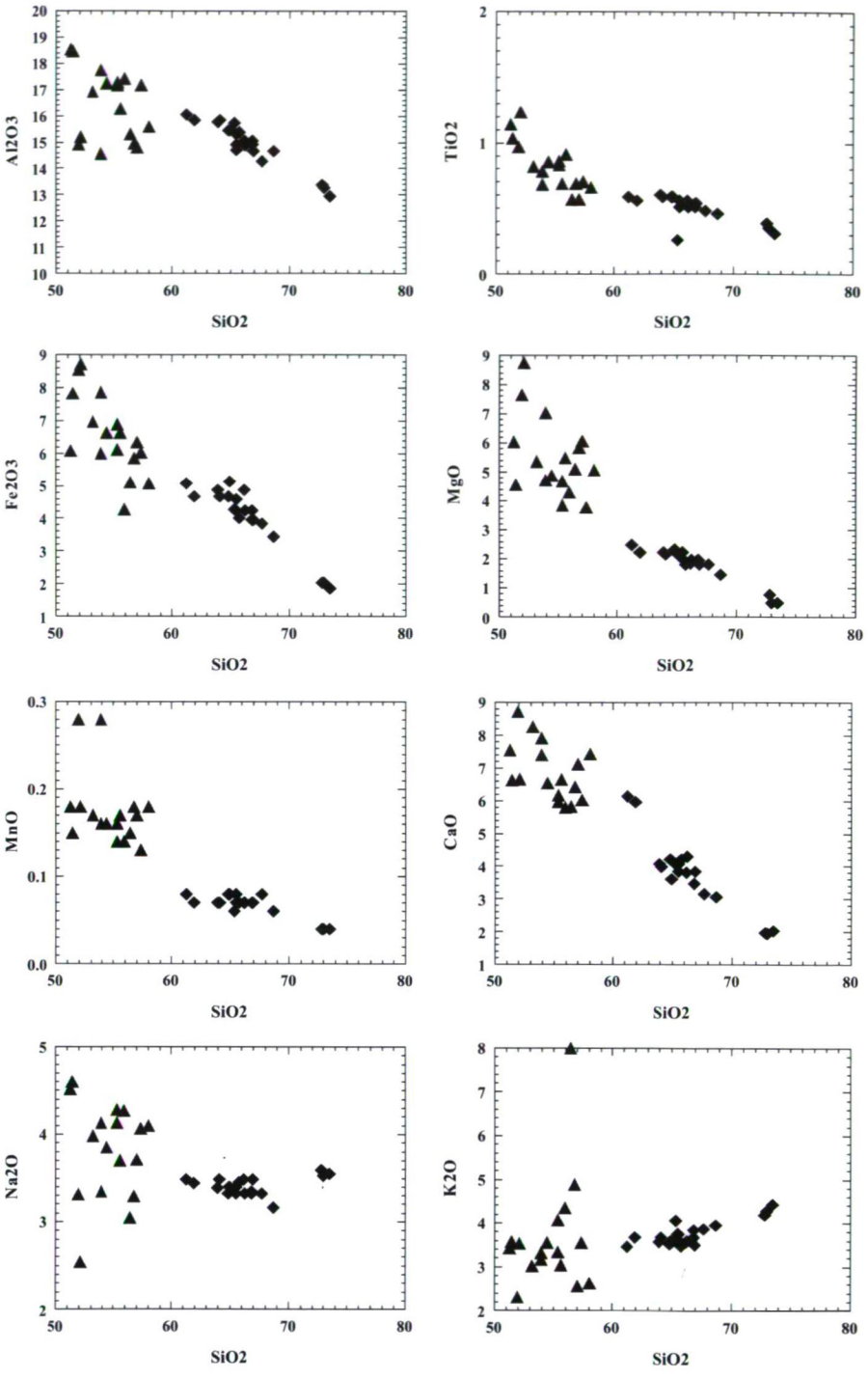

Fig. 5. Silica vs. major oxides variation diagram of the studied MMEs and host rock granodiorite samples. Symbols: (▲ Enclaves) and (♦ Host rock).

vary widely in the enclave samples. It is observed that the Y and Zr abundances increase relative to decreasing SiO_2 although the scatter of values has little linear trend. The Sr plot is marked by curved pattern, and shows the maximum Sr amount at 60% SiO_2.

It is observed that the behavior of some major and trace elements relative to silica contents (Fig. 5 and 6), especially Al, Na, and K, confirms that chemical variations among micro-granular enclaves are not explained by magmatic differentiation processes. These chemical variations related mostly to hybridization resulting from a mingling process as suggested petrographically.

The Zr/SiO_2, Y/SiO_2, Nb/SiO_2 diagrams of Collins *et al.* (1982), shown in Fig. 6 indicates also

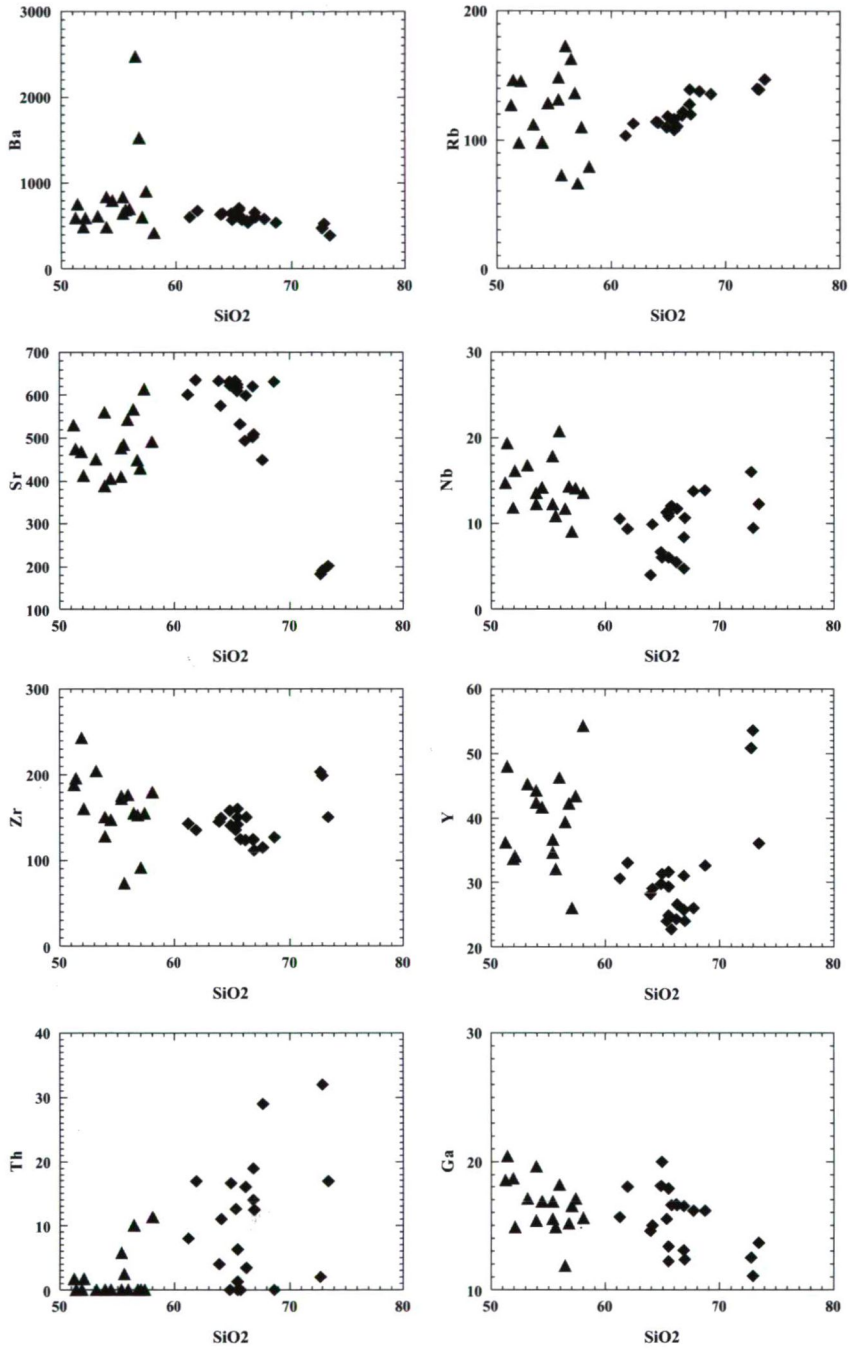

Fig. 6. Silica vs. trace elements variation diagram of both MMEs and host rock granodiorite samples.

that all the analyzed calc–alkaline granodiorite samples fall within the I-type granite field (Nb values are less than 21 ppm, Zr values are less than 250 ppm and Y contents are less than 55 ppm).

By using Shand index diagram (Fig. 7), it is evident that the host rock has meta-aluminous characteristics

Applying the diagram of Pearce et al. (1984) shown in Fig. 8 and 9, it is evident that the analyzed microgranular enclave samples occupy the subduction-related volcanic arc granite field (VAG) near the separating line of the (WPG) field.

By applying the diagram of Pearce et al. (1984) shown in Fig. 6, the analyzed granodiorite samples fall in the volcanic arc or syncollision granite field and occupy the same site of the enclave samples and still near the separating line of the (WPG) field.

On the diagram R1 vs. R2 (Fig. 10), it is evident that the host rock granodiorite and enclaves occupy the field of the pre-plate collision and post-collision uplift area.

Chemically (Debon and Le Fort 1982), the granitoid rocks are granodiorite , adamellite , and quartz monzodiorite . The majority of the analyzed samples lie within the granodiorite field.. According to Debon and Le Fort (1982) this cafemic association indicates a mantle–derived source.

White and Chappell (1977) suggested that linear trends on variation diagrams have been interpreted as evidence either of magma mixing or of restite unmixing.

However Wall et al. (1987) have shown that under certain conditions fractional crystallization can also generate linear trends. Dorais et al. (1990) reported that, if the compositional spectrum of enclave samples ranges from 46 to 57 wt% SiO_2, this will be related to fractional crystallization.

Discussion and Conclusions

It is worthy to mention that the present study revealed that the mafic microgranular enclaves, (MMEs) in the Egyptian granitoids needs more investigations in order to reach a new plateau in the understanding of their genesis and also to formulate a basic hypothetical model for their evolution.

The existence of MMEs within the granitoid rocks represents an important characteristic feature of the granitic magma and the petrogenesis of these enclaves is controversial. Various hypotheses have been advanced by several authors to explain the petrogenesis of these enclaves and their host granitic magma.

The enclaves are fragments of earlier mafic parental magma. The trapping or these basic fragments by acidic magma has been called magma mingling. The trapped basic magma was generally considered of mantle origin, (Clarke 1992), whereas the acidic magma may represent either products of crustal melting or residues from the differentiation of basic magma. Bailey (1984) suggested also that mafic microgranular enclaves and their host granites are hybrid rocks resulting from incomplete mixing and mingling of acidic and basic components. Clarke (1992) indicated also that continental arc metaluminous

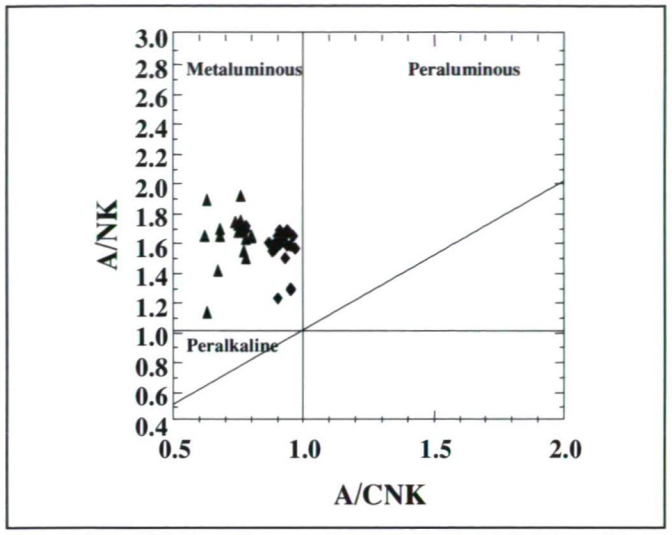

Fig. 7. Shand Index diagram for the studied MMEs and host rock granodiorite samples, (Maniar and Piccoli 1989). Symbols are the same than in the previous figures.

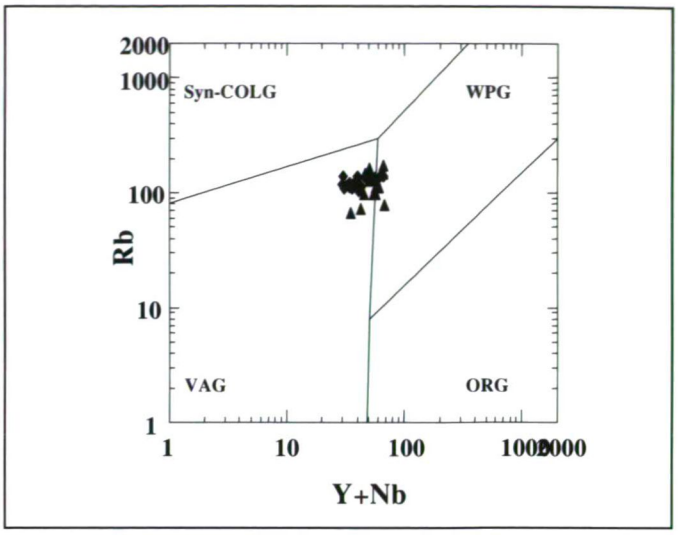

Fig. 8. Rb vs. Y+Nb tectonic diagram for the investigated host rock granodiorite, (Pearce *et al.* 1984).

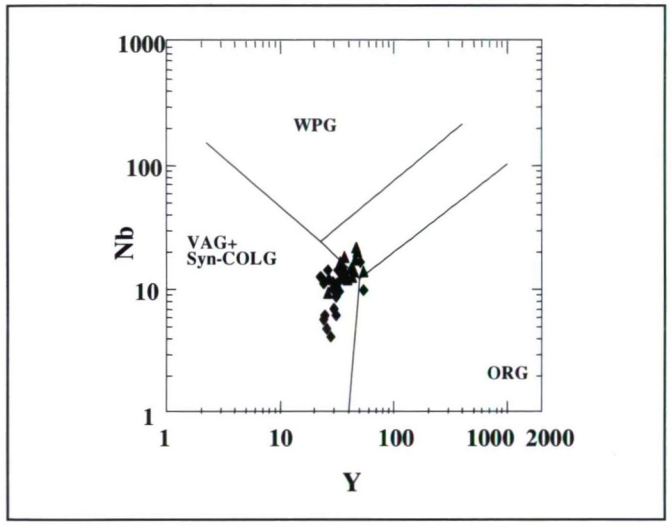

Fig. 9. Nb vs. Y tectonic diagram for the investigated host rock granodiorite, (Pearce *et al,* 1984).

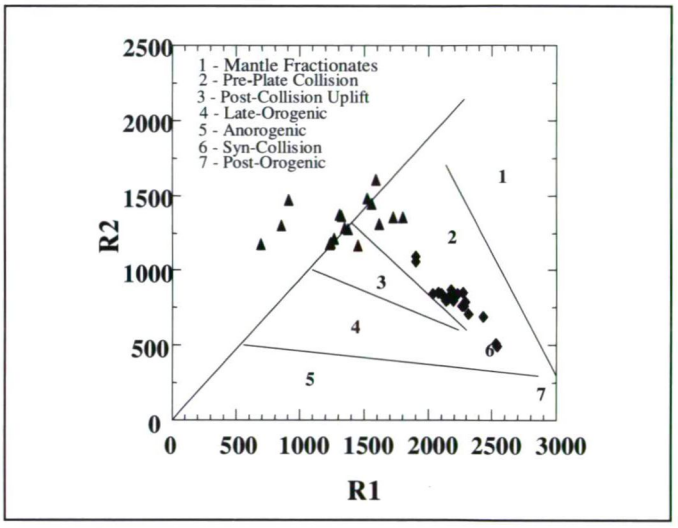

Fig. 10. R1 vs R2 diagram of the host rock granodiorite.

granitoids created by the partial melts of basaltic rocks that were previously derived from the partial melts of the mantle. Orsini et al. (1991) suggested that mixing involves thermal equilibration and various types of interactions between the two coeval magmas, such as material exchanges between the two components through either mechanical transfers of crystals or chemical transfers. During chemical transfer, the migration of alkali elements from the acid towards the basic components is recognized by chemical analyses.

Field relations revealed that the contact between enclaves and their host rocks is often marked by a chilled margin with no sign of solid state deformation.

Hybrid quartz diorite-granodiorite rocks are mesocratic to melanocratic in composition. They represent zones of mafic-felsic magma mixing. Hybrid quartz diorite-monzodiorite-granodiorite is exclusive to the granodiorite at the southwest of Wadi Rahaba. Their texture is porphyritic to equigranular showing growth textures compatible with magma mixing.

The hybrid zone is surrounded by granodioritic rocks. An important feature of the hybrid zone is that the mineral constituents of the granodiorite and the monzogranite show a good linear relationship, suggesting dynamics of a mafic magma batch. The hybrid zone is another type of mafic microgranular enclave, formed by magma mixing/mingling process where mafic magma is more abundant than granitic magma.

The interaction between magma and country rocks (assimilation) is also present. Although there could have been assimilation, there was little chance for chemical interaction. These are mostly unmodified rocks that show only scarce hornfels structure.

Bussy and Ayrton (1990) indicated that the quartz ocelli are result of the mechanical transfer of the quartz xenocrysts from the acid system into the more basic environment. The mingling process followed by mixing process. During the incomplete mixing process some igneous textures are developed in the enclaves, Hibbard (1995).

The microgranular enclaves neither contain andalusite, sillimanite, cordierite, garnet nor residual minerals formed from mica dehydration. There is no continuous variation in the meta-aluminosity from enclaves to granodiorite; so they do not represent restites.

Some of the MMEs contain quartz and plagioclase megacrysts of similar size and composition to those of the host rock, suggesting that these megacrysts have been mechanically transferred from the host granitic magma to the enclave.

There is no regular decrease in anorthite content of plagioclase from the granodioritic enclave to the host granite. This observation does not support fractional crystallization model, suggesting that the microgranular enclaves do not represent autoliths. The fine grain size of the studied enclaves than the host rock, the existence of double enclaves, the rounded and ovoid shapes of them, the complex oscillatory zoning of plagioclase phenocrysts in the granodioritic enclaves and the acicular apatite crystals found in the majority of enclaves, suggest that a mixing process between both mafic and felsic magma can be operated and the enclaves have been incorporated by the host granitic melt as magma globules.

The studied MMEs are enriched in biotite, the mafic magma had a higher water content, which enable it to remain liquid inside the granite magma and favored chemical mixing (Grasset and Albarede 1994). Biotite crystallized early during the fast cooling stage and was chemically re-equilibrated after the thermal equilibration, during the slow cooling stage of the basic magma inside the granite magma. Biotites from the cores and rims of the small granodioritic enclaves show some chemical differences suggesting that the rims have more fully equilibrated with the host rock

The textural features in the MMEs such as poikilitic K–feldspars and plagioclase, irregular poikilitic quartz patches, quartz ocelli rimmed by mafic minerals, skeletal relic plagioclase crystals, are all consistent with magma mixing process between felsic (host) and mafic (enclave) magma. The relic pyroxenes in the enclaves represent residual crystals of initial basic magma.

The important textural variations described for the granitoids at the outcrop scale reflect slow cooling and the presence of a volatile, which facilitates mineral growth. In the same way, biotite and amphibole indicate the availability of water and elevated pressure during crystallization. However, it is possible that not all crystals of amphibole are products of magmatic crystallization. In some crystals, commonly preserved relic patches of clinopyroxene, indicate late magmatic or post-magmatic crystallization replacement. Reactions involving water-rich fluids also include late magmatic overgrowth processes responsible for the replacement of pyroxene by green hornblende especially at the contact with the gabbroid rocks.

During magma mingling/mixing process, mechanical and chemical transfers developed from acidic to basic magma. A mafic magma intruded and mingled with the granite magma, which were partially crystallized, because phenocrysts of host granite were transferred to microgranular enclaves as xenocrysts. Quick crystallization took place due to the thermal contrast and mechanical mixing, which was important in the petrogenesis of granodioritic enclaves.

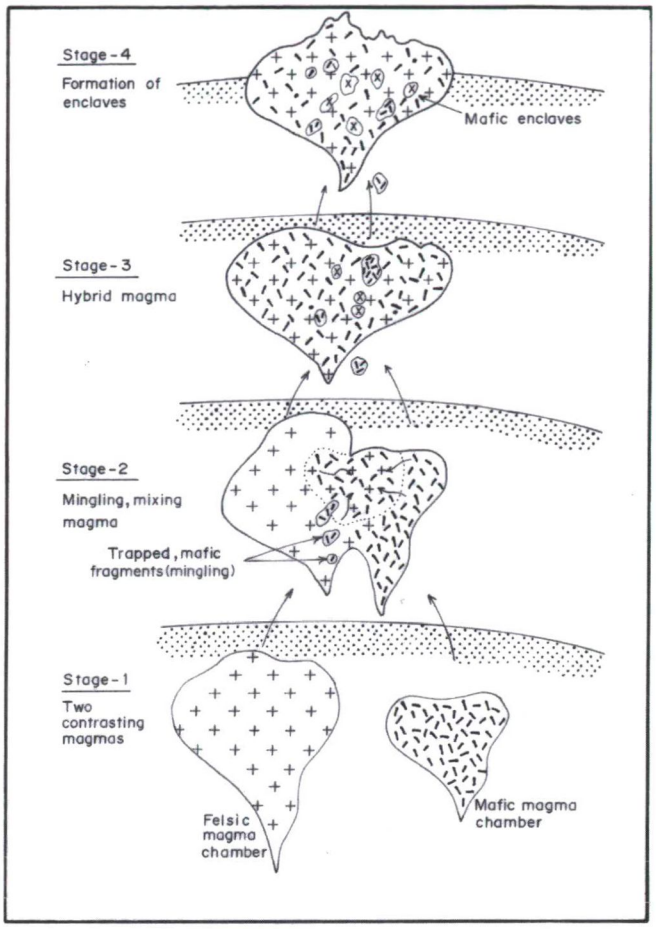

Fig. 11. Hypothetical diagram shows the evolution of the MMEs and their granodiorite host rock.

However, the differences in viscosity of the contrasting magmas, decrease the rate of the chemical mixing between them.

Evidence of disequilibrium are manifested in feldspars by oscillatory zoning, resorbed rims, mantling and punctuated growth, together with overgrowth of clinopyroxene/amphibole on quartz crystals, as well as the development of Fe–Ti oxides along clinopyroxene cleavages. According to Hibbard (1995) spongy cellular texture is formed as a result of dissolution or direct melting caused by reheating of a Ca-plagioclase component in more a felsic plagioclase composition. These observations suggest that the MMEs are derived from a hybrid-magma formed as a result of the intrusion of a mafic magma into the base of a felsic magma chamber, (Fig. 11.).

The higher contents of some major oxides (except SiO_2 and K_2O) and Nb, Y ratios in the enclaves related to the chemical transfer of trace and major elements.

Granodiorite is metaluminous, I–type, calc-alkaline in character. The enclaves have intermediate composition. They are classified as mafic microgranular enclaves on the basis of their dark color, grain size and textural properties. Petrographic and geochemical studies of the MMEs and their granodioritic host rock indicate that the latter is a product of partial melting and fractional crystallization of basic magma and that the MMEs are trapped blobs of basic magma in acidic magma. The mineralogical compositions of mafic microgranular enclaves are more or less similar to the

granodioritic host rock but have different proportions of the mineral constituents.

The Y and Nb contents of the enclaves are generally higher than those of the host rock; these high contents are similarly explained by a chemical transfer of trace and major elements out of the acid component.

REFERENCES

AMMAR, S.E., ABDELWAHED, A.A., EL-HUSSEINY, M.O. (2003): Enclaves in the El-Delihimmi-Nusla granitic pluton, central Eastern Desert, Egypt; petrography, geochemistry and origin, Egypt. J. Geol., **47/2**, 583–596

BAILEY, J.C. (1984): Geochemistry and origin of hornblende–bearing xenoliths in the I–type Petford Granite, north–eastern Queensland. Aust. J. Earth Sci., **31**, 7–23.

BARBARIN B. (2005): Mafic magmatic enclaves and mafic rocks associated with some granitoids of the central Sierra Nevada batholith, California: nature, origin, and relations with the hosts. Lithos, **80**, 155–177

BARBARIN, B. (1986): Comparison of mineralogy of mafic magmatic enclaves and host granitoids, central Sierra Nevada, California, Abstracts with Programs-Geological Society of America 18 (1986), 83.

BARBARIN, B. (1988) Field evidence for successive mixing and mingling between the Piolard Diorite and the Saint Julien-la-Vêtre Monzogranite (Nord Forez, Massif Central, France). Canadian Journal of Earth Sciences, **25**, 49–59.

BARBARIN, B. DIDIER, J. (1991): Conclusions: enclaves and granite petrology. In: Didier, J., Barbarin, B. (Eds.): Enclaves and granite petrology, Elsevier, Amsterdam, 545–549.

BARBARIN, B. DIDIER, J. (1992): Genesis and evolution of mafic microgranular enclaves through various types of interaction between coexisting felsic and mafic magmas. Trans. R. Soc. Edinburgh Sci., **83**, 145–153.

BUSSY, F. AYRTON, S. (1990): Quartz textures in dioritic rocks of hybrid origin. Schweiz. Mineral. Petrog. Mitt., **70**, 223–235.

CASTRO, A., MERENO-VENTAS, I., DE LA ROSA, J. D. (1990): Microgranular enclaves as indicators of hybridization processes in granitoid rocks. Hercynian Belt, Spain. Wally Pitcher Conference, University of Liverpool, January 1990. Geological Journal, **25**, 391–404.

CASTRO, A., MORENO-VENTAS, I., DE LA ROSA, J.D. (1991): H-type (hybrid) granitoids: a proposed revision of the granite-type classification and nomenclature. Earth Sciences, **31**, 237–253.

CHAPPELL B. W. (1996): Magma mixing and the production of compositional variation within granite suites: Evidence from the granites of Southeastern Australia". J. Petrol, l449–470.

CLARKE, D.B. (1992): Granitoid Rocks. Chapman and Hall Publications, Hong Kong, 283.

COLLINS, W.J., BEAMS, S.D., WHITE, A.J.R., CHAPPELL, B.M. (1982): Nature and origin of A–type granites with particular reference to Southeastern Australia. Contrib. Mineral. Petrol., **80**, 189–200.

DAHLQUIST, J.A. (2002): Mafic microgranular enclaves: early segregation from metaluminous magma (Sierra de Chepes), Pampean Ranges, NW Argentina. Journal of South America Earth Sciences, **15**, 643–655.

DEBON, F. LE FORT, P. (1982): A chemical–mineralogical classification of common plutonic rocks and associations. Royal Soc. of Edinburg Transaction, **73**, 135–149.

DIDIER, J. (1973): Granites and their Enclaves, Elsevier, Amsterdam, 393.

DIDIER, J. (1973): Granite and Their Enclaves: The Bearing of Enclave on the Origin of Granites, Development in Petrology, 3, Elsevier, Amsterdam, 393.

DIDIER, J. (1984): The problem of enclaves in granitic rocks, a review of recent ideas on their origin. In: Xu, K.Q. and Tu, G.C. (eds.): Geology of Granites and their Metallogenetic Relations, Proceeding of International Symposium, Nanjing, October 1982, Science Press, Beijing, 137–144.

DIDIER, J. (1987): Contribution of enclave studies to the understanding of origin and evolution of granitic magmas. Geologische Rundschau, **79**, 41–50.

DIDIER, J. BARBARIN, B. (1991): The different types of enclaves in granites-Nomenclature. In: Didier, J. and Barbarin, B. (eds.): Developments in Petrology 13: Enclaves and granite petrology. Elsevier, Amsterdam, 19–24.

DODGE, F.C.W. KISTLER, R.W. (1990): Some additional observations on inclusions in the granitic rocks of the Sierra Nevada. Journal of Geophysical Research, **95**, 17841–17848.

DORAIS, M.J., WHITNEY, J.A., RODEN, M.F. (1990): Origin of mafic enclaves in the Dinkey Creek Pluton, Central Sierra Nevada batholith, California. J. Petrol., **31**, 853–881.

EL-METWALLY, A. A. (1993): Microgranular enclaves in the Pan African granites from the Sinai massif; petrography, mineralogy and geochemistry. J. Afri. Sci., **14**, 111–119.

EYAL, M. BARTOV, Y. SHIMRON, A. E., BENTOR, Y. K. (1980): Sinai geological map (1:500,000); Geological Survey of Israel.

GRASSET, O. ALBAREDE, F. (1994): Hybridization of mingling magmas with different denisties. Earth Planet. Sci. Lett., **121**, 327–332.

HASSEN, I. S. (1997): Mineralogy, petrology and geochemistry of granitiod rocks of St. Katherine area, South Sinai, Egypt. Ph.D. Thesis (Unpublished), Eötvös Lorand University, Budapest, Hungary, 83.

HIBBARD, M.J. (1995): Petrography to Petrogenesis. Prentice Hall, 587.

MAAS, R., NICHOLLS, I. A. LEGG, C. (1997): Igneous and metamorphic enclaves in the S-type Deddick Granodiorite, Lachlan Fold Belt, SE Australia: petrographic, geochemical and Nd-Sr isotopic evidence for crustal melting and magma mixing. J. Petrol., **38**, 815–841.

MANIAR, P. D. PICCOLI, P. M. (1989): Tectonic discrimination of granitoids. Geol. Soc. Am. Bull., **101**, 635–643.

ORSINI, J.B., CORCIRTA, C., ZORPI, M. J. (1991): Genesis of mafic microgranular enclaves through differentiation of basic magmas, mingling and chemical exchanges with their host granitoid magmas. In: Didier, J., Barbarin, B. (eds.): Developments in Petrology 13: Enclaves and Granite Petrology. Elsevier, Amsterdam, 445–464.

PEARCE, J.A., HARRIS, N.B.W., TINDLE, A.G.W. (1984): Trace element discrimination diagrams for the tectonic interpretation of granitic rocks. J. Petrol., **25**, 56–983.

SINHA, K. K., NAUTIYAL-KULDEEP, SHARMA, P.K., GUPTA, R.K. (2001): Petrochemical evidences of magma mingling and mixing in Bundelkhand Massif, Rajghat, Uttar Pradesh, Gondwana. Geological Magazine, **13**, 1–11.

SUROUR, A.A. KABESH, M.L. (1998): Calc-alkaline magmatism and associated mafic microgranular enclaves of Wadi Risasa area, southeastern Sinai, Egypt, Annals Geol. Surv. Egypt, V.XXI; 35-54.

TOBISCH, O.T., MCNULTY, B.A., VERNON, R.H. (1997): Microgranitoid enclave swarms in granitic plutons, Central Sierra Nevada, California. Lithos, **40**, 321–339.

VERNON, R.H. (1983): Restite, xenoliths and microgranitoid enclaves in granites. J. Proc. R. Soc. N. S. W., **116**, 77–103.

VERNON, R.H. (1984): Microgranitoid enclaves: Globules of hybrid magma quenched in a plutonic environment. Nature, **304**, 438–439.

VERNON, R.H. (1990): K-feldspar megacrysts in granites: Phenocrysts not Porphyroblasts. Earth Sci. Rev., **23**, 1–36.

VERNON, R.H. (1991): Interpretation of microstructures of microgranitoid enclaves. In: Didier, J., Barbarin, B. (Eds.): Enclaves and Granite Petrology, Elsevier, Amsterdam, 277–292.

VERNON, R.H., ETHERIDGE, M.A., WALL, V. J. (1988): Shape and microstructure of microgranitoid enclaves: indicators of magmatic mingling and flow. Lithos, **22**, 1–12.

WHITE, A.R. CHAPPELL, B.W. (1977): Ultrametamorphism and granitoid genesis. Tectonophysics, **43**, 7–22.

WINCHESTER, J. A. FLOYD, P. A. (1977): Geochemical discrimination products using immobile elements. Chem. Geol., **20**, 325-343.

WYLLIE, P.J., COX, K.G., BIGGAR, G.M. (1962): The habit of apatite in synthetic systems and igneous rocks. J. Petrol., **3**, 238–243.

Received: April 6, 2008; accepted: July 29, 2008

*Acta Mineralogica-Petrographica, Szeged 2008, Vol. **48**, pp. 17-31.*

ACTA Mineralogica Petrographica

SHOCK METAMORPHISM AT TERRESTRIAL IMPACT STRUCTURES: MINERALOGICAL AND GEOLOGICAL CONSEQUENCES

ARNOLD GUCSIK

Max Planck Institute for Chemistry, Department of Geochemistry, Joh.-J.-Becherweg 27., D-55128, Mainz, Germany.
e-mail: gucsik@mpch-mainz.mpg.de

ABSTRACT

The impact cratering as a leading process in the formation of the planetary bodies and surfaces and their geological as well as mineralogical consequences have been summarized in this review article, which is based on PhD. thesis of Arnold Gucsik at Univeristy of Vienna. The purpose of this study is to provide the most important lithological and shock diagnostic features of shock metamorphism accompanied with terrestrial impact structures. The first section of this study gives a brief summary of the formation mechanism and stages of an impact structure as well as a short description of basics of the sock wave physics of an impact event. The next section deals with the types of terrestrial impact structures. The lithological shock-metamorphic indicators and diagnostic shock features in the target rocks are mentioned in the following sections.

Key words: shock metamorphism, impact crater, shock wave, impact-derived glasses, shock-induced microdeformations

INTRODUCTION

Shock metamorphism is the sum of irreversible chemical, mineralogical and physical changes in the target materials that occur during the hypervelocity impact event (Melosh 1989). The following chapters have been summarized from reviews by French and Short (1968), Sharpton and Grieve (1990), Stöffler and Langenhorst (1994), Grieve et al. (1996), Koeberl (1997) and French (1998). When an extraterrestrial projectile (comet or asteroid) hits target rocks of a planetary surface, geologic materials are subjected to shock pressures above their Hugoniot Elastic Limit (HEL), which is on the order of 5 to 10 Gigapascals (GPa) (Sharpton and Grieve 1990). Shock metamorphism provides evidence for conditions associated with impact cratering (e.g., French and Short 1968, Stöffler and Langenhorst 1994, Grieve et al. 1996, Koeberl 1997, French 1998 and references therein) including the high pressures, temperatures, and strain rates (106-108 s-1), which lead to characteristic structural and phase changes in minerals. Figure 1 shows a comparative pressure-temperature diagram of endogenic metamorphism and shock metamorphism (Koeberl 1997). The most characteristic products of shock metamorphism, as well as the associated diagnostic features are listed in Tables 1 and 2. These diagnostic shock features are the most important criterion to evaluate the impact origin of a crater, in particular when characteristic features of progressive shock metamorphism, as listed in Tables 1 and 2, are found.

Large impact events differ in many ways from endogenic processes such as volcanic explosions, earthquakes, and plate tectonics (French 1998):

- There have been no historical records or examples of large meteorite impacts.
- The impact energy is limited only by the mass and velocity of the projectile and concentrated within a fraction of time compared to the hundreds or thousands of years through volcanism, earthquakes, tectonic processes, and heat flow.
- The energy is released in an impact event shattering, deforming, melting, and even vaporising large volumes of target rock in a fraction of seconds.
- Large impact events cause biological extinctions, because their impact energy is released near the surface and directly into the biosphere.
- Unique deformation effects occurred as changes in minerals such as mineral deformations and melting under the extreme high pressure and temperature (e.g., the shock pressure is approximately 60 GPa and post-shock temperature is about 2000°C).

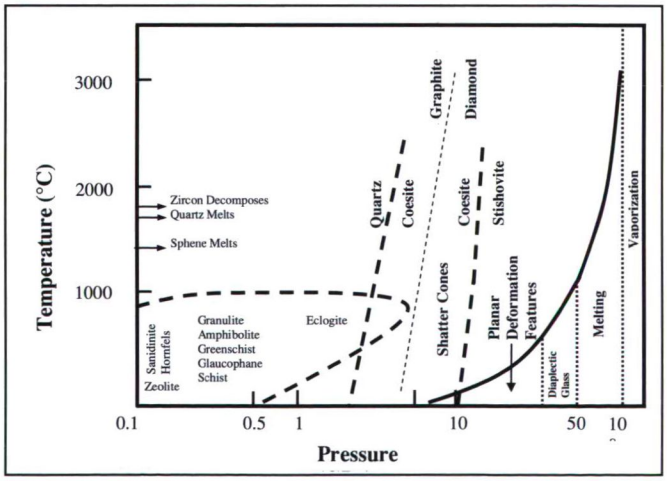

Fig. 1. Conditions of endogenic metamorphism and shock metamorphism in the pressure-temperature fields. This comparison diagram exhibits the onset pressures of various irreversible structural changes in the rocks due to shock metamorphism and the relationship between pressure and post-shock temperature for shock metamorphism of granitic rocks (after Koeberl 1997, his Fig. 2).

Table 1. Shock pressures and effects (from Stöffler and Langenhorst, 1994; French, 1998).

Approximate Shock Pressure (GPa)	Estimated Post Shock Temperature (°C)	Effects
2-6	<100	Rock fracturing; breccia formation; Shatter cones
5-7	100	Mineral fracturing: (0001) and $\{10\bar{1}\,0\}$ in quartz
8-10	100	Basal Brazil twins (0001)
10	100	
		Quartz with PDFs $\{10\bar{1}\,3\}$
12-15	150	Quartz → stishovite
13	150	Graphite → diamond
20	170	
		Quartz with PDFs $\{10\bar{1}\,2\}$, etc.
		Quartz, feldspar with reduced refractive indices, lowered birefringence
>30	275	Quartz → coesite
35	300	
		Diaplectic quartz, feldspar glasses
45	900	Normal (melted) feldspar (vesiculated)
60	>1500	Rock glasses, crystallised melt rocks (quenched from liquids)
80-100	>2500	Rock glasses (condensed from vapor)

*For dense nonporous rocks. For porous rocks (e.g., sandstones), postshock temperatures = 700°C (P = 10 GPa) and 1560°C (P = 20 GPa).

Table 2. Characteristics and formation pressures of various shock deformation features.

Pressure (GPa)	Features	Target characteristics	Feature characteristics
2-30	Shatter cones	Best developed in homogeneous, fine-grained, massive rocks, both sedimentary and crystalline.	Conical fracture surfaces with subordinate striations radiating from a focal point.
5-45	Planar fractures (PF) and planar deformation features (PDFs)	Highest abundance in crystalline rocks; found in many rock- forming minerals; e.g., quartz, feldspar, olivine, and zircon	PDFs: Sets of extremely straight, sharply defined parallel lamellae; occur often in multiple sets with specific crystallographic orientations.
30-40	Diaplectic glass	Most important in quartz and feldspar (e.g., maskelynite from plagioclase).	Isotropization through solid-state transformationunder preservation of crystal habit as well as primary defects and sometimes planar features. Index of refraction lower than in crystal but higher than in fusion glass.
15-50	High-pressure Polymorphs	Quartz polymorphs (coesite, stishovite) most common, but also ringwoodite from olivine, jadeite from plagioclase, and majorite from pyroxene.	Recognisable by crystal parameters, confirmed usually with XRD or NMR; abundance influenced by post-shock temperature and shock duration; Stishovite is temperature liable.
>35	Impact diamond	From carbon (graphite) present in target rocks; rare	Cubic and hexagonal form; usually very small but occasionally up to millimetre-size; inherit graphite crystal shape
45->70	Mineral melts	Rock-forming minerals (e.g., lechatelierite from quartz)	Contrary to diaplectic glass, liquid-state transformation of a mineral into glass.
>60	Rock melt	Best developed in massive silicate rocks. Occur as individual melt bodies (millimetre to meter size) or as coherent melt sheets, up to >1000 km3.	Either glassy (fusion glasses) or crystalline; of macroscopically homogeneous, but microscopically often heterogeneous composition. Large melt sheets may be medium to coarse-grained, and resemble endogenetic igneous rocks.

GPa = Gigapascals; XRD = X-ray diffraction; NMR = nuclear magnetic resonance; PDFs = planar deformation features (after Koeberl, 1997, his Table 1).

IMPACT CRATERING MECHANICS

The impact cratering process is commonly divided into the contact and compression, excavation, and modification stages (Gault et al. 1968, Melosh 1989, 1992). During the compression stage, structural modifications and phase changes occurred in the target rocks. The morphology of a crater is developed in the excavation and modification stages (Fig. 2).

Contact and compression stage

During the contact and compression stage, the projectile or impacting object first hits the planet's surface (the target) and transfers its energy and momentum to the underlying rocks. The projectile traveling at a few kilometers per second produces large specific kinetic energy ($E=½\ mv^2$, m = mass, v = velocity) (Melosh 1992). For instance, a stony meteorite of only 6 m diameter, colliding with the Earth at 20 km/s, releases as much energy [8.3 x 1023 Joules (J) or 20,000 tons (20 kT) of TNT] as an atomic bomb (French 1998).

This stage lasts only a bit longer than the time required for the impacting object to travel its own diameter,

$$t_{cc}= L/v_i, \quad (1)$$

where t_{cc} is the duration of contact and compression, L the projectile diameter, and v_i the impact velocity.

The shock wave in the projectile reaches its back (or top) surface in contact and compression stage. Simultaneously, the pressure is released as the surface of the compressed projectile expands upward (wave of pressure relief propagates back downward toward the projectile-target interface). During the irreversible compression process, the projectile has been compressed to high pressure (hundreds of gigapascals) producing liquid or gaseous state due to heat deposited in the projectile (Melosh 1992).

Very high velocity jets of highly shocked material are formed, where strongly compressed material is close to a free surface. The jet velocity depends on the angle between the converging surface of the projectile and the target, but may exceed the impact velocity by factors as large as five (Melosh 1992).

Hugoniot Elastic Limit (HEL)

The projectile hits the target, generating strong shock waves, which leads to compression of the target rocks at pressures far above a material parameter called the Hugoniot elastic limit (Melosh 1989). The Hugoniot Elastic Limit (HEL) describes the maximum stress in an elastic wave that a material can be subjected to without permanent deformation (Melosh 1989). The value of the HEL is about 5-10 GPa for most minerals and whole rocks. The only known natural process that generates these high shock pressures exceeding the HELs is hypervelocity impact. The strength of the shock waves can be demonstrated or measured from the Hugoniot equations, relating quantities in front of the shock wave (subscript 0) to quantities behind the shock wave (Melosh 1989)

$$\rho(U-\mu_p) = \rho_0 U \quad (2)$$

$$P-P_0 = \rho_0 \mu_p U \quad (3)$$

$$E-E_0 = ½(P + P_0)(1/\rho_0-1/\rho) \quad (4)$$

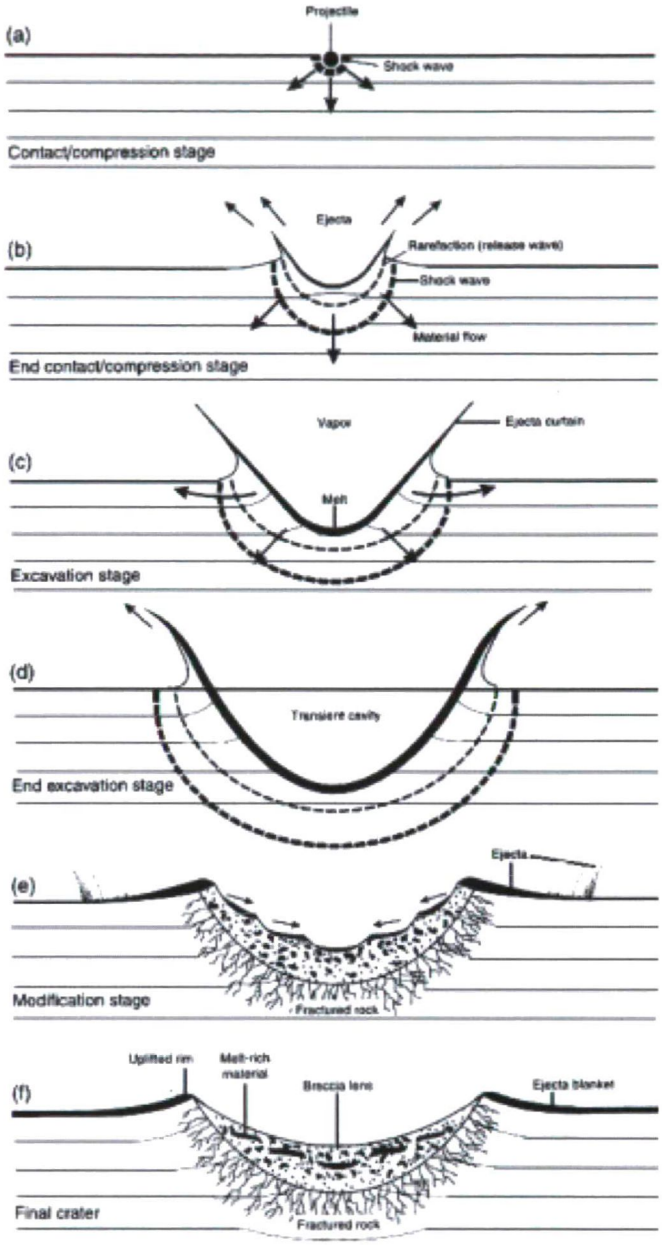

Fig. 2. Schematic diagram of the stages of the formation of a simple impact crater (from French, 1998; Fig.3.3).

where P is pressure, ρ density, μ_p particle velocity after the shock, U the shock velocity, and E energy per unit mass. These three equations are equivalent to the conservation of mass, momentum, and energy, respectively, across the shock front. The Hugoniot equations must be supplemented by a fourth equation, the equation of state, that relates the pressure to the density and internal energy in each material,

$$P = P(\rho, E) \quad (5)$$

Alternatively, a relation between shock velocity and particle velocity may be specified,

$$U = U(\mu_p) \quad (6)$$

As this relation is frequently linear, it often provides the most convenient equation of state in impact processes. Thus, we can write:

$$U = c + S\mu_p \quad (7)$$

where c and S are empirical constants. Table 3 lists the measured values of c and S for a variety of materials. These equations can be used to compute the maximum pressure, particle velocity, shock velocity, etc. in an impact (Melosh 1992). A Hugoniot equation of state curve is a shock wave equation of state data, which are plotted on a P-V plane (Fig. 3). It defines the locus of all shock states achievable in any material by shock waves of variable intensity, e.g., by various impact velocities of a projectile (Melosh 1989, Koeberl 1997).

Temperatures in the shocked states can be determined by integrating the following equation because of the internal energy, which is related to temperature and volume through an equation of state (Martinez et al. 1995, Martinez and Agrinier 1998):

$$\frac{dt}{dV} = -T\left(\frac{\gamma}{V}\right) + \left[\frac{dP}{dV}(V_0 - V) + (P_0 - P)\right]\frac{1}{2C_v} \quad (8)$$

where V0 and P0 are initial volume and pressure.

Models of specific heat Cv and Grüneisen parameters γ (which are quantities that are relatively constant by the product of three times the coefficient of linear expansion divided by the product the compressibility with the specific heat per unit volume) at high temperature and compression are therefore required for calculating shock temperatures (Melosh 1989, Martinez and Agrinier 1998).

Post-shock temperatures in the material can be related to temperatures in the shocked state using

$$\frac{dT}{dV} = -T\left(\frac{\gamma}{V}\right) \quad (9)$$

which is the adiabatic part of the Hugoniot equation and represents the adiabatic decompression from the shock state to the final surface-pressure state (Melosh 1989, Martinez and Agrinier 1998).

Excavation stage

As Figure 4 shows, the expanding shock waves open the actual impact crater during the excavation stage (Melosh 1989, Grieve 1991). The transient cavity is a freshly opened bowl-shaped crater and surrounded by an ejecta curtain that develops is several orders of magnitude larger than the diameter of the projectile.

At the high pressures and post-shock temperatures the rocks may melt or even vaporise upon release. The lower pressures cause pervasive fracturing and planar deformation elements in individual crystals and produce characteristic cone-in-cone fractures called shatter cones. The target material strength and gravity become important near the end of excavation. This stage ends much longer than the contact and compression stage, requiring seconds or minutes to reach completion, depending upon the several factors as follows: crater size, direction of the impact, impact velocities, presence of a water table or layers of different strength, rock structure, joints, or initial topography in the target (Melosh 1992).

Modification stage

The modification stage begins when the transient crater collapses under gravity, and elastic rebound of the underlying, compressed rock layers may also play a role. It was suggested from volume conservation that the crater collapse appears almost immediately after formation of the transient crater, which produces an increase of the original diameter of the crater by about 15%. During modification, loose debris slides down the steep interior walls of small craters, pooling on the floor of the final bowl-shaped depression (Melosh 1992). The normal geologic processes of gradation, isostatic adjustment, infilling by lavas, sediments, etc. on geologic time scales may eventually result in obscuration or even total obliteration of the crater (Melosh 1992).

Table 3. Linear shock-particle velocity equation of state parameters (from Melosh, 1989, 1992).

Material	ρ_0 (g/cm^3)	c (km/s)	S
Aluminium	2.750	5.30	1.37
Basalt	2.860	2.60	1.62
Calcite (carbonate)	2.670	3.80	1.42
Coconino sandstone	2.000	1.50	1.43
Diabase	3.000	4.48	1.19
Dry sand	1.600	1.70	1.31
Granite	2.630	3.68	1.24
Iron	7.680	3.80	1.58
Permafrost (water saturated)	1.960	2.51	1.29
Serpentinite	2.800	2.73	1.76
Water (25°C)	0.998	2.393	1.33
Water ice (-15°C)	0.915	1.317	1.53

ρ_0 is the density of material in front of shock wave, c and S are empirical constants.

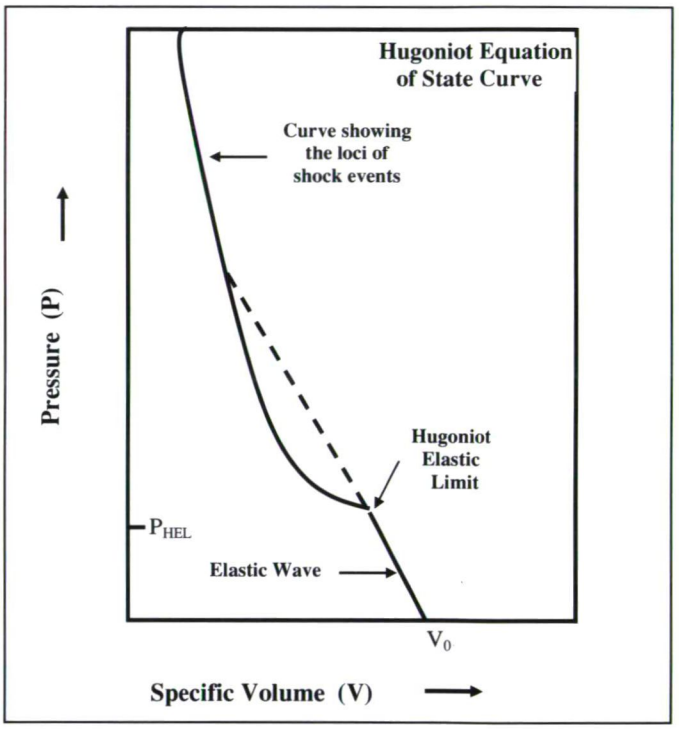

Fig. 3. The Hugoniot equation state curve does not represent a continuum of states as in thermodynamic diagrams, but the loci of individual shock compression events. The yielding of the material at the Hugoniot Elastic Limit is indicated (after Koeberl 1997, his Fig. 1).

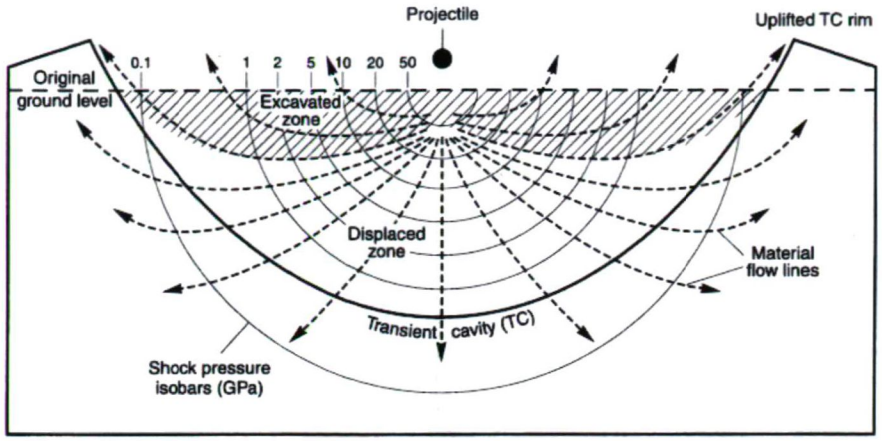

Fig. 4. Theoretical cross section showing development of the transient crater during the excavation stage immediately after the contact/compression stage. The hemispherical isobars around the impact point are original peak shock pressures in Gigapascals (GPa). The subsequent rarefaction wave produces an outward excavation flow (dashed arrows) that opens up the transient crater. In the upper part of this region (excavated zone; ruled area), target material is fractured, excavated, and ejected beyond the transient rim. In the lower region (displaced zone), target material is driven downward and outward, more or less coherently, and thus does not reach the surface (from French 1998, his Fig.3.4).

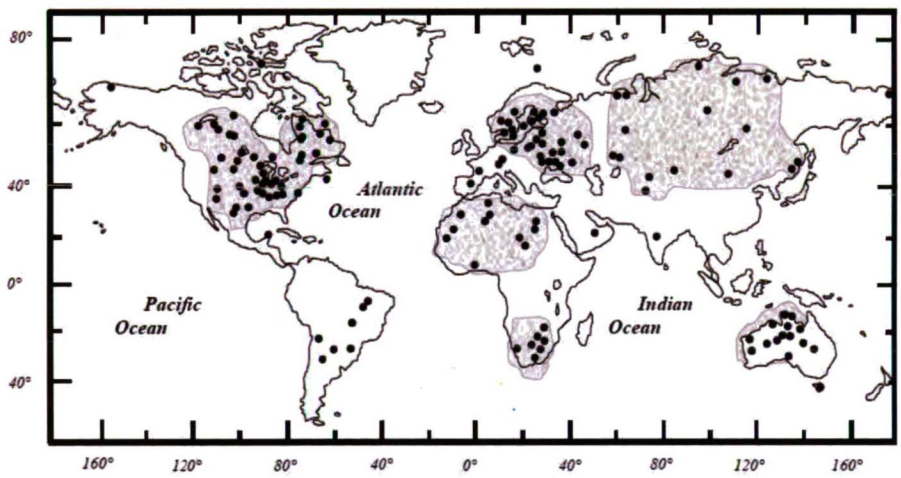

Fig. 5. Distribution of currently (2009) known impact structures on Earth. The confirmed impact craters are concentrated mainly to the cratonic areas (as indicated by grey regions) of continents. So far no impact structures on the ocean floor have been identified (data from www.unb.ca/passc/Impact Database).

Fig. 6. A young, well-known and well-preserved simple impact crater (1.2 km in diameter): Barringer Meteor Crater (Arizona, USA). This crater was formed about 50.000 years ago, when an iron meteorite approximately 30 m across struck the horizontal sediments of northern Arizona's Colorado Plateau. The photo, looking northwest, shows the uplifted rim (photo by the author).

TYPES OF IMPACT CRATERS

The Earth Impact Database is a resource that has been assembled since 1985 by researchers at the Geological Survey of Canada (a division of Natural Resources, Canada). It has now been transferred to the Planetary and Space Science Centre at the University of New Brunswick, Department of Geology. Here, 175 impact structures (2009) were registered on the webpage: www.unb.ca/passc/ImpactDatabase/. These confirmed terrestrial impact craters (Fig. 5) have two basic morphological forms: simple and complex. The two forms differ only in the diameter range at which the transition from one form to another takes place. On the Earth, simple craters occur up to a diameter of 4 km in crystalline and 2 km in sedimentary target rocks (Dence 1972). Terrestrial craters with a diameter greater than 4 km show a complex form. Depending on their size, complex craters may be further subdivided into peak ring crater and multiring basins.

Simple Craters

Simple craters are the smallest impact structures and occur as bowl-shaped depressions (French 1998). These craters can be characterized by a structurally upraised and fractured rim area (e.g., Barringer Crater, Arizona, USA) (Fig. 6). The sizes of these craters are up to 2 km (sedimentary target rocks) to about 4 km in diameter (crystalline target rocks) on Earth, depending on the strength of the target rocks (Dence 1972, Melosh 1992). The interior of the crater has a smoothly sloping parabolic profile and its rim-to-floor depth is about one-fifth of its rim-to-rim diameter. The surrounding plain is blanketed with a mixture of ejecta (proximal ejecta) and debris scoured from the pre-existing surface for a distance of about one crater diameter from the rim (Melosh 1992). The floor of simple craters is underlain by a lens of broken rock, breccia, which slid down the inner walls of the crater shortly following excavation. This breccia typically includes representatives from all the formations intersected by the crater and may contain layers of melted or highly shocked rocks (Fig. 7).

Complex craters

The complex craters have flat interior floors or internal rings instead

of central peaks and formed with diameters larger than 4 km on Earth (depending on the target lithology). These craters are believed to have formed by collapse of an initially bowl-shaped transient crater, and because of this more complicated structure they are known as complex craters (Melosh 1992). The floors of complex craters are covered by melted and highly shocked debris. The surfaces of the terrace blocks tilt outward into the crater walls, and melt pools are also common in the depressions thus formed (Fig. 8). The central peaks consist of material that is pushed upward from the deepest levels excavated by the crater. Complex craters are generally shallower than simple craters of equal size and their depth increases slowly with increasing crater diameter. Rim height also increases rather slowly with increasing diameter because much of the original rim slides into the crater bowl as the wall collapses (Melosh 1992). The amount of structural uplift (SU) at complex craters can be measured, where the subsurface stratigraphy is known (Fig. 8). The relationship is:

$$SU=0.06D^{1.1} \qquad (10)$$

where SU is the amount of stratigraphic uplift undergone by the deepest lithology now exposed at the surface in the center and D is the diameter of the crater (Grieve 1991). The uplifted area may consist of parts of the upper crust at the larger complex craters (e.g., Siljan, SU=4 km; Manicouagan, SU=9.5 km). The ejecta blankets of complex craters show some similarities to those of simple craters. However, the hummocky texture characteristics of simple craters are replaced by more radial troughs and ridges as size increases (Melosh 1992).

Submarine impact structures

Only a few confirmed submarine impact craters are known, including: Montagnais, located offshore of Nova Scotia, Canada (50.5 Ma, D=45 km), Tvären, Sweden (455 Ma, D=2 km), Mjølnir in the Barents Sea, north of Norway (Jurassic, D=40 km), and Chesapeake Bay offshore of the Atlantic coast of Virginia, USA (35 Ma, D=90 km). The half of the Chicxulub multiring impact basin is

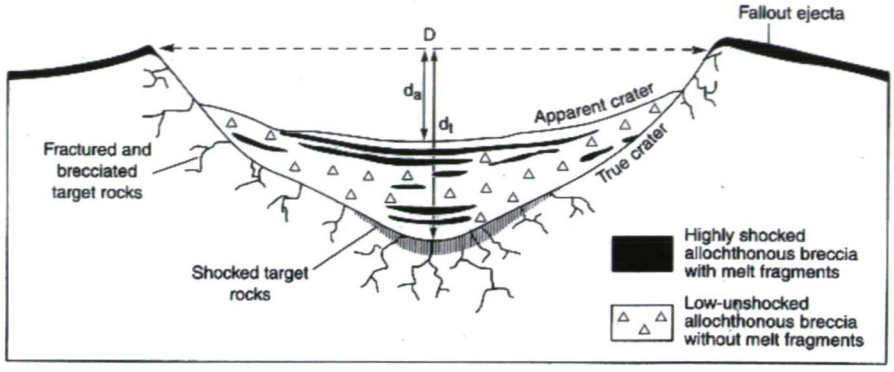

Fig. 7. Schematic cross section of a simple impact structure, showing the locations of impactite types. Fractured and brecciated target rocks lie below the true crater floor without distinctive shock effects. Only the shocked target rocks as a small zone (fine vertical ruling) contain shock metamorphic effects in the center of the structure. The fallout ejecta overlies the uplifted crater rim and surrounds the crater, which is easily eroded and is presented only in the youngest and best-preserved structures. D= final crater diameter; dt= true depth of the final crater; da= apparent depth of the crater (from French 1998, his Fig.3.7).

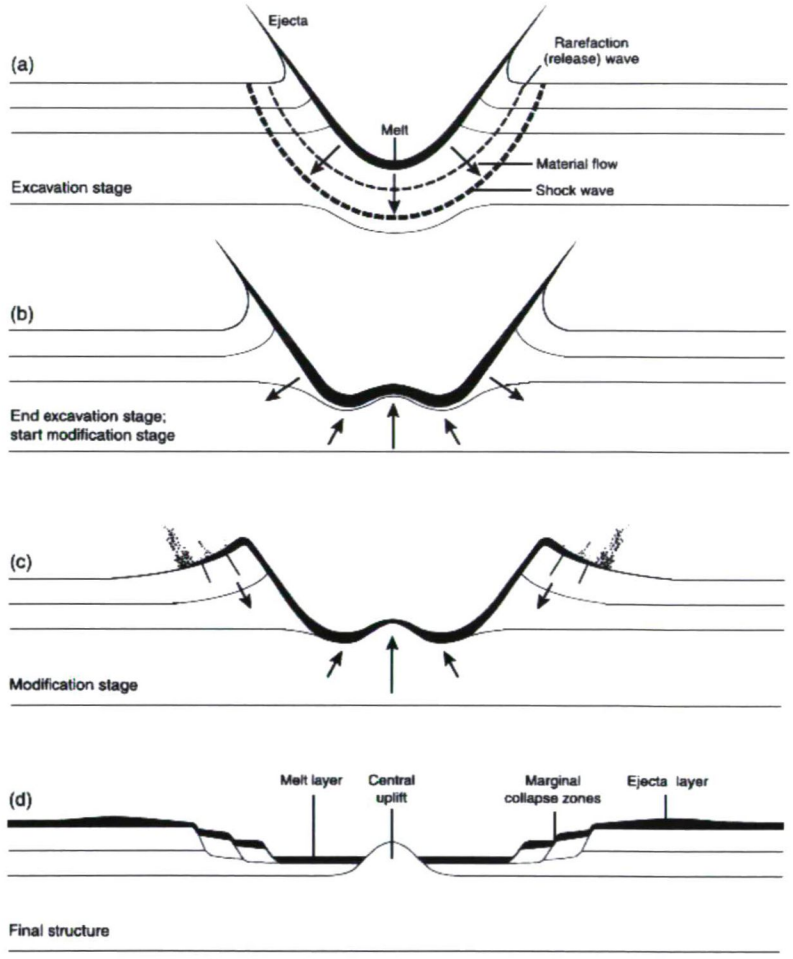

Fig. 8. Stages of progressive development of a large, complex impact structure in a horizontal layered target: (a) formation of a large transient crater in the excavation stage; (b) initial development of central uplift during the modification stage; (c) start of peripheral collapse in the modification stage; (d) final structure showing a central uplifted area, which is surrounded by a relatively flat plain and by a terraced rim produced by inward movement along stepped normal faults. The central uplift is surrounded by an annular deposit of allogenic breccias and impact melt (black). An ejecta layer (stippled) covers the target rocks around the structure. (from French, 1998; his Fig.3.10).

buried by under roughly 1 km of Cenozoic sediments, which is located at the tip of the Yucatan Peninsula. The Kara Sea in Russia shows relics of a twin impact structure (71 Ma), Kara and Ust-Kara craters. The evidence for a Late Pliocene impact are described such as occurrence of microtektites and an iridium anomaly in abyssal sediments in an area of about 300 000 km^2 in the South Pacific (Eltanin Sea Mt.). However, the small-sized projectile (D= 0.5 km) probably did not reach the ocean floor (at a depth of ca. 5000 m). Craters on oceanic crust are unknown to date, reflecting not only the young mean age of the oceanic crust, but also our relatively poor knowledge of two thirds of the Earth's solid surface (Deutsch 1998).

LITHOLOGICAL INDICATORS OF IMPACT STRUCTURES

An impact event is a surface process that produces circular, shallow, rootless structures in contrast to volcanic processes (French 1998). The lithological indicators for an impact structure may be a layer of fragmental breccia, which is found as crater filling or overlying a possibly raised, partially brecciated, and up- or over-turned rim (Koeberl 1997).

Breccia types at impact structures

The impact-derived breccias contain shocked minerals, impact melts, and impact glasses in an impact crater (Stöffler and Grieve 1994, Koeberl 1997). The monomict and polymict breccias that formed during impact processes could be divided into three main types: (1) cataclastic (fragmental breccias), (2) suevitic (fragmental with a melt fragment component) breccias (Fig. 9), or (3) impact melt (melt breccia - i.e., melt in the matrix with a clastic component) breccias. The breccias can be allochthonous or autochthonous. Additionally, the basement rocks contain dikes of injected or locally formed fragmental or pseudotachylitic breccias (Reimold 1995). Whether all these breccia types are actually present at an impact crater depends on factors including the size of the crater, the composition of the target area (e.g., Kieffer and Simonds 1980), and the level of erosion (see Roddy et al. 1977, Hörz 1982, Grieve 1987 and references therein).

Complete melting

The target rocks undergo complete (bulk) melting to form impact melts at pressures in excess of about 60 GPa. The resulting melts are deposited as splash-form glass particles and "bombs" in suevitic breccias or as coherent impact melt body. The presence of inclusions of minerals, such as lechatelierite (monomineralic quartz melt that forms from pure quartz at temperatures of 1700°C), or baddeleyite (thermal decomposition product of zircon forming at a temperature of at least 1680°C), is associated with very high temperatures. Lechatelierite as a good indicator of meteorite impact origin is not found in any other natural rock, except in fulgurites, which form by fusion of soil or sand when lightning hits the ground (Stöffler and Langenhorst 1994, and references therein).

Impact glasses

Impact glasses are more commonly found at relatively young impact craters rather than at old impact structures, because glass is not stable over geological times. Such

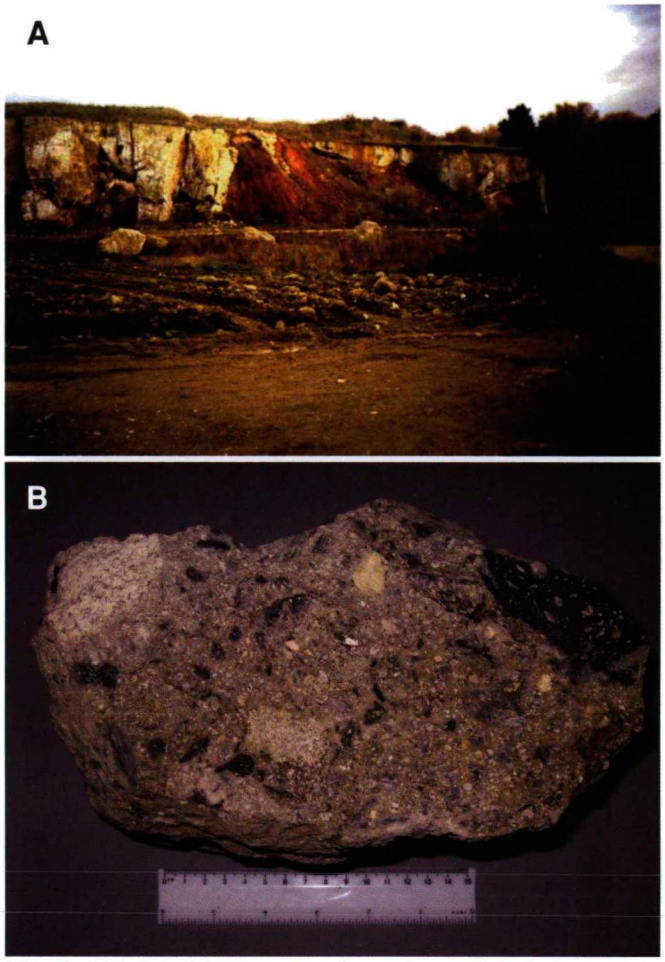

Fig. 9. (A) Aumühle quarry of suevite, which is located in the northwest of the Ries impact structure (Germany). This image shows a dark Jurassic clay and red clay and sandstones of the Keuperian. (B) Suevite: the elongated, grey parts of suevite are impact glasses (photos by author).

impact-derived glasses have chemical and isotopic compositions that are similar to those of the target rocks. The similarities in chemical and isotopic composition between impactites and crater target rocks have been employed in several source crater investigations (e.g., French et al. 1970, Blum et al. 1993, Meisel et al. 1995). Impact glasses have much lower water contents (about 0.001-0.05 weight %) than volcanic or other natural glasses (Koeberl 1992a). These impact melts and glasses are useful for the dating of an impact structure using K-Ar, ^{40}Ar-^{39}Ar, fission track, Rb-Sr, Sm-Nd, or U-Th-Pb isotope age-dating methods (Montanari and Koeberl 2000). The age that should be obtained for an impact event is different from that of volcanism because impact melts or glasses give a unique (local), much younger age as compared to the target rocks, which are usually old crustal rocks.

Tektites and microtektites

The centimeter-sized tektites as chemically homogeneous glasses have been ejected from a few terrestrial impact structures and spread over thousands of kilometers. They found on land and have been subdivided into three groups: (a) normal or splash-form tektites, (b) aerodynamically shaped tektites, and (c) Muong Nong-type tektites (or layered

tektites). Tektites can be associated with smaller (≤1 mm) microtektekties (Montanari and Koeberl 2000).

Currently, on the basis of differences in location, age, and to some extent, the characteristics of tektites and microtektites, four strewn fields are known: (1) Australasian (0.78 Ma, source crater no yet identified); (2) Central European (15 Ma) from the Ries Crater, Germany; (3) Ivory Coast (1.07 Ma) from the Bosumtwi Crater, Ghana (Koeberl et al. 1997a); and (4) North American (35 Ma) from the Chesapeake Bay impact structure, USA (Koeberl et al. 1997a) (Fig. 10).

Tektites are formed as the product of melting and quenching of terrestrial rocks during hypervelocity impact on the Earth (see Montanari and Koeberl 2000, for a recent review). Their chemical and isotopic compositions are identical with those of the target rocks where the impact occurred:

- Typically high in silica composition (>65 weight %), but their chemical and isotopic compositions are not volcanic, but closer to those of shales and similar sedimentary rocks. Containing low water content (≤0.02 wt %), and their flow-banded structure includes particles and bands of lechatelierite (monomineralic quartz melt).
- A few tektites contain partly melted inclusions of shocked and unshocked mineral grains (quartz, apatite, zircon) as well as coesite (Glass and Barlow 1979).

The Aouelloul crater is situated at 20°15'N and 12°41'W in the Ardar region, Western Sahara Desert, Mauritania (e.g., Koeberl 1994). The fission track and K-Ar dating of the impact glass show that this crater was formed 3.1 ± 0.3 Ma ago (Fudali and Cressy 1976, Storzer and Wagner 1977). The crater has a rim to rim diameter of 390 meters is exposed in an area of Ordovician Oujeft quartzite and Zli sandstone (Koeberl et al. 1998). Aouelloul impact glasses contain lechatelierite and baddeleyite (El Goresy 1965, El Goresy et al. 1968), , as well as partly digested quartz and feldspar grains, have a low water content (Beran and Koeberl 1997), and abundant schlieren of different chemical composition (Koeberl 1994). The composition of the glass is similar to that of the sandstone in which the crater is exposed, but some siderophile elements are enriched in the glass (Koeberl and Auer 1991). Re-Os isotope studies of the target sandstone and the impact glass were performed and demonstrated the presence of a distinct extraterrestrial component in the glass (Koeberl et al. 1998).

Muong Nong-type tektites are a subgroup of tektites that are abundant in the Australasian strewn field, These tektites differ in some characteristics from "normal" tektites: (1) they have higher concentrations of volatile elements (e.g., Cl, Br, Zn, Cu, Pb); (2) they are chemically inhomogeneous on a millimeter scale; (3) they contain dark and light layers with different chemical composition; (4) they may contain relict mineral inclusions (e.g., zircon, chromite, rutile, quartz, monazite) (e.g., Glass 1972, Deloule et al. 2001); (5) they contain large and more abundant bubbles that may be ellipsoidal, showing glass flow; (6) they have a large and irregular sample size with no sign of ablation (cf. Koeberl 1992b).

Libyan Desert Glass (LDG) is a natural glass found in an area of about 3500 km^2 between linear sand dunes of the southwestern corner of the Great Sand Sea in western Egypt, near the Libyan border. This glass occurs as fragments of a broad range of sizes (from centimeter -to decimeter-sized irregular and strongly wind-eroded blocks) (Barrat et al. 1997). In terms of chemical composition, LDG is very silica-rich (approximately 98 wt% of SiO_2 content) and has low abundances of most major oxides. The age of LDG was determined by fission-track analysis giving ages ranging from 28.5±2.3 Ma to 29.4±0.5 Ma (plateau age) (e.g., Bigazzi and de Michele 1996; Horn et al. 1997). The origin of LDG has been the subject of much debate since it was discovered early in the 20th century. Many workers were of the opinion that LDG is an impact glass, but were deterred by the lack of a suitable impact crater. Most researchers have now accepted the geochemical and geological evidence for an impact origin of LDG (McHone et al. 2000). Evidence for an impact origin includes the presence of lechatelierite (Diemer 1997), baddeleyite (Storzer and Koeberl 1991, Rocchia et al. 1997), and the likely existence of an extraterrestrial component in the glass (e.g., Rocchia et al. 1997, Murali et al. 1997). Previous cathodoluminescence data by Piacenza (1997) were interpreted to show evidence for a granular structure and the presence of lechatelierite. Cathodoluminescence microphotographs were used by Cipriani et al. (2000) in the determination of a possible extraterrestrial body signature in LDG. They concluded that the luminescence of Libyan Desert Glass is intrinsic, not induced by particle damage as in the case of amorphous silica.

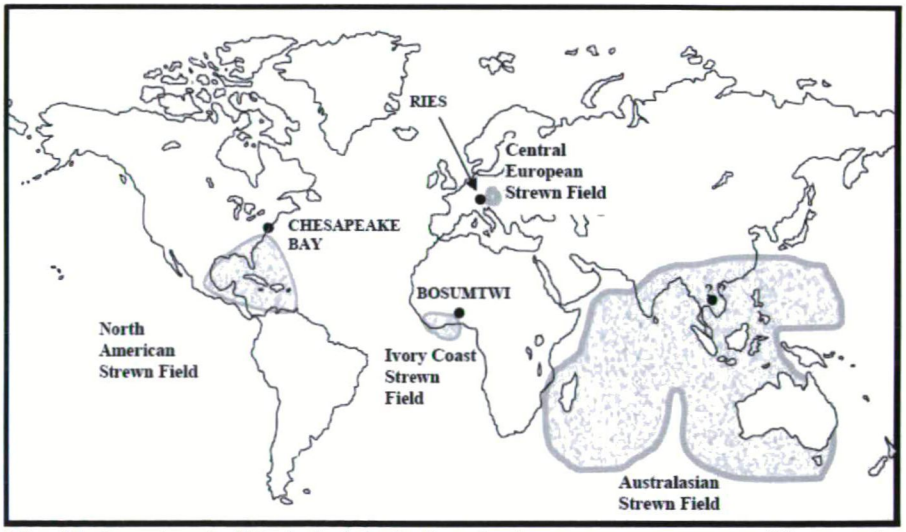

Fig. 10. Location (solid circles) including the known source craters (Chesapeake Bay, Ries, and Bosumtwi craters) and extension of the four tektite strewn fields, which were classified by differences in location, age, and to some extent, the characteristics of tektites and microtektites on Earth (after Montanari and Koeberl 2000, their Fig. 2.4.1.1).

DIAGNOSTIC SHOCK FEATURES IN IMPACT CRATERS

The best diagnostic indicators for shock metamorphism are features that can be studied easily by using the polarizing microscope. They include planar microdeformation features; optical mosaicism; changes in refractive index, birefringence and optical axis angle; isotropization; and phase changes (Stöffler 1972, 1974, Stöffler and Langenhorst 1994, Grieve et al. 1996, Koeberl 1997).

Shatter cones

Shatter cones (Fig. 11) are regarded as the only distinctive and unique shock deformation feature that develops on a macroscopic scale as hand specimen (Dietz 1968, French 1998). They are distinctive conical fractures produced in target rocks by shock waves of relatively low intensity, usually below the crater floor or in the central uplifts of large structures. They form in all kinds of target rocks subjected to the appropriate pressures, but they are most strikingly developed in fine-grained rocks, especially carbonates. Shatter cones can be distinguished from similar deformation features by the distinctive radiating striations ("horsetailing") along the cone surface, and by the fact that the cones originally point in the direction of the source of the shock wave, i.e., inward and upward. They develop in a large volume of target rock and have been widely used to identify terrestrial impact structure. Shatter cones are good diagnostic structural criteria that are easy to recognize and are found in many terrestrial impact structures.

The formation mechanism for shatter cones is poorly understood. The conical shapes might be related to the interactions of shock waves with point inhomogeneites in rocks, or interactions between the main compressive shock and rebound waves (Gash 1971). However, these models do not explain the dominant features of shatter cones such as characteristic striations, the "horse-tail" cone hierarchy, and the variety of complete cones. More recently, Shagy at al. (2002) have shown that the shatter cones are branched tensile fractures. Shatter-cone striations are the preserved tracks of fracture front waves. Their analysis of the striations shows that shatter cones develop only at extreme propagation velocities, between $0.9V_R$ and the maximal permitted velocity of V_R. The angles of the striations (α), which are shown to increase systematically with the distance from the impact, reflect both the stresses and the energy flux driving the fracture at a given site, and may be used as a general tool to evaluate extreme local stresses in the field (Shagy et al. 2002).

Fig. 11. Well-developed finely sculptured shatter cone, in fine-grained Ordovician limestone from the Charlevoix impact crater, Canada (photo by the author).

Mosaicism

The term mosaicism describes the internal fragmentation of a single crystal into a mosaic of slightly disoriented crystal domains. Mosaicism is a microscopic expression of shock metamorphism observed in a number of rock-forming minerals (see, e.g., Hörz and Quaide 1973) and appears as an irregular, mottled optical extinction pattern. This is distinctly different from the undulatory extinction that occurs in tectonically deformed quartz and, generally, accompanied in many minerals by indications of plastic deformation structures or deformation bands (Stöffler 1972). Mosaicism can be semi-quantitatively investigated by X-ray diffraction.

Kink Bands

Kink bands appear in sheet silicates, other sheet-like structures in shocked quartz and feldspar (Bunch 1968). They are not oriented parallel to rational crystallographic planes and display variable disorientation with respect to the host lattice compared to the deformation twins. Kink banding is considered as supporting evidence for the impact origin of

Table 4. Characteristics of planar fractures and planar deformation features in quartz. Data from Stöffler and Langenhorst (1994).

Nomenclature	1. Planar fractures (PF) 2. Planar deformation features (PDF) 2.1. Nondecorated PDFs 2.2. Decorated PDFs
Crystallographic orientation	1. PFs: usually parallel to $(00\bar{1}1)$ and $\{10\bar{1}1\}$ 2. PDFs: usually parallel to $\{10\bar{1}3\}$,$\{10\bar{1}2\}$, $\{10\bar{1}1\}$, (0001), $\{11\bar{2}2\}$, $\{11\bar{2}1\}$, $\{10\bar{1}0\}$, $\{11\bar{2}0\}$, $\{21\bar{3}1\}$, $\{51\bar{6}1\}$, etc.
Optical microscope properties	Multiple sets of PFs or PDFs (up to 15 orientations per grain) Thickness of PDFs: <2-3 μm Spacing: >15 μm (PFs), 2-10 μm (PDFs)
TEM properties (PDFs)	Two types of primary lamellae are observed: 1. Amorphous lamellae with a thickness of about 30 nm (at pressures of <25 GPa) and about 200 nm (at pressures of >25 GPa) 2. Brazil twin lamellae parallel to (0001)

a structure, but it cannot be used as a single diagnostic criterion, as it occurs also in metamorphic rocks.

Planar microstructures

Two types of planar microstructures are apparent in shocked minerals: planar fractures (PFs) and planar deformation features (PDFs). Their essential characteristics are summarized in Table 4. The PDFs occur as either non-decorated or decorated PDFs (Stöffler and Langenhorst 1994). Planar deformation features in rock-forming minerals (e.g., quartz, feldspar, or olivine) are generally accepted to provide diagnostic evidence for shock deformation (see, e.g., French and Short 1968, Stöffler and Langenhorst 1994, Grieve et al. 1996, French 1998, and references therein).

Planar Fractures (PF)

Planar fractures are parallel sets of multiple planar cracks or cleavages in quartz grains; they develop at the lowest pressures characteristic of shock waves (~5-8 GPa) (French, 1998). As French (1998) noted, they are parallel to rational crystallographic planes with low Miller indices, such as (0001) and $\{10\bar{1}1\}$. The fractures are typically 5-10 μm wide and spaced 15-20 μm or more apart in individual quartz grains. Similar cleavage occurs also rarely in quartz from non-impact settings, and therefore planar fractures cannot be used independently as a single criterion for meteorite impact. However, the development of intense, widespread, and closely spaced planar fractures are frequently accompanied in impact structures by other features clearly formed at higher shock pressures (French 1998, and references therein). Planar deformation features, together with the somewhat less specific planar fractures (PFs) (Fig. 12), are usually well developed in quartz (Stöffler and Langenhorst 1994).

Planar Deformation Features (PDFs)

PDFs in various minerals (especially in quartz) have long been known as evidence of impact-induced deformation. In contrast to planar fractures, PDFs are not open cracks. They occur as multiple sets of more closely spaced (typically 2-10 μm), narrow (typically <2-3 μm), parallel planar regions than planar fractures (Fig. 13). PDFs occur in planes corresponding to specific rational crystallographic orientations. The basal (0001) or c, $\{10\bar{1}3\}$ or ω, and $\{10\bar{1}2\}$ or π, orientations are the most common planes in quartz. In addition, PDFs often occur in more than one crystallographic orientation per grain. At pressures about ≥35 GPa, the distances between the planes decrease, and the PDFs become more closely spaced and more homogeneously distributed over the grain. Depending on the peak pressure, PDFs are observed in 2 to 10 (maximum 18) orientations per grain (Robertson et al. 1968, Stöffler 1972, Stöffler and Langenhorst 1994, Grieve et al. 1996, Koeberl 1997). To properly characterize PDFs, it is necessary to measure their crystallographic orientations optically by using either a universal stage (Emmons 1943) or a spindle stage (Medenbach 1985), or by transmission electron microscopy (see, e.g., Goltrant et al. 1991, Leroux et al. 1994).

The formation mechanisms of these features in naturally shocked quartz might be explained by the pressure dependence of the shear modulus (decreasing linearly with increasing pressure and, for some planes even discontinuously, for a critical pressure of the order of 10 GPa) of quartz for various planes and directions. The Si-O-Si bonds are more easily broken, allowing the corresponding atoms to move towards energetically more favourable positions. This progressive reorganization leads to the formation of a new structure (dense amorphous silica lamellae). The transformation occurs very rapidly, as it is

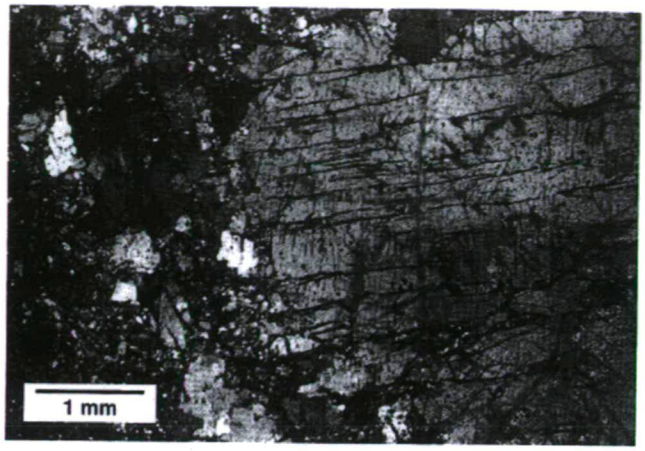

Fig. 12. A quartz grain from metamorphosed orthoquartzite target from the Gardnos impact structure (Norway) exhibits numerous subparallel palanar fractures (longer, dark, subhorizontal lines) and much shorter planar features (short, dark, near-vertical lines). These latter features may be relicts of true PDFs or of Brazil twins parallel to the base (0001) (from French 1998, his Fig. 4.15).

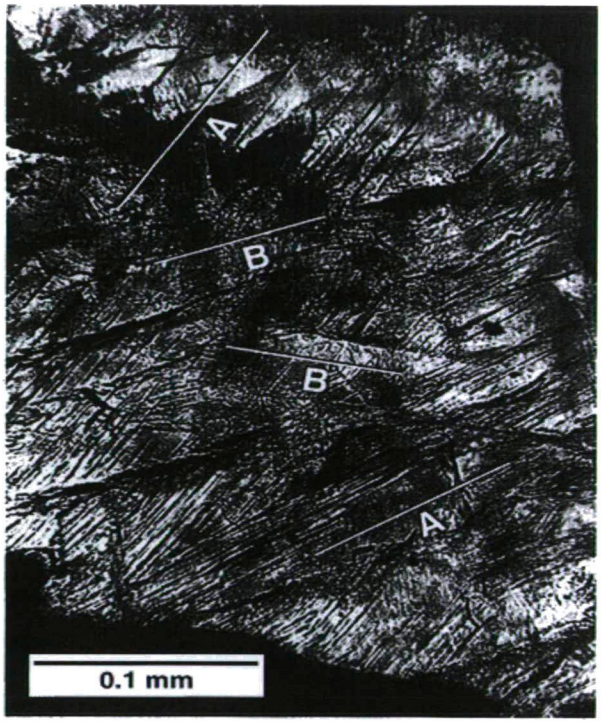

Fig. 13. Multiple sets of PDFs developed in a quartz grain from a shocked granite inclusion in suevite from the Ries Crater (Germany). "A" indicates PDFs parallel to $\{10\bar{1}3\}$ identical $\{01\bar{1}3\}$; "B" indicates PDFs parallel to $\{10\bar{1}1\}$ identical $\{01\bar{1}1\}$. Note the irregular extinction within the quartz grain (from French, 1998; his Fig. 4.16).

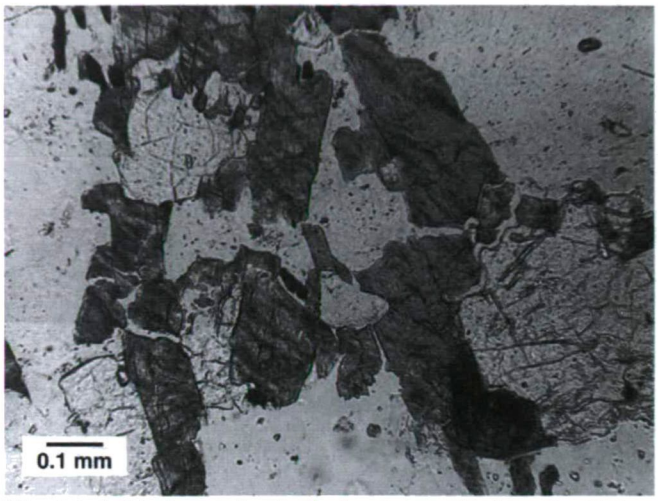

Fig. 14. A biotite gneiss inclusion in suevite breccia, Otting, Ries Crater (Germany) contains diaplectic feldspar glass (maskelynite) (clear, low relief; e.g., upper right) and diaplectic quartz glass (clear, higher relief, e.g., lower right). The associated biotite crystals (dark) have retained their original shape and have remained crystalline and birefrigent, despite the complete transformation of adjacent quartz and plagioclase into glassy phases. Biotite gneiss (from French 1998, his Fig. 4.32).

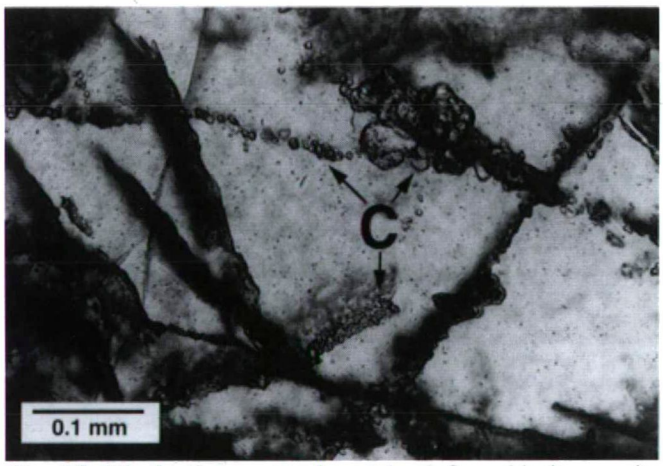

Fig. 15. Diaplectic quartz glass (clear) from biotite granite inclusion in suevite breccia, Aufhausen, Ries Crater (Germany) appears, with strings of small, high-relief crystals of coesite ("C") (from French 1998, his Fig. 4.12).

driven by the front of the shock wave. This explanation predicts that the density of PDFs should markedly increase with shock intensity (Goltrant et al. 1992).

DIAPLECTIC GLASS, LECHATELIERITE AND HIGH-PRESSURE POLYMORPHS

Diaplectic glass

Diaplectic glass is formed (Tables 1 and 2) at shock pressures in excess of about 35 GPa without melting by solid-state transformation and has been described as a phase intermediate between crystalline and normal glassy phases (Stöffler and Hornemann 1972). It is found at numerous impact craters and shows the original crystal defects, planar features, and absence of flow structures and vesicles. Maskelynite is a diaplectic plagioclase glass formed in a similar way and at similar pressure range as diaplectic quartz glass. Diaplectic glass has a refractive index that is slightly lower than that of synthetic quartz glass (Fig. 14). Other minerals (mafics) tend to oxidize or decompose.

Lechatelierite

At pressures that exceed about 50 GPa, lechatelierite forms by fusion of quartz. In contrast to diaplectic glass, lechatelierite is formed by a liquid state transformation associated with the melting of quartz at higher temperatures (>1700°C) than occur in volcanic processes. This is a good indicator of a meteorite impact origin. Other minerals also melt at sufficiently high temperatures, e.g., feldspar (Stöffler and Langenhorst 1994).

High-pressure polymorphs

The high-pressure SiO_2 polymorphs, coesite (Fig. 15) and stishovite, occur as very fine-grained aggregates that are formed by partial transformation of the host quartz during shock metamorphism (Grieve et al. 1996). Under conditions of static equilibrium, where reaction rates are slower and kinetic factors less important, coesite forms from quartz at lower pressures (>2 GPa) than does stishovite (10-15 GPa) (French 1998). The identification of coesite and stishovite at several impact sites in the early 1960s provided one of the earliest criteria for establishing the impact origin of several structures, most notably the Ries crater, Germany (Chao et al. 1960, Shoemaker and Chao 1961), and the Bosumtwi crater (Littler et al. 1961). Impact-derived coesite occurs as very fine-grained, colorless to brownish, polycrystalline aggregates, up to 100-200 μm in size, usually embedded in diaplectic quartz glass, or rarely, in nearly isotropic quartz with abundant planar deformation features and a mean refractive index below 1.48 (Stöffler and Langenhorst 1994) (Fig. 15). Coesite occurs also in metamorphic rocks of ultra-high pressure origin.

Other high-pressure mineral phases include jadeite formed from plagioclase, majorite from pyroxene, and ringwoodite from olivine (Stöffler 1972). Impact derived diamonds (the high-pressure cubic modification of carbon) have also been found at various craters. These diamonds form from carbon in the target rocks, mainly in graphite-bearing (e.g., graphitic gneiss) or coal-bearing rocks (Koeberl et al. 1997b).

A new mineralogical indicator of shock metamorphism: zircon

Zircon is a refractory and weathering-resistant mineral that has been proven useful as an indicator of shock metamorphism in the study of impact structures and formations that are old, deeply eroded, and metamorphically overprinted. Thus, it has advantages compared to quartz or other shock-metamorphosed minerals that have been previously used as impact indicators, but are far less refractory than zircon.

Shock-induced microdeformation in zircon has been described in samples from a variety of impact environments, including material from confirmed impact structures (Åberg and Bollmark (1985), Bohor et al. (1993), Krogh et al. (1984), Wittmann et al. (2006) from the Cretaceous-Tertiary boundary, and from the Upper Eocene impact ejecta layer Bohor et al. (1993), Kamo and Krogh (1995), Glass and Liu

(2001), as well as in experimentally shock-deformed single-crystal zircon (Deutsch and Schärer 1990, Leroux et al. 1999, Gucsik et al. 2002). Two different types of shock deformation have been observed: (i) planar microdeformations and (ii) granular (also called polycrystalline, microcrystalline, *strawberry*) texture. Some effort, especially by transmission electron microscopy (TEM), has been made to determine whether the planar microdeformations discernable at the optical scale in shock-metamorphosed zircon represent *bona fide* planar deformation features (PDFs), well-known from many other shock-metamorphosed rock-forming minerals French (1998), Stöffler and Langenhorst (1994) Grieve et al. (1996), or whether they represent planar fractures or some other type of microdeformation (Reimold et al. 2002). To date, this problem has not been solved. Leroux et al. (1999) established that, on a nanometer scale, amorphous phases in the form of planar lamellae were formed in experimentally shocked zircon (pressure range: 20-40 GPa). However, these authors were not able to confirm that these micro-lamellae, resembling PDFs, indeed corresponded to the optically resolved, several μm wide, planar/subplanar microdeformations.

The granular texture of zircon was first observed by Bohor et al. (1993) in zircon from the Cretaceous/Tertiary distal impact ejecta layer. Since then, it has been observed in zircon from a number of impact structures (Kamo et al. 1996 and references therein), in zircon from a Late Eocene microkrystite layer, and in tektites (Glass and Liu 2001, Deloule et al. 2001). Complete breakdown of zircon to baddeleyite, presumably as a result of high-temperature dissociation, has been identified in Libyan Desert Glass and corroborated the impact origin of these enigmatic glasses Kleinmann (1969).

Leroux et al. (1999) confirmed through their TEM investigations of experimentally shocked zircon that the phase transformation from the zircon structure to a scheelite ($CaWO_4$)-type phase that had been previously observed in shock-metamorphosed zircon by Kusaba et al. (1985) was nearly complete at 60 GPa shock pressure. In the 60 GPa samples of Leroux et al. (1999) shock deformation effects (nanometer-sized PDFs) were observed in a few relict domains consisting of zircon. More recently, new techniques and methodologies such as SEM, CL, micro-Raman and IR have been applied to identify reidite from shocked zircon samples of shock recovery experiments and naturally shock-metamorphosed samples from Ries impact structure (Gucsik et al. 2004).

Shocked clay minerals

Clay minerals have been found from different shock metamorphic environments such as Cretaceous/Tertiary Boundary layers (Pollastro and Bohor 1993, Salge et al. 2000), terrestrial impact structures (Dypvik and Ferrell 1998, Krisimäe et al. 2002, Dypvik et al. 2003, Uysal et al. 2003, Horton et al. 2006), and meteorites (Scott and Krott 1998).

In a pioneering study, shocked clay samples from a Barents Sea borehole near the Mjølnir Impact Structure were used to investigate changes in the clay assemblage associated with the submarine impact (Dypvik and Ferrell 1998). They found increased abundance of a smectite, a randomly interstratified smectite-illite with 85% smectite layers, forms the basis for a two-layer oceanic impact clay model that differs from published terrestrial cases. The smectite is assumed to represent seawater-altered impact glass from the ejecta blanket material that was mixed with resuspended shelf sediments by the collision generated waves. The smectite-rich interval is overlained by a coarser unit containing abundant smectite, shocked quartz grains, and anomalous Ir contents at its base. This interval may have originated as a density/turbidity current, generated by the impact and the collapse and erosion of the crater rim.

More recently, clay minerals were described from shocked granitoid basement rocks of Woodleigh impact structure (Australia), which are mainly smectite-rich (>75%) mixed-layer illite-smectite with some discrete illite formed as an alteration-product (replacement) of biotite (Uysal et al. 2003). They concluded that these clay minerals formed by post-shock hydrothermal alteration processes.

ACKNOWLEDGEMENTS

As this study was a part of my Ph.D. thesis, I would like to express thank to Profs. Christian Koeberl, Eugen Libowitzky, Uwe Reimold, and Franz Brandstätter supervising my Ph.D. studies at the University of Vienna, Austria.

REFERENCES

ÅBERG, G., BOLLMARK, B. (1985): Retention of U and Pb in zircons from shocked granite in the Siljan impact structure, Sweden. Earth and Planetary Science Letters, **74**, 347–49.

BARRAT.A., JAHN, B.M., AMOSSE, J., ROCCHIA, R., KELLER, F., POUPEAU, G.R., DIEMER, E. (1997): Geochemistry and origin of Libyan Desert glasses. Geochimica et Cosmochimica Acta, **61**, 1953–959.

BERAN, A. KOEBERL, C. (1997) Water in tektites and impact glasses by FTIR spectrometry. Meteoritics and Planetary Science, **32**, 211–16.

BIGAZZI, G., DE MICHELE, V. (1996): New fission-track age determination on impact glasses. Meteoritics and Planetary Science, **31**, 234–36.

BLUM, J.D., CHAMBERLAIN, C.P., HINGSTON, M.P, KOEBERL, C., MARIN, L.E., SCHURAYTZ, B.C., SHARPTON, V.L. (1993): Isotopic comparison of K-T boundary impact glass with melt rock from the Chicxulub and Manson impact structures. Nature, **364**, 325–327.

BOHOR, B. F., BETTERTON, W. J., KROGH, T. E. (1993): Impact-shocked zircons: discovery of shock-induced textures reflecting increasing degrees of shock metamorphism. Earth and Planetary Science Letters, **119**, 419–424.

BUNCH, T.E. (1968): Some characteristics of selected minerals from craters. In: French, B.M., Short, N.M. (Eds.), Shock metamorphism of natural materials. Mono Book Corporation, Baltimore, 413–432.

CHAO, E.C.T., SHOEMAKER, E.M., MADSEN, B.M. (1960): First natural occurrence of coesite. Science, **132**, 220–222.

CIPRIANI, C., CORAZZA, M., GIULI, G., CECCHI, V. N., PRATESI, G., ROSSI, P., VITTONE, E. (2000): Ion beam study of a possible extraterrestrial body signature in Lybian desert glass. Nuclear Instruments and Methods in Physical Research B, **170**, 187–192.

DELOULE, E., CHAUSSIDON, M., GLASS, B.P., KOEBERL, C. (2001): U-Pb isotopic study of relict zircon inclusions recovered from Muong Nong-type tektite. Geochimica et Cosmochimica Acta, 65, 1833-1838.

DENCE, M. R. (1972): The nature and significance of terrestrial impact structures. 24th International Geological Congress, Montreal, Canada. Proceedings Section, **15**, 77–89.

DEUTSCH, A. (1998): Examples for terrestrial impact structures. In: MARFUNIN, S.A. (Ed.), Mineral matter in space, mantle, ocean floor, biosphere, environmental management, and jewelry. Springer-Verlag, Berlin, Heidelberg, Advanced Mineralogy, **3**, 119–129.

DEUTSCH, A., SCHARER, U. (1990): Isotope systematics and shock-wave metamorphism: I. U-Pb in zircon, titanite, and monazite, shocked experimentally up to 59 GPa, Geochimica and Cosmochimica Acta, **54**, 3427–3434.

DIEMER, E. (1997): Libyan Desert Glass: an impactite. State of the art in July 1996. In: de Michelle V. (ed.), Silica '96 Proceedings of Meeting on Libyan Desert Glass and related events: Milan, Italy, Pyramids, 29–36.

DIETZ, R.S. (1968): Shatter cones in cryptoexplosion structures. In: FRENCH, B.M., SHORT, N.M. (Eds.), Shock metamorphism of natural materials. Mono Book Corporation, Baltimore, 267–285.

DYPVIK, H., FERREL, R.E. (1998): Clay mineral alteration associated with meteorite impact in the marine environment (Barents Sea). Clay Minerals, **33**, 51–64.

DYPVIK, H., FERREL, R.E., SANDBAKKEN, P.T. (2003): The clay mineralogy of sediments relate to the marine Mjolnir impact crater. Meteoritics and Planetary Science, **38**, 1437–1450.

EL GORESY, A. (1965): Baddeleyite and its significance in impact glasses. Journal of Geophysical Research, **70**, 3453–3456.

EL GORESY, A., FECHTIG, H., OTTEMANN, T. (1968): The opaque minerals in impactite glasses. In: French, B.M., Short, N.M. (Eds.), Shock Metamorphism of Natural Materials, Mono Book Co., Baltimore, Maryland, USA, 531–553.

EMMONS, R.C. (1943): The Universal Stage (With Five Axes of Rotation). Geological Society of America Memoir, **8**, 205.

FRENCH, B.M. (1998): Traces of Catastrophe: A Handbook of Shock-Metamorphic Effects in Terrestrial Meteorite Impact Structures. LPI Contribution No. 954, Lunar and Planetary Institute, Houston, 120.

FRENCH, B.M., SHORT, N. M., (Eds) (1968): Shock metamorphism of natural materials. Mono Book Corporation, Baltimore, 644 pp.

FRENCH, B.M., HARTUNG, J.B., SHORT, N.M., DIETZ, R. S. (1970): Tenoumer crater, Mauritania: Age and petrologic evidence for origin by meteorite impact. Journal of Geophysical Research, **75**, 4396–4406.

FUDALI, R.F., CRESSY, P.J. (1976): Investigation of a new stony meteorite from Mauritania with some additional data on its find site: Aouelloul crater. Earth and Planetary Science Letters, **30**, 262–268.

GASH, P.J.S. (1971): Dynamic mechanism for the formation of shatter cones. Nature, **230**, 32–35.

GAULT, D.E., QUAIDE, W.L., OBERBECK, V.R. (1968): Impact cratering mechanics and structures. In: French, B.M., Short, N.M. (Eds.), Shock Metamorphism of Natural Materials. Mono Book Corporation, Baltimore, 87–99.

GLASS, B.P. (1972): Crystalline inclusions in a Muong Nong-type indochinite. Earth and Planetary Science Letters, **16**, 23–26.

GLASS, B.P., LIU, S. (2001): Discovery of high-pressure $ZrSiO_4$ polymorph in naturally occurring shock-metamorphosed zircons. Geology, **29**, 371–373.

GLASS, B.P., BARLOW, R.A. (1979): Mineral inclusions in Muong Nong-type indochinites: Implications concerning parent material and process of formation. Meteoritics, **14**, 55–67.

GOLTRANT, O., LEROUX, H., DOUKHAN J.-C., CORDIER, P. (1992): Formation mechanism of planar deformation features in naturally shocked quartz. Physics of the Earth Planetary Interiors, **74**, 219–240.

GOLTRANT, O., CORDIER, P., DOUKHAN, J.C. (1991): Planar deformation features in shocked quartz: a transmission electron microscopy investigation. Earth and Planetary Science Letters, **106**, 103–115.

GRIEVE, R.A.F. (1991): Terrestrial impact: The record in the rocks. Meteoritics, **26**, 175–194.

GRIEVE, R.A.F. (1987): Terrestrial impact structures. Annual Reviews of Earth and Planetary Science, **15**, 245–270.

GRIEVE, R.A.F., LANGENHORST, F., STÖFFLER, D. (1996): Shock metamorphism of quartz in nature and experiment: II. Significance in geoscience. Meteoritics and Planetary Science, **31**, 6–35.

GUCSIK, A., KOEBERL, C., BRANDSTATTER, F., LIBOWITZKY, E., REIMOLD, W.U. (2004): Cathodoluminescence, electron microscopy, and Raman spectroscopy of experimentally shock metamorphosed zircon crystals and naturally shocked zircon from the Ries impact crater. In Dypvik, H., Burchell, M., Claeys, PH. (eds.): Cratering in Marine Environments and on Ice, Springer-Verlag, Heidelberg, 281–322.

GUCSIK A., KOEBERL, C., BRANDSTATTER, F., REIMOLD, W.U., LIBOWITZKY, E. (2002): Cathodoluminescence, electron microscopy, and Raman spectroscopy of experimentally shock-metamorphosed zircon. Earth and Planetary Science Letters, **202**, 495–509.

HORN, P., MÜLLER-SOHNIUS, D., SCHAAF, P., KLEINMANN, B., STORZER, D. (1997): Potassium-argon and fission-track dating of Lybian Desert Glass, and strontium and neodymium isotope constraints on its source rocks. In: de MICHELE, V. (Ed.), Proceedings of Meeting on Libyan Desert Glass and related events: Milan, Italy, Pyramids, 59–73.

HORTON, W.J, JR., VANKO, D.A., NAESER, CH.W. (2006): Postimpact hydrothermal conditions at the central uplift, Chesapeake Bay impact structure, Virginia, USA. 38th Lunar and Planetary Science Conference, #1642.

HÖRZ, F. (1982): Ejecta of the Ries crater, Germany. In: SILVER, L. T., SCHULTZ, P. H. (Eds.), Geological implications of impacts of large asteroids and comets on the Earth. Geological Society of America Special Paper, **190**, 39–55.

HÖRZ, F., QUAIDE, W.L. (1973): Debye-Scherrer investigations of experimentally shocked silicates. The Moon, **6**, 45–82.

KAMO, S.L., KROGH, T.E. (1995): Chicxulub crater source for shocked zircon crystals from the Cretaceous-Tertiary boundary layer, Saskatchewan: Evidence from new U-Pb Data. Geology, **23**, 281–284.

KAMO, S.L., REIMOLD, W.U., KROGH, T.E., COLLISTON, W.P. (1996): A 2.023 Ga age for the Vredefort impact event and first report of shock metamorphosed zircons in pseudotachylitic breccias and Granophyre. Earth and Planetary Science Letters, **144**, 369–387.

KIEFFER, S.W., SIMONDS, C.H. (1980): The role of volatiles and lithology in the impact cratering process. Reviews of Geophysics and Space Physics, **18**, 143–181.

KLEINMANN, B. (1969): The breakdown of zircon observed in the Libyan Desert Glass as evidence of its impact origin. Earth and Planetary Science Letters, **5**, 497–501.

KOEBERL, C. (1997): Impact cratering: the mineralogical and geochemical evidence. In: Johnson, K.S., Campbell, J.A. (eds.),

Ames structure in northwest Oklahoma and similar features: origin and petroleum production (1995 symposium). Oklahoma Geological Survey Circular, **100**, 30–54.

KOEBERL, C. (1994): African meteorite impact craters: Characteristics and geological importance. Journal of African Earth Sciences, **18**, 263–295.

KOEBERL, C. (1992a): Water content of glasses from the K/T boundary, Haiti: indicative of impact origin. Geochimica et Cosmochimica Acta, **56**, 4329–332.

KOEBERL, C. (1992b): Geochemistry and origin of Muong Nong-type tektites. Geochimica and Cosmochimica Acta **56**, 1033–1064.

KOEBERL, C., AUER, P. (1991): Geochemistry of impact glass from the Aouelloul crater, Mauritania. 22nd Lunar and Planetary Science Conference, 731–732.

KOEBERL, C., REIMOLD, W.U., SHIREY, S.B. (1998): The Aouelloul crater, Mauritania: On the problem of confirming the impact origin of a small crater. Meteoritics and Planetary Science, **33**, 513–517.

KOEBERL, C., BOTTOMLEY, R., GLASS B.P., STORZER, D. (1997a): Geochemistry and age of Ivory Coast tektites and microtektites. Geochimica et Cosmochimica Acta, **61**, 1745–1772.

KOEBERL, C., MASAITIS, V.L., SHAFRANOVSKY, G.I., GILMOUR, I., LANGENHORST, F., SCHRAUDER, M. (1997b): Diamonds from the Popigai impact structure, Russia. Geology, **25**, 967–970.

KUSABA K., SYONO Y., KIKUCHI M., FUKUOKA K. (1985) Shock behaviour of zircon: phase transition to scheelite structure and decomposition. Earth and Planetary Science Letters, **72**, 433–439.

KRISIMAE, K., SUUROJA, S., KIRS, J., KARKI, A., POLIKARPUS, M., PUURA, V., SUUROJA, K. (2002): Hornblende alteration and fluid inclusions in Kardla impact crater, Estonia: evidence for impact-induced hydrothermal activity. Meteoritics and Planetary Science, **37**, 449–457.

KROGH, T.E., DAVIS, W.D., CORFU, F. (1984): Precise U-Pb zircon and baddeleyite ages for the Sudbury area. In: Pye, E.G., Naldrett, P.E., Giblin, P.E. (eds.), The Geology and Ontario Geolological Survey Special Paper, **1**, 431–446.

LEROUX H., REIMOLD W.U., KOEBERL C., HORNEMANN U., DOUKHAN J.-C. 1999. Experimental shock deformation in zircon: a transmission electron microscopic study. Earth and Planetary Science Letters, **169**, 291–301.

LEROUX, H., REIMOLD, W.U., DOUKHAN, J.C. (1994): A T.E.M. investigation of shock metamorphism in quartz from the Vredefort dome, South Africa. Tectonophysics, **230**, 223–239.

LITTLER, J., FAHEY, J.J., DIETZ, R.S., CHAO, E.C.T. (1961): Coesite from the Lake Bosumtwi crater, Ashanti, Ghana. Geological Society of America Special Paper, **68**, 218.

MARTINEZ, I., AGRINIER, P. (1998): Meteorite impact craters on Earth: major shock induced effects in rocks and minerals. Earth and Planetary Sciences, **327**, 75–86.

MARTINEZ, I., DEUTSCH, A., SCHARER, U., ILDEFONSE, P., GUYOT, F., AGRINIER, P. (1995): Shock recovery experiments on dolomite and thermodynamical calculations of impact induced decarbonation. Journal of Geophysical Research, **100**, 15,465–15,476.

MCHONE, J.F., KILLGORE, M., KUDRYAVTSEV, A. (2000): Cristobalite inclusions in Libyan Desert Glass: confirmation using Raman spectroscopy. 31st Lunar and Planetary Science Conference, #1877.

MEDENBACH, O. (1985): A new microrefractometer spindle stage and its application. Fortschritte der Mineralogie, **63**, 111–133.

MEISEL, T., KRAHENBÜHL, U., NAZAROV, M.A. (1995): Combined osmium and strontium isotopic study of the Cretaceous-Tertiary boundary at Sumbar, Turkmenistan: A test for an impact vs. volcanic hypothesis. Geology, **23**, 313–316.

MELOSH, H.J. (1992): Impact crater geology. In: Nierenberg, W.A. (Ed.), Encyclopedia of Earth System Science 2. Academic Press, San Diego, 591–605.

MELOSH, H.J. (1989): Impact Cratering: A geologic process. Oxford University Press, New York, 245.

MONTANARI, A., KOEBERL, C. (2000): Impact Stratigraphy: The Italian Record. Lecture Notes in Earth Sciences 93, Springer, Heidelberg, 364.

MURALI, A.V., ZOLENSKY, M.E., UNDEWOOD, J.R., JR., GIEGENGACK, R.F. (1997): Chondritic debris in Libyan Desert Glass. In: de Michelle V. (Ed.), Proceedings of Meeting on Libyan Desert Glass and related events: Milan, Italy, Pyramids, 133–142.

PIAZENZA, B. (1997): Evidence of granular structure of Libyan Desert Silica Glass by SEM cathodoluminescence. In: de Michelle V. (Ed.), Proceedings of Meeting on Libyan Desert Glass and related events: Milan, Italy, Pyramids, 85–90.

POLLASTRO, R. M., BOHOR, B.F. (1993): Origin and clay-mineral genesis of the Cretaceous/Tertiary Boundary Unit, Western Interior of North America. Clays and Clay Minerals, **41**, 7–25.

REIMOLD, W.U. (1995): Pseudotachylite in impact structures – generation by friction melting and shock brecciation?: A review and discussion. Earth Science Reviews, **39**, 247–265.

REIMOLD, W.U., LEROUX, H., GIBSON, R.L. (2002): Shocked and thermally metamorphosed zircon from the Vredefort impact structure, South Africa: A transmission electron microscopic study. European Journal of Mineralogy, **14**, 859–868.

ROCCHIA, R., ROBIN, E., FRÖCHLICH F., AMOSE, J., BARRAT, J-A., MEON, H., FROGET, L., DIEMER, E., (1997): The impact origin of Libyan Desert Glass. In: de Michele, V. (Ed.), Proceedings of Meeting on Libyan Desert Glass and related events: Milan, Italy, Pyramids, 143–149.

RODDY, D.J., PEPIN, R.O., MERRILL, R.B., (Eds.) (1977): Impact and explosion cratering. Pergamon Press, New York, 1301.

ROBERTSON, P.B., DENCE, M.R., VOS, M.A. (1968) : Deformation in rock-forming minerals from Canadian craters. In: French, B.M., Short, N.M., (Eds.) Shock metamorphism of natural materials. Mono Book Corporation, Baltimore, 433–452.

SALGE, T., TAGLE, R., CLAEYS, P. (2000): Accretionary lapilli from the K/T Boundary site of Guayal, Mexico: Preliminary insights of expansion plume formation. 63rd Annual Meteoritical Society Meeting, #5124.

SCOTT, E.R.D., KROT, A.N. (1998): Formation of pre-impact interstitial carbonates in the ALH84001 Martian meteorite. 61st Annual Meteoritical Society Meeting, #5296.

SHAGY, A., RECHES, Z., FINEBERG, J., 2002. Dynamic fracture by large extraterrestrial impacts as the origin of shatter cones. Nature, **418**, 310–313.

SHARPTON, V.L., GRIEVE, R.A.F. (1990): Meteorite impact, cryptoexplosion, and shock metamorphism; A perspective on the evidence at the K/T boundary. Geological Society of America Special Paper, **247**, 301–318.

SHOEMAKER, E.M., CHAO, E.C.T. (1961): New evidence for the impact origin of the Ries Basin, Bavaria, Germany. Journal of Geophysical Research, **66**, 3371–3378.

STORZER, D., KOEBERL, C. (1991): Uranium and zirconium enrichments in Libyan Desert Glass. Zircon, baddeleyite and high-temperature history of the glass. 22nd Lunar and Planetary Science Conference, 1345–1346.

STORZER, D., WAGNER, G.A. (1977): Fission track dating of meteorite impacts. Meteoritics, **12**, 368.

STÖFFLER, D. (1974): Deformation and transformation of rock-forming minerals by natural and experimental processes: II. Physical properties of shocked minerals. Fortschritte der Mineralogie, **51**, 256–289.

STÖFFLER, D. (1972): Deformation and transformation of rock-forming minerals by natural and experimental shock processes: I. Behaviour of minerals under shock compression. Fortschritte der Mineralogie, **49**, 50–113.

STÖFFLER, D., GRIEVE, R.A.F. (1994): Classification and nomenclature of impact metamorphic rocks. 25th Lunar and Planetary Science Conference, 1347–1348.

STÖFFLER, D., LANGENHORST, F. (1994): Shock metamorphism of quartz in nature and experiment: I. Basic observation and theory. Meteoritics, **29**, 155–181.

STÖFFLER, D., HORNEMANN, U. (1972): Quartz and feldspar glasses produced by natural and experimental shock. Meteoritics, **7**, 371–394.

UYSAL, I.T., GOLDING, S.D., GLIKSON, A.Y., MORY, A.J., GLIKSON, M. (2003): K-Ar evidence from illitic clays of a Late Devonian age of the 120 km diameter Woodleigh impact structure, Southern Carnarvon Basin, Western Australia. Earth and Planetary Science Letters, **192**, 281–289.

WITTMANN, A., KENKMANN, T., SCHMITT, R.T. STÖFFLER, D. (2006): Shock metamorphosed zircon in terrestrial impact craters. Meteoritics and Planetary Sciences, **40**, 1–16.

Received: June 13, 2008; accepted: December 9, 2008

*Acta Mineralogica-Petrographica, Szeged 2008, Vol. **48**, pp. 33-41.*

ACTA Mineralogica Petrographica

PETROLOGY OF PĂULIŞ GRANITES (APUSENI MTS., ROMANIA)

ELEMÉR PÁL-MOLNÁR[1], EDUÁRD ANDRÁS[1], ZSOMBOR KASSAY[1], GYÖRGY BUDA[2], ANIKÓ BATKI[1]

[1]Department of Mineralogy, Geochemistry and Petrology, University of Szeged. H-6701 Szeged, P. O. Box 651, Hungary.
[2]Department of Mineralogy, Institute of Geology, Eötvös L. University, H-1117 Budapest, Pázmány Péter sétány 1/c, Hungary
e-mail: palm@geo.u-szeged.hu

ABSTRACT

This paper presents new data of the highly evolved part of the Highiş Granitoid Suite. Two types of texture represent the suite: equigranular, medium-grained leucogranites and aplite veins. Main rock forming minerals are quartz, orthoclase, microcline, plagioclase feldspar, biotite and muscovite. Based on geochemical investigations which were performed on both selected mineral phases and whole rock composition the Highiş Granitoids from Păuliş are S-type, felsic-peraluminous alkali granites, with alkali-calcic character, formed in post-collisional (post-orogenic) tectonical setting, mainly from metasedimentary source.

Keywords: Păuliş granites, S-type granitoids, Variscan granitoids, Biharia Nappe System, Highiş Mts., Apuseni Mts., Romania.

INTRODUCTION

The studied rocks are highly evolved Variscan granites from Highiş Mountains which are located in the south-western part of the Apuseni Mts., Romania (Fig. 1A).

The Apuseni Mts. are built up by two major tectono-stratigraphic units, the Tisia Mega-Unit and the Dacia Mega-Unit; these structures were formed during Alpine tectonic events. Their basement is formed of pre-alpine metamorphites and igneous suites from earlier tectonic events, including Variscan granitoids.

Detailed studies on these Variscan granitoids were performed by many authors (Giuşcă 1979, Tatu 1998, Pană 1998); however, their correlations with other variscides have not been well clarified.

Two granitic intrusions can be distinguished within the Highiş Mts.: the Şiria Granitoids in the north-western part and the Highiş Granitoids in the southern part of the massif. There are significant differences between the two intrusions. The Şiria Granitoids are the part of the Codru Nappe System, component of the Tisia Mega-Unit in contrast with the Highiş Granitoids which are the part of the Biharia Nappe System, recently considered to be the part of the Dacia Mega-Unit (Fig. 1B). The studied rocks originate from the countryside of Păuliş, Highiş Granitoid Suite, therefore we use the term Păuliş Granitoids for them.

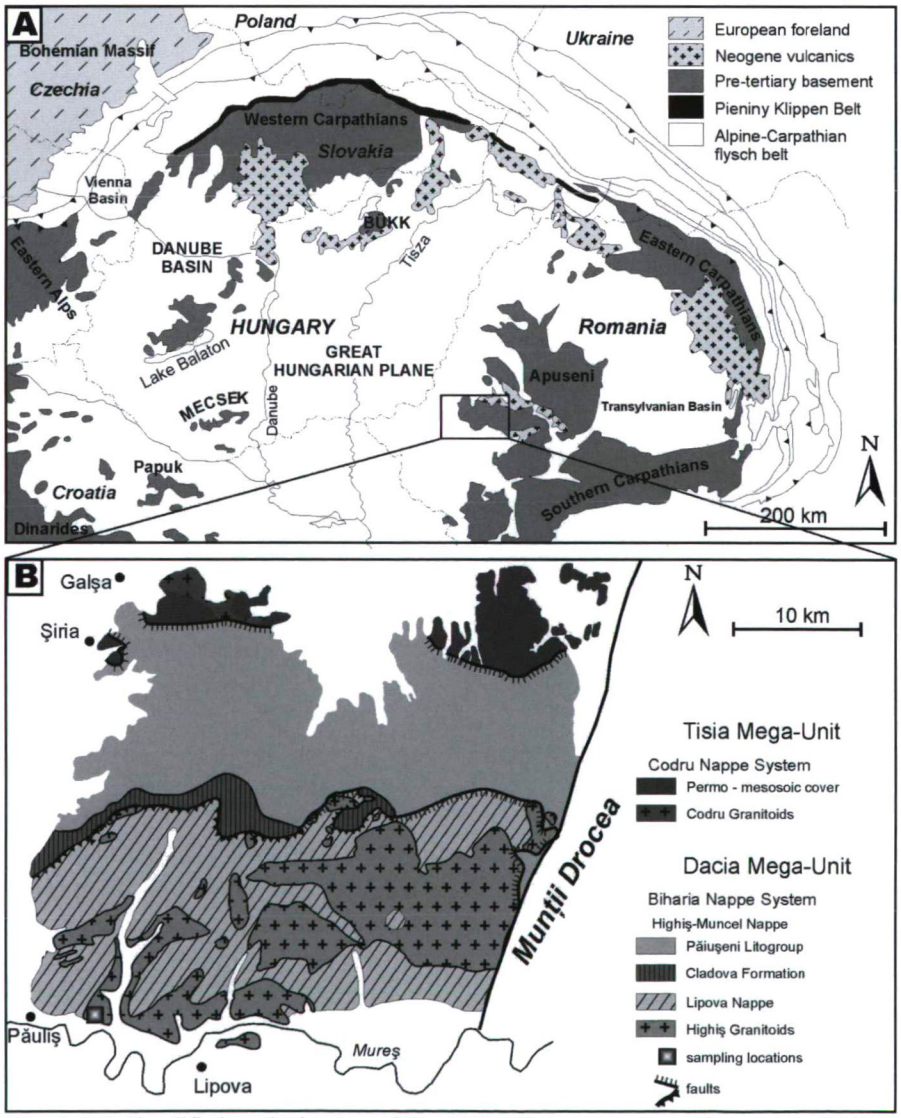

Fig. 1. (A) Simplified geologic map of the Alpine-Carpathian-Pannonian region *(B)* Pre-Neogene geology of the Highiş Mts. after Balintoni (1986) and Balintoni and Puşte (2002).

Geological Setting and Location

The Highiş Mts. are located in the W-SW part of the Apuseni Mts., Romania. Previous researches of the geological structure of Highiş Mts. were made by Lóczy (1883), Rozlozsnik (1913), Paucă (1941), Giuşcă (1948, 1962, 1979), Giuşcă et al. (1964), Dimitrescu (1962, 1967, 1988), Savu (1965), Balintoni (1986, 1994), Tatu (1998), Pană (1998), Balintoni, Puşte (2002).

In the northern part of Highiş Mts. the crystalline basement is formed by the Tisia Mega-Unit while the center and southern regions are formed by the Dacia Mega-Unit considered as Biharia Nappe System (Schmid et al. 2008). These mega-units are represented in the Highiş Mts. by alpine nappes belonging to Biharia Nappe System (Dacia Mega-Unit) and Codru Nappe System (Tisia Mega-Unit) (Fig. 1B). The Biharia Nappe System shows a two stage poly-metamorphic history within Dacia Mega-Unit, beginning in the Middle to Late Jurasic and finishing in the Early Cretaceous. The final emplacement of both of the nappe systems occurred in Cretaceous (Turonian), during the pre-Gosau tectogenesis but with strikes of opposite direction. The Codru Nappe System is in lower position than the Biharia Nappe System. Both of the nappe systems are positioned in the Biharia Unit (Săndulescu 1984), and both of them contain granitoids of variscan age (Pană 1998).

The granitoids of the Biharia Nappe System, located in the Highiş Mts., are emplaced in the Highiş-Muncel Nappe, in contact with the Cladova Formation, part of the Păiuşeni Litho-group, which is overthrusted by the Lipova Nappe. The Cladova Formation is formed by sandstones, argillites, basic tuffs and basalts, and it is metamorphosed at the contact of the Highiş granitoids. In their contact zones hornfelses do appear. Highiş granitoids are Variscan, postcinematic granites, containing aplitic and pegmatitic veins (Giuşcă 1979). Giuşcă et al. (1964) estimated a 350 Ma age of the Highiş Granitoid Complex by K/Ar (WR) method. Nevertheless, Pană (1998) determined a 264-267 Ma age from zircon fractions by the more reliable U/Pb method, and explained the formation of Highiş granitoids by a short lasting magmatism at the end of the early Permian.

Sampling and Analytical Methods

The studied 28 rock samples were collected from Păuliş (Fig. 1B). During the research 82 mineral chemical analyses were made at Department of Mineralogy and Petrology, University of Graz. Measurements were performed at a 15 kV acceleration voltage and 10 nA current. Spectra were evaluated with Oxford-Isis software. Geochemical analyses were performed on 10 samples at the University of Stockholm with inductively coupled plasma atomic emission spectroscopy (ICP-AES) and inductively coupled plasma mass spectrometry ICP-MS methods. Processing of raw data was made by MinPet 2.0, Mica+1.0 and GCDkit 2.7.0 softwares.

Petrography

On the basis of modal analyses, rocks from Păuliş are alkali granites to syenogranites with moderate mica content (1-3 vol. %) (Le Maitre 1989, not shown). The granitoids have a pinkish, sometimes greyish colour. Their texture is phenocrystalline, equigranular and medium-grained (Pál-Molnár et al. 2004). Light grey coloured aplitic veins are also present cutting the whole mass of the rock in various directions.

Weakly foliation can be observed on some samples, but mostly the phyllosilicates are oriented along fractures. The average size of the main mineral constituents is similar, both quartz and feldspar grain sizes falls between 1-4 mm. The only exception is biotite which is appearing in 2-4 cm clots.

Mineralogy and Mineral Chemistry

Mineral chemical analyses were performed on feldspar, biotite and muscovite. Representative compositions are shown in Table 1 and 2.

Quartz: xenomorphic, mean grain size is between 2-4 mm. It has always undulating extinction and it is frequently recrystallized, which leads to the decrease of grain size and the development of subgrains forming fine grained mosaics.

Orthoclase: hypidiomorphic with tabular habit, mean grain size is 4-5 mm. Carlsbad twins are common, they occasionally have perthitic structure.

Microcline: hypidiomorphic, rarely xenomorphic, 3-4 mm grains, tabular habit and polysynthetic twinning is characteristic.

The analyzed K-feldspars have $Or_{93,70-97,77}Ab_{2,23-6,30}An_0$ composition (Table 1.).

Plagioclase feldspars: hypidiomorphic, tabular, often zoned, mean grain size is 3-5 mm, polysynthetic, albite twins are common. The plagioclase feldspars are albites with anorthit composition between 0,30-1,65wt% (Table 1). The distribution of feldspars according to Or-Ab-An can be seen in Fig. 2.

Biotite group

The representative chemical compositions of the minerals of the biotite group are presented in Table 2. Hypidiomorphic tabular or xenomorphic grains are characteristic, mean grain sizes are 1-3 mm. Their pleochroism is light brown to dark green. In intergrown with muscovite they often contain opaque minerals, apatite and zircon. Along microtectonical deformations they have a slight orientation. Biotites frequently compose clots of 2-4 cm.

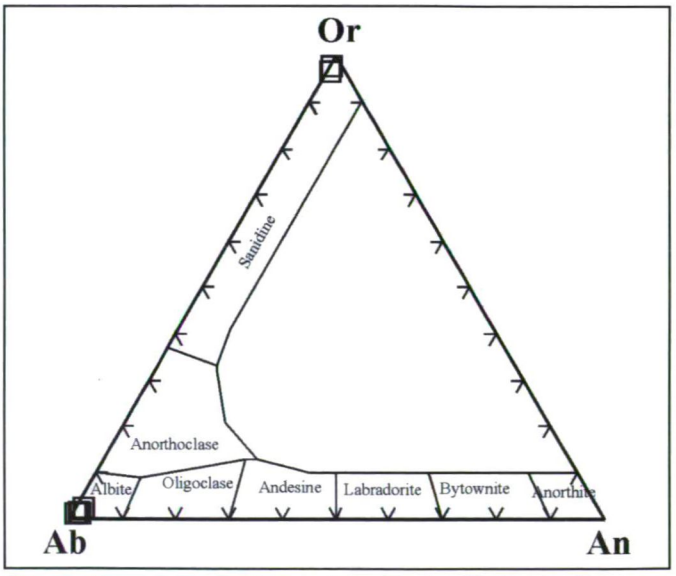

Fig. 2. Feldspar compositions plotted in the Ab-Or-An diagram.

Table 1. Representative chemical composition of the feldspars.

	Plagioclase feldspars											K-feldspars					
	7260/18	7260/22	7260/23	7262 /1	7262/5	7262/10	7262 /11	7264 /1	7264/3	7264 /5	7264 /7	7260 /1	7260/2	7260/17	7260 /21	7264 /2	7264 /11
Na_2O	10.44	10.77	10.87	10.96	10.38	10.75	9.54	10.66	10.98	10.41	10.70	0.33	0.55	0.70	0.31	0.30	0.26
MgO	0.05	0.00	0.01	0.06	0.29	0.00	0.22	0.20	0.19	0.09	0.00	0.10	0.22	0.23	0.00	0.16	0.00
Al_2O_3	19.90	19.64	19.84	18.68	19.44	19.00	19.21	19.68	19.97	19.66	19.36	17.87	18.00	17.60	17.64	17.92	18.39
SiO_2	70.49	70.62	71.02	66.57	69.60	68.88	69.89	70.57	69.87	70.76	71.05	64.15	63.99	63.7	65.17	64.74	64.57
K_2O	0.08	0.09	0.07	0.07	0.04	0.06	0.85	0.11	0.10	0.06	0.08	16.21	16.17	15.81	16.23	16.63	16.63
CaO	0.32	0.14	0.19	0.06	0.06	0.07	0.08	0.32	0.46	0.13	0.23	0.00	0.00	0.00	0.00	0.02	0.00
TiO_2	0.02	0.00	0.05	0.02	0.01	0.02	0.00	0.01	0.00	0.04	0.04	0.06	0.02	0.07	0.00	0.01	0.00
MnO	0.00	0.00	0.00	0.00	0.00	0.09	0.00	0.00	0.02	0.00	0.07	0.04	0.02	0.06	0.01	0.11	0.11
FeO	0.13	0.11	0.07	0.02	0.09	0.00	0.02	0.16	0.06	0.05	0.00	0.06	0.05	0.01	0.10	0.00	0.02
∑oxide	101.43	101.38	102.12	96.45	99.91	98.86	99.82	101.72	101.65	101.21	101.52	98.82	99.02	98.18	99.47	99.89	99.98
Na	0.87	0.90	0.90	0.96	0.87	0.92	0.81	0.89	0.92	0.87	0.89	0.03	0.05	0.06	0.03	0.03	0.02
Mg	0.00	0.00	0.00	0.00	0.02	0.00	0.01	0.01	0.01	0.01	0.00	0.01	0.02	0.02	0.00	0.01	0.00
Al	1.01	0.99	1.00	0.99	1.00	0.99	0.99	0.99	1.01	1.00	0.98	1.00	0.99	0.98	0.97	0.97	0.99
Si	3.02	3.03	3.03	3.01	3.02	3.03	3.05	3.02	3.01	3.04	3.05	3.00	2.99	3.00	3.04	3.01	3.02
Cl	0.00	0.00	0.00	0.00	0.00	0.00	0.00	0.00	0.00	0.00	0.00	0.00	0.00	0.00	0.00	0.00	0.00
K	0.00	0.00	0.00	0.00	0.00	0.00	0.00	0.01	0.01	0.00	0.00	0.97	0.96	0.95	0.96	0.98	0.97
Ca	0.01	0.01	0.01	0.00	0.00	0.00	0.00	0.01	0.02	0.01	0.01	0.00	0.00	0.00	0.00	0.00	0.00
Ti	0.00	0.00	0.00	0.00	0.00	0.00	0.00	0.00	0.00	0.00	0.00	0.00	0.00	0.00	0.00	0.00	0.00
Mn	0.00	0.00	0.00	0.00	0.00	0.00	0.00	0.00	0.00	0.00	0.00	0.00	0.00	0.00	0.00	0.00	0.00
Fe	0.00	0.00	0.00	0.00	0.00	0.00	0.00	0.01	0.00	0.00	0.00	0.00	0.00	0.00	0.00	0.00	0.00
O	8.00	8.00	8.00	8.00	8.00	8.00	8.00	8.00	8.00	8.00	8.00	8.00	8.00	8.00	8.00	8.00	8.00
∑cation	4.91	4.93	4.94	4.96	4.91	4.94	4.86	4.94	4.98	4.93	4.93	5.01	5.01	5.01	5.00	5.00	5.00
Or	0.43	0.54	0.41	0.41	0.18	0.30	5.51	0.66	0.52	0.31	0.42	97.01	95.09	93.7	97.18	97.30	97.77
Ab	97.92	98.81	98.69	99.29	99.51	99.39	94.11	97.77	97.23	99.06	98.96	2.99	4.91	6.30	2.82	2.66	2.23
An	1.65	0.65	0.90	0.30	0.31	0.30	0.37	1.57	2.25	0.63	0.61	0.00	0.00	0.00	0.00	0.04	0.00

Table 2. Representative chemical composition of the micas.

	Biotite					Muscovite											
	7260 /3	7260 /10	7260/13	7260 /19	7264 /8	7260/8	7260/9	7260/15	7260/16	7260/20	7262/4	7262/8	7262/9	7262/12	7262/13	7264/4	7264/10
Na_2O	0.24	0.05	0.7	0.05	0.16	0.30	0.45	0.83	0.69	0.16	0.15	0.20	0.09	0.12	0.12	0.14	0.11
MgO	5.29	5.43	4.38	5.27	4.72	1.87	1.81	2.10	1.85	1.71	2.98	3.35	3.35	2.67	3.39	1.29	1.85
Al_2O_3	13.63	13.42	12.74	14.12	13.77	28.04	25.59	25.61	25.32	27.31	25.48	27.41	28.62	29.76	27.46	28.53	26.73
SiO_2	34.38	34.88	34.79	35.87	37.62	49.55	45.41	47.13	47.29	48.40	45.77	50.52	50.29	48.00	50.11	48.70	48.54
K_2O	9.38	9.29	3.06	9.58	6.50	9.33	9.19	10.17	8.86	9.76	8.66	8.68	9.38	7.87	9.41	9.37	9.50
CaO	0.00	0.02	0.33	0.06	0.25	0.07	0.00	0.00	0.04	0.00	0.07	0.07	0.00	0.80	0.06	0.05	0.00
TiO_2	1.47	1.51	0.15	1.52	0.04	0.30	0.46	0.40	0.39	0.44	0.24	0.28	0.33	0.26	0.24	0.34	0.37
MnO	0.48	0.40	0.43	0.46	0.37	0.05	0.05	0.00	0.00	0.06	0.00	0.00	0.08	0.00	0.01	0.05	0.07
FeO	27.34	26.49	27.95	27.28	26.03	7.48	7.24	6.89	6.95	6.95	2.46	2.73	2.94	3.00	2.79	6.70	7.44
∑oxide	92.21	91.49	84.53	94.22	89.46	96.99	90.20	93.13	91.39	94.78	85.81	93.24	95.09	92.48	93.58	95.17	94.62
Na	0.08	0.01	0.24	0.02	0.05	0.08	0.13	0.23	0.19	0.04	0.04	0.05	0.02	0.03	0.03	0.04	0.03
Mg	1.31	1.34	1.14	1.27	1.16	0.37	0.39	0.44	0.39	0.35	0.66	0.67	0.66	0.54	0.68	0.26	0.38
Al	2.66	2.62	2.63	2.69	2.68	4.42	4.37	4.25	4.24	4.42	4.43	4.36	4.50	4.78	4.37	4.56	4.33
Si	5.70	5.79	6.09	5.79	6.21	6.62	6.58	6.64	6.72	6.65	6.75	6.82	6.70	6.54	6.77	6.61	6.67
Cl	0.05	0.05	0.08	0.05	0.00	0.01	0.00	0.00	0.00	0.00	0.00	0.01	0.00	0.00	0.01	0.00	0.00
K	1.98	1.96	0.68	1.97	1.37	1.59	1.70	1.83	1.61	1.71	1.63	1.49	1.59	1.37	1.62	1.62	1.67
Ca	0.00	0.00	0.06	0.01	0.04	0.01	0.00	0.00	0.01	0.00	0.00	0.01	0.00	0.12	0.01	0.01	0.00
Ti	0.18	0.19	0.02	0.18	0.01	0.03	0.05	0.04	0.04	0.05	0.03	0.03	0.03	0.03	0.02	0.03	0.04
Mn	0.07	0.06	0.06	0.06	0.05	0.01	0.01	0.00	0.00	0.01	0.00	0.00	0.01	0.00	0.00	0.01	0.01
Fe	3.79	3.67	4.10	3.68	3.59	0.84	0.88	0.81	0.83	0.80	0.30	0.31	0.33	0.34	0.32	0.76	0.85
O	22.00	22.00	22.00	22.00	22.00	22.00	22.00	22.00	22.00	22.00	22.00	22.00	22.00	22.00	22.00	22.00	22.00
∑cation	15.82	15.69	15.1	15.72	15.16	13.98	14.11	14.24	14.03	14.03	13.84	13.75	13.84	13.75	13.83	13.90	13.98
mg#	26	27	22	26	24												
Al(IV)	2.29	2.20	1.91	2.21	1.79												
Al(VI)	0.38	0.43	0.73	0.48	0.89												

According to Foster (1960) the sum of cations in X position and in Y position of biotites is between 1,60 – 2,20 (mean: 1,91) and above 5,00 (mean: 5,15), respectively. The average TiO_2 content of biotites is 0,90%. The Mg content of biotites is low (mg#=21,8-26,8; mean mg#=24,8), and they are replaced by phlogopites along fractures: mg#= 67,8-69,5 (mean mg#=68,7). Based on compositional classifications and the IMA nomenclature, biotites are Magnesian-siderophyllites (Fe-biotites; Foster 1960) and Ferroan-phlogopites, respectively (Fig.3A).

According to the Mg vs. Al_{tot} distribution of biotites (Nachit et al. 1985), the Păuliş granitoids are of subalkaline character (Fig. 3B).

The high Mg content of the phlogopites signs postgenetic transformations, which is supported as well by the fact that phlogopites occur only along fractures, they are often weathered, and appear in combination with muscovite. Textural orientation is also characteristic.

Muscovite: hypidiomorphic tabular and elongated lamellar, the mean grain size is 1–3 mm. It appears often along with biotite, and at some places it is oriented. Small sized muscovite grains are frequent in the fractures of the rock. The studied rocks contain ferrum-rich muscovites, the FeO content of Păuliş Granites varies between 2,46% and 7,48%, with significant magnesium content (1,29%–3,35%). The representative chemical compositions of muscovites are shown in Table 2.

Accessory minerals are apatite, monazite and zircon

Apatite crystals usually have an idiomorphic, partly hypidiomorphic shape, and often appear in biotite crystals. Zircon crystals are idiomorphic, rarely hypidiomorphic, and represent two types of habit. The one is squattish, reddish-brown, and yellowish-brown; the other one is colorless, pinkish with an elongated columnar appearance. Opaque inclusions are quite frequent; numerous grains are zoned, which refers to several crystallization phases.

GEOCHEMISTRY

Representative geochemical compositions are shown in Table 3. Păuliş syenogranites have high silica content, between 70.95 and 72.30 wt% (mean value 71.60), aplites are even more saturated in SiO_2, with mean 75.44 wt% of SiO_2. Their alkaline content is also high, K_2O content is higher (4.42-49.0 wt%, mean 4.56 wt%) than Na_2O (3.25-3.68 wt%, mean 3.48 wt%), K_2O/Na_2O ratio ranges from 1.26 to 1.49.

Modified alkali lime index (MALI) shows alkali-calcic character (Frost et. al 2001) (Fig. 4E). Low concentrations of CaO (0.40 to 0.55 wt%) and MgO (0.26 to 0.30 wt%) along with low TiO_2 (Ti mineral phase is absent) and Sr (which is coordinated by basic plagioclase feldspar phase) concentrations suggest a highly fractionated rock. $Fe_2O_3/(Fe_2O_3+MgO)$ ratio is relatively high, 0.81. According to Chappel and White (2001) on the basis of CaO and Fe_2O_3 content, the studied rocks are S-type granitoids (Fig. 4A). Based on the R1-R2 multicationic distribution diagram (De La Roche et al. 1980) Păuliş granitoids are alkali granites [R1=4Si-11(Na+K)-2(Fe+Ti) and R2=6Ca+2Mg+Al] (Fig. 4D).

Based on their saturation in alumina, the studied rocks are slighty peraluminous, mean A/CNK value is 1.07. This feature is also supported by the presence of modal muscovite, and CIPW normative corundum (Shand 1943) (Fig. 4B). For further subdivision within peraluminous group *A* [Al - (K + Na + 2 Ca)] *vs. B* [Fe + Mg + Ti] distribution diagram has been chosen (Villaseca et al. 1998). The studied rocks have felsic-peraluminous character (Fig. 4C).

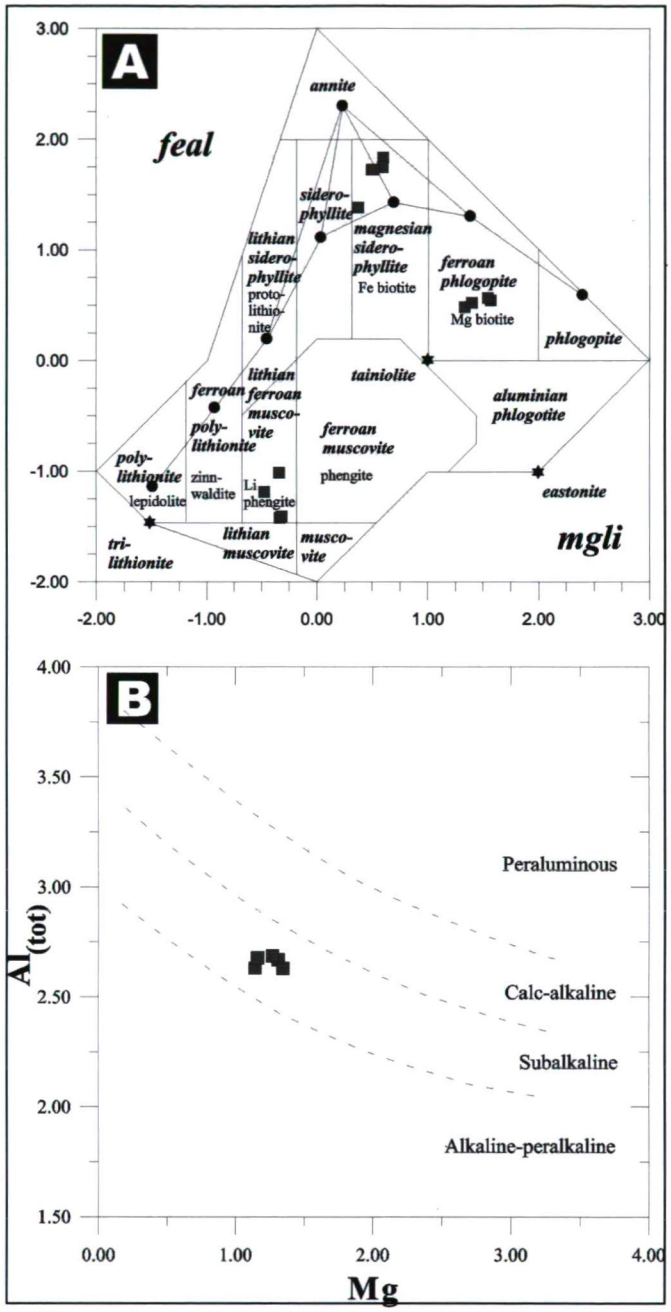

Fig. 3. (A) Compositional classification of the biotites after Tischendorf et al. (1997). ***(B)*** Mg vs. Al_{tot} plot after Nachit et al. (1985).

The MORB-normalized (Pearce 1983) trace element patterns show that Păuliş granites are enriched in LILE, mostly in Rb, K, Ba with the exception of Sr which is strongly depleted, and are slightly enriched in HFS elements (Zr, Hf, Nb) (Fig. 5B).

The chondrite-normalized (Nakamura 1974) REE concentrations of most granites and aplites show smooth patterns. The studied aplites are less enriched in LREE than

Table 3. Representative whole rock chemical composition.

	SiO_2	Al_2O_3	Fe_2O_3*	MnO	MgO	CaO	Na_2O	K_2O	TiO_2	Total	Ba	Be	Ce	Co	Cr	Cu	Dy	Er	Eu	Ga
7259	71.66	11.87	1.27	0.02	0.26	0.47	3.57	4.49	0.18	93.80	316.46	3.15	61.78	2.72	6.35	18.52	6.57	4.82	0.38	<42.83
7260	71.40	11.85	1.16	0.01	0.26	0.45	3.44	4.47	0.17	93.20	313.02	3.15	55.44	2.11	4.68	18.46	6.21	4.76	0.41	<42.83
7261	71.15	12.50	1.17	0.02	0.27	0.43	3.30	4.42	0.17	93.44	306.37	3.13	55.80	2.11	5.38	17.82	6.16	4.73	0.43	<42.83
7263	72.12	12.09	1.32	0.02	0.30	0.49	3.66	4.90	0.21	95.11	321.06	3.15	61.98	2.78	6.69	19.12	6.58	4.91	0.38	<42.83
7264	72.30	12.57	1.28	0.02	0.31	0.55	3.68	4.64	0.18	95.52	326.37	3.15	65.95	3.24	7.03	16.83	6.98	4.95	0.35	<42.83
7265	70.95	12.68	1.19	0.02	0.28	0.40	3.25	4.42	0.17	93.36	302.48	3.13	55.87	2.09	5.90	17.53	5.97	4.69	0.43	<42.83
7269	75.20	11.95	0.49	0.00	0.19	0.10	3.51	4.90	0.08	96.41	225.40	2.34	38.96	3.52	3.65	20.63	5.48	4.14	<0.07	<42.83
7270	75.68	12.03	0.42	0.01	0.17	0.11	3.43	5.10	0.06	97.01	216.55	2.29	39.37	3.67	3.48	22.18	5.13	4.07	<0.07	<42.83
	Gd	Hf	La	Lu	Mn	Mo	Nb	Nd	Ni	Pb	Rb	S	Sc	Sm	Sr	V	Y	Yb	Zn	Zr
7259	7.81	4.84	30.24	0.79	80.36	6.77	5.58	20.03	4.68	122.83	400.76	55.78	3.33	7.45	23.59	7.42	42.00	3.57	32.13	148.91
7260	7.33	3.76	30.53	0.78	76.61	2.61	5.42	19.97	3.20	118.56	398.58	37.28	3.21	7.45	23.34	7.36	36.70	3.50	33.44	143.18
7261	7.27	4.13	29.68	0.77	74.70	3.04	5.41	18.86	3.12	116.76	379.16	37.45	3.24	7.25	23.26	7.51	34.90	3.48	33.71	139.81
7263	8.00	6.59	29.95	0.81	92.47	7.82	6.08	20.32	5.38	126.84	405.32	60.89	3.38	7.86	26.75	7.63	42.34	3.86	30.90	161.73
7264	8.46	6.51	33.69	0.86	100.17	8.91	6.43	23.42	6.64	129.82	413.98	67.36	3.58	8.33	28.98	8.57	40.94	3.90	31.48	171.66
7265	7.18	4.25	28.34	0.77	70.64	3.67	5.21	18.67	3.03	115.67	359.54	39.73	3.26	7.24	23.11	7.52	34.30	3.34	33.83	137.61
7269	5.30	6.95	16.11	0.74	22.22	10.57	9.64	10.24	81.56	48.86	305.53	35.75	1.55	6.16	11.12	3.46	30.89	3.50	11.11	118.13
7270	5.41	7.24	17.33	0.73	15.67	11.95	9.45	10.35	92.63	42.62	288.32	35.75	1.24	6.02	13.67	3.64	31.68	3.54	9.08	102.28

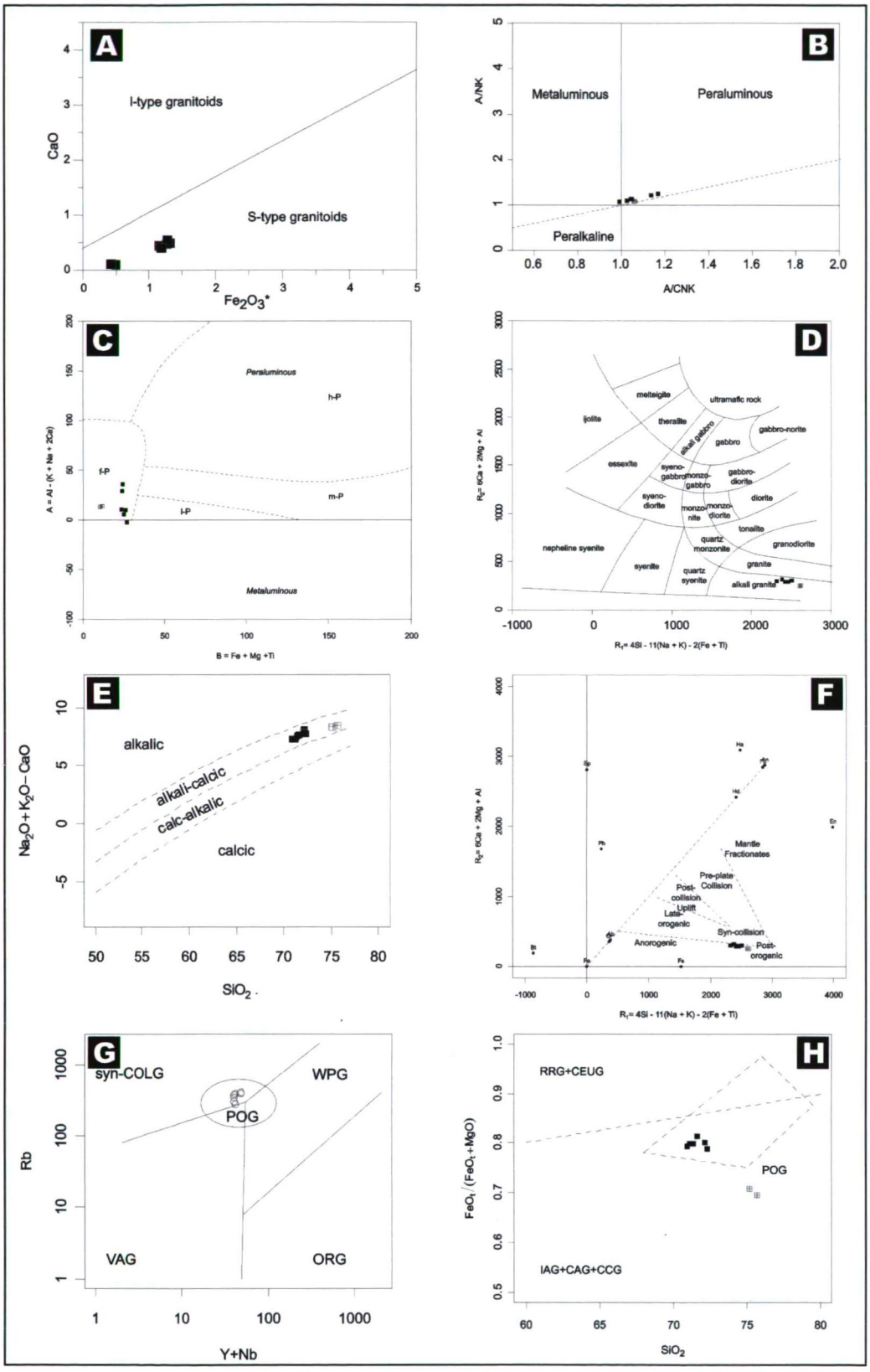

Fig. 4. ***(A)*** CaO vs. Fe_2O_3 diagram (Chappell and White, 2001) discriminating I-type (Igneous) and S-type (Sedimentary) source. ***(B)*** A/CNK vs. A/NK diagram of Shand (1943) discriminating metaluminous, peraluminous and peralkaline compositions. ***(C)*** BA plot modified by Villaseca et al. (1998) (f-P; h-P; m-P; l-P; – felsic-; high-; medium-; and low-peralumious granitoids). ***(D)*** Granite classification diagram based on R1 vs. R2 distribution plot after De la Roche et al. (1980). ***(E)*** Modified Alkali-Lime Index (MALI) (Frost et al., 2001). ***(F)*** Tectonic discrimination diagram based on R1 vs. R2 after Batchelor, Bowden (1985). ***(G)*** Tectonic discrimination diagram based on Y+Nb vs. Rb (Pearce, 1996). ***(H)*** Tectonic discrimination diagram based on $FeO^t/(FeO^t/MgO)$ vs. SiO_2 (Maniar, Piccoli, 1989).

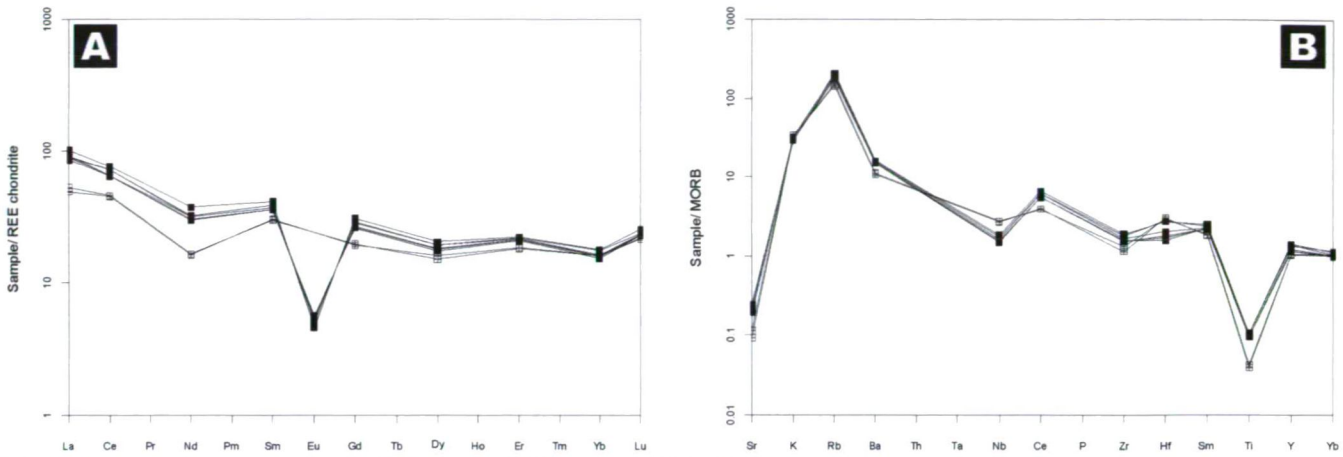

Fig. 5. (A) Chondrite-normalized REE pattern (Nakamura, 1974). *(B)* MORB-normalized trace element pattern (Pearce, 1983).

the granites. The granites have very strong negative Eu anomaly (mean value of Eu/Eu* is 0.16), while the Eu content of the aplites is below the detection limit (Fig. 5A).
The low CaO/Na_2O and medium Al_2O_3/TiO_2 ratios in the studied granites (excluding aplites), (mean CaO/Na_2O is 0,13; mean Al_2O_3/TiO_2 is 68,59) are typical for peraluminous variscan granitic suites (Sylvester 1998). Low values of CaO/Na_2O ratio suggest pelitic origin of the granites, and medium values of Al_2O_3/TiO_2 ratio suggest medium to high temperatures (~875-900 ^{0}C) of the melts. Rb/Sr vs. Rb/Ba distribution also confirms the pelitic source (Sylvester 1998).

Based on the distributions of SiO_2 vs. $FeO^t/(FeO^t+MgO)$ (Maniar and Piccoli 1989) (Fig. 4H), Rb vs. Y+Nb (Pearce 1996) (Fig. 4G), and R1 vs. R2 (Batchelor and Bowden 1985) (Fig. 4F) multiple discrimination diagrams Păuliş granites were formed in post-orogenic tectonic setting.

Conclusions

Păuliş Granites except aplites are holocrystalline, equigranular and medium-grained. In some samples textural orientation can be observed, but it is unusual regarding the whole studied suite.

The main rock forming minerals are: quartz, orthoclase, microcline, plagioclase feldspar (albite), biotite and muscovite. Apatite, monazite and zircon occur as accessory minerals. Păuliş Granites are leucogranites with very high silica and relatively high alkali content. Based on the concentration of major elements the studied rocks are alkali granites. According to their alumina saturation, Păuliş Granites are felsic peraluminous granites. Muscovite which is a typical mineral phase for slightly peraluminous granites is present in the studied rocks as a significant component. The composition of biotites indicates subalkali character of the granites, while whole rock compositions plotting in the modified alkali lime index (MALI) show alkali-calcic character. Păuliş Granites are highly evolved S-type granites (Chappell and White 2001). Due to crystal fractionation, their CaO and Sr^{2+} content is very low, plagioclase feldspars are albites. First generation of biotites is ferric type as well. Păuliş granites are enriched in Rb, K and Ba. The chondrite-normalized (Nakamura 1974) Rare earth elements show smooth pattern, with very strong Eu anomaly. These characteristics of granites are well known from late Variscan suites (Sylvester 1998) where due to the relatively thin lithosphere the main source of heat is provided from the asthenosphere. The source of the highly evolved Păuliş Granites is proposed mainly pelitic. Previous authors assigned mixed source for the whole suite which contains rock types from alkali granites to more basic type of igneous rocks. According to Tatu (1998) it is confirmed that Păuliş Granites were formed in post-orogenic tectonic setting in a late Variscan tectogenetic stage, following the main collision event.

Acknowledgements

The financial background of this work was ensured by the Hungarian National Science Found (OTKA) (Grant number 67787).

References

Balintoni, I. (1986): Petrologic and tectonic features of Highiş - Drocea crystalline massif. D.S. Inst. Geol. Geofiz., **70-71**, 5, 5–12.

Balintoni, I. (1994): Structure of the Apuseni Mountains. ALCAPA II, Field Guidebook, Suppl. 2 to Rom. J. Tect. & Reg. Geol., **75**, 51–57.

Balintoni, I., Puşte, A. (2002): New lithostratigraphic and structural aspects in the southern part of the Bihor Massif (Apuseni Mountains). St. Univ. Babeş-Bolyai Geol., **47**, 2, 13–18.

Batchelor, R. A., Bowden, P. (1985): Petrogenetic interpretation of granitoid rock series using multicationic parameters. Chemical geology, **48**, 43–55.

Chappell, B.W., White, A.J.R. (2001). Two contrasting granite types: 25 years later. Australian Journal of Earth Sciences, **48**, 489–500.

De La Roche, H., Leterrier, J., Grandclaude, P., Marchal, M. (1980): A classification of volcanic and plutonic rocks using R_1,R_2-diagrams and major element analysis - its relationshipwith current nomenclature. Chemical Geology, **29**, 183–210.

Dimitrescu, R. (1962): Cercetări geologice în regiunea Şiria. D.S. Inst. Geol., **45** (1957-1958), 75–87.

Dimitrescu, R. (1967): Contribuţii la cunoaşterea structurii părţii de N-V a masivului cristalin Highiş. D.S. Inst. Geol., **53**, 1, (1965-1966), 39–50. (in Romanian)

Dimitrescu, R. (1988): Apuseni Mountains. In Zoubek, V., Cogné, J., Kozhoukharov, D., (eds.): Precambrian in Younger Fold Belts 665–674.

Foster, M. D. (1960): Interpretation of the composition of trioctahedral micas. Geol. Surv. Prof. Paper. 354-B, 49.

FROST, B.R., BARNES, C.G., COLLINS, W.J., ARCULUS, R.J., ELLIS, D.J., FROST, C.D. (2001): A geochemical classification for granitic rocks. Journal of Petrology, **42**, 2033–2048.

GIUŞCĂ, D. (1948): Raport preliminar asupra zăcămintelor metalifere din regiunea Munţilor Highiş. Arh. Com. Geol. (in Romanian)

GIUŞCĂ, D. (1962): Observaţii asupra formaţiunilor cristaline şi metamorfismul de contact al granitelor din masivul Highiş. St. Cerc. Geol. **7**, 2, 319–327. (in Romanian)

GIUŞCĂ, D. (1979): Masivul cristalin al Highişului. St. Cerc. Geol. Geofiz. Geogr., Geol. **24**, 15–43. (in Romanian)

GIUŞCĂ, D., IONESCU, J., UDRESCU, C. (1964): Contribuţii la studiul geochimic al masivului Highiş. St. Cerc. Geol. **9**, 2. Bucureşti.

LE MAITRE, R. E. (ed.) (1989): A classification of the igneous rocks and glossary of geological terms. Blackwell, Oxford.

LÓCZY, L. (1883) A Maros és a Fehér-Kőrös közötti hegyvidéken és az Arad-Hegyalján eszközölt földtani részletes felvételről. Földt. Közl., 1884, **XIV**, p.196–213.

MANIAR, P.D, PICCOLI, P. M., (1989): Tectonic discrimination of granitoids. Geol. Soc. of Am. Bull., v. 101, p. 635–643.

NACHIT, H., RAZAFIMAHEFA, N., STUSSI, J.M., CARRON, J.P. (1985): Composition chimique des biotite et typologie magmatique des granitoides. CR Acad Sci Paris, **301**, 813–822. (in French)

NAKAMURA, N. (1974): Determination of REE, Ba, Fe, Mg, Na, and K in carbonaceous and ordinary chondrites. Geochim. Cosmochim. Acta **38**, 757–775.

PANĂ, D. (1998): Petrogenesis and tectonics of the basement rocks of the Apuseni Mountains: significance for the Alpine tectonics of the Carpatho-Pannonian region. PhD Thesis, University of Alberta, Alberta, Canada. 356p.

PAUCĂ, M. (1941): Recherches géologiques dans la région de Şiria. C.R. Inst. Géol. Roum., **25** (1936-1937). (in Romanian)

PEARCE J A (1983): Role of the sub-continental lithosphere in magma genesis at active continental margins. In Hawkesworth C J & Norry M J (eds) Continental Basalts and Mantle Xenoliths. Shiva, Nantwich, 230–249.

PEARCE, J.A (1996): Sources and settings of granitic rocks. Episodes, **19**, no. 4.

ROZLOZSNIK, P. (1913): Geologische Beobachtungen in verschiedenen Gliedern der im weitern Sinne genommenen Bihar-Gebirgsgruppe. Jahresb. kgl. ung. geol. R.A.f. 1914. (in German)

SAVU , H. (1965): Masivul eruptiv de la Bârzava (Munţii Drocea). Mem. Com. Geol., **8**, 148. (in Romanian)

SĂNDULESCU, M., (1984): Geotectonica României. Ed. Tehn., Bucureşti. 336. (in Romanian)

SCHMIDT, S.M., BERNOULLI, D., FÜGENSCHUH, B., MATENCO, L., SCHEFER, S., SCHUSTER, R., TISCHLER, M. & USTASZEWSKI, K. (2008): The Alpine-Carpathian-Dinaridic orogenic system: correlation and evolution of tectonic units. Swiss Journal of Geoscience, **101** 139–183

SHAND, S.J. (1943): Eruptive Rocks. Wiley, London, New York.

SYLVESTER, P.J. (1998): Post-collisional strongly peraluminous granites. Lithos, **45**, 29–44.

TATU, M. (1998): Le Massif Highis (Roumanie), un exemple de l'evolution du magmatism alcalin anorogenique. PhD Thesis, Université de Paris-Sud Centre d'Orsay, Paris, France, 206. (in French)

TISCHENDORF, G., GOTTESMANN, B., FÖRSTER, H.J., TRUMBULL, R.B. (1997): On Li-bearing micas: estimating Li from electron microprobe analyses and improved diagram for graphical representation. Mineral. Mag., **61**, 809–834.

VILLASECA, C., BARBERO, L., ROGERS, G. (1998): Crustal origin of Hercynian peraluminous granitic batholiths of Central Spain: petrological, geochemical and isotopic Sr, Nd constraints. Lithos, **43**, 55–79.

Received: March 23, 2008; accepted: June 3, 2008

*Acta Mineralogica-Petrographica, Szeged 2008, Vol. **48**, pp. 43-48.*

ACTA Mineralogica Petrographica

NORDSTRANDITE – A NEW OCCURRENCE FROM HUNGARY

PÉTER KOVÁCS-PÁLFFY[1], FELICITÁSZ VELLEDITS[2], PÉTER KÓNYA[1], MÁRIA FÖLDVÁRI[1], KAMILLA GÁLNÉ SÓLYMOS[3]

[1]Geological Institute of Hungary, H-1143, Stefánia út 14, Budapest, Hungary.

[2]Volterra Bt., H-2120 Dunakeszi, Andrássy Gy. u. 6, Hungary.

[3]Department of Mineralogy, Eötvös Loránd University of Sciences, H-1117, Pázmány sétány 1/C, Budapest, Hungary
e-mail: kpp@mafi.hu (Péter Kovács-Pállfy), fvelledits@freemail.hu (Felicitász Velledits), kope@mafi.hu (Péter Kónya), foldvari@mafi.hu (Mária Földvárai)

ABSTRACT

A new occurrence of nordstrandite was described from NE Hungary (Aggtelek-Rudabánya Mts). This mineral appeared in red clayed matrix of conglomerates accumulated in dolines from Triassic platform limestone. It was investigated by X-ray diffractometry, thermal analyses, SEM-EDS. By X-ray analyses it was possible to separate the nordstrandite from other crystalline modifications of $Al(OH)_3$. Nordstrandite appears as individual or radial crystal aggregates in voids (fissures or cavities). In our case the nordstrandite precipitated from amorphous $Al(OH)_3$ gels, from the alkaline phreatic solutions, infiltrating along the fissures of the clayed matrix of conglomerates. Nordstrandite was most probably formed during Late Miocene-Pleistocene.

Key words: Nordstrandite, Aggtelek-Rudabánya Mountains (NE Hungary), terra rossa, X-ray diffractometry, thermal analyses, SEM-EDS.

INTRODUCTION

A half of century ago Van Nordstrand et al. (1956) synthesized a new form of $Al(OH)_3$, what was later named nordstrandite by Papée et al. (1958). Many natural occurrences have since been reported (Table 1). According to Milton et al. (1975), Chao and Baker (1982) and Dani et al. (2001) these may be classified into five groups of natural occurrences of nordstrandite (Table 1):

1. the most important, as a weathering product in bauxitic profiles influenced by carbonatic rocks,
2. as a vein or fissure-filling mineral in dolomitic oil shale,
3. as an alteration product of dawsonite and alumohydrocalcite,
4. as a late-forming mineral in pegmatitic pockets and miarolitic cavities associated with nepheline syenite and sodalite alkaline rocks,
5. weathering product in bauxite derived from alkalic igneous rocks,
6. as recent products in discharged caustic waste.

WHAT IS NORDSTRANDITE?

There are four naturally occurring polymorphous $Al(OH)_3$: gibbsite (JCPDS-cards: 7-0324, 29-0041, 33-0018), bayerite (JCPDS-card: 20-0011), nordstrandite (JCPDS-card: 24-0006), and doyleite (JCPDS-card: 38-0376). All occur in the nature, in natural conditions most frequently gibbsite.

The structure of all these minerals is build up from octahedral layers of $Al(OH)_6$. Differences are in the ways of stacking the layers of $Al(OH)_3$ octahedra. This determinates the symmetry and size of the unit cell of minerals, causing smaller differences. The general structure of the four modifications of $Al(OH)_3$ is presented in the Figure 1.

HISTORICAL BACKGROUND OF THE HUNGARIAN NORDSTRANDITE OCCURRENCES

Nordstrandite was first described in Hungary by Náray-Szabó and Péter (1967), based on the X-ray investigations from the 1–5 μm fraction of brick clays. According to Viczián (1999) although based on chemical analyses these fractions contain $Al(OH)_3$, but these can not be assigned to nordstrandite and bayerite. The determination of the above mentioned two minerals by X-ray analyses is uncertain, because their reflections coincide/interfier with the peaks of kaolinite, chlorite and plagioclase. Consequently the $Al(OH)_3$ determined by Náray-Szabó and Péter (1967) refer to amorphous phase.

Koch (1985) mentioned the presence of nordstrandite in bauxite samples from Csordakút (Transdanubian Range), also investigated by X-ray diffractometry. Albert and Mátrai (1970), Albert et al. (1973) mentioned bayerite and nordstrandite in brick clays (in 1-5μm fraction), but according to Viczián (1999) these were not prooved with certainty.

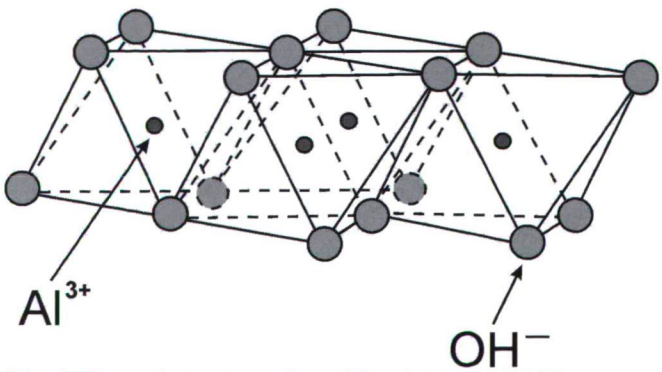

Fig. 1. General structure of modifications of $Al(OH)_3$.

Table 1. Reported geological occurrences of nordstrandite.

Geological setting, location	Type	Associated Al-minerals	Geological age	References
Ferruginous limestone and bauxite (Jamaica)	1	Gibbsite, boehmite	Upper Miocene	Davis & Hill 1973 (in Milton et al. 1975)
Interface limestone and fossil soil derived from basalts and tuffs (Sarawak, Borneo)	1	Gibbsite, diaspore?	Upper Miocene	Wall et al. 1962
Interface limestone and weathered intermediate to basic igneous rock (Guam)	1	Gibbsite, boehmite	Upper Miocene	Hathaway and Schlanger 1962
Interface limestone and weathered volcanic rocks (French Polynesia)	1	Gibbsite, boehmite	Pleistocene	Jamet et al. 1991
Brick clay (Hungary)	1(?)	Gibbsite, bayerite?	Upper Miocene	Náray-Szabó and Péter 1967
Karst limestone, terra rossa (Montenegro)	1	Gibbsite, boehmite	Upper Miocene	Tertian 1966 (in Millot et al. 1975)
Karst limestone, terra rossa (Croatia)	1	Gibbsite, boehmite	Upper Miocene	Marič 1968
Solution cavities on the surface of carbonate rocks (Magnetite mines, Sokolovsko-Sarbay, Russian Federation)	1	Hematite, gibbsite, goethite, magnetite, kaolinite	No data	Kulikova et al. 1974
Karst limestone, terra rossa (Hungary)	1	Kaolinite, hematite, Al-goethite, boehmite	Upper Miocene	This study
Fissure fillings in dolomitic marlstone and oil shale (Rio Blanco, Colorado, USA)	2	Dawsonite	Miocene	Milton et al. 1975
Authigenic in marine and in fluviodeltaic strata (Sydney Basin, New South Wales, Australia)	3	Dawsonite, alumohydrocalcite	Pleistocene	Goldberry and Loughnan 1970
Cavities in nepheline syenite (Narssarssuk, Greenland)	4	No data	No data	Petersen et al. 1976
Pegmatites, miarolitic cavities and xenoliths in nepheline syenite (Mont St-Hilaire, Quebec, Canada)	4	Doyleite, dawsonite	No data	Chao and Baker 1982
Cavities in hauyn-nephelinite (Stradner Hill, Gleichenberg, Austria)	4	Hydrotalcite, motukoreait	Upper Tertiary (Later Pliocene)	Alker et al. 1981
Bauxite derived from phonolite	5	Gibbsite, boehmite	Upper Tertiary (Pliocene?)	Dani et al. 2001
New products in discharged caustic waste (Campbell Island, Southwest Pacific)	6	Bayerite, gibbsite, brucite, pseudoboehmite	Recente	Rodgers et al. 1991

Szakáll and Gatter (1993), Szakáll et al. (2005) consider that the presence of these minerals is not proved properly from the Hungarian occurrences.

The present paper describes the new occurrence of nordstrandite from the Aggtelek-Rudabánya-Mountain, NE-Hungary (Szőlőhegy, Kápolna).

Geological background

The Aggtelek carbonate platform in which the nordstrandite was detected forms a 1–3 km wide belt in the karstified Aggtelek Hills. It strikes NW/SE over a distance of about 7 km between Aggtelek, Jósvafő and Égerszög in NE Hungary. The Triassic formations building up the Aggtelek Karst belong to the Silica Nappe, which forms the uppermost nappe of the Inner West Carpathians (Kozur and Mock 1973).

The Aggtelek platform as part of the non-metamorphosed Aggtelek–Rudabánya Hills belong to the North Pannonian – Inner West Carpathian terrane collage and they are situated in the NE part of the large, composite Pelso Megaunit (Fülöp et al. 1987, Haas ed. 2001) or Pelsonia Composite Terrane (Kovács et al. 2000) (Fig. 2).

On the Middle Triassic carbonate platform lagoonal and reef limestone were deposited. In the Miocene (Sarmatian-Badenian) the Triassic platform carbonates were uplifted and during the denudation period in the karstic doline conglomerates with red clay matrix cement were formed. In the Pleistocene terra rossa with considerable SiO_2 content filled the karstic dolina. The conglomerates were formed during the Miocene or Pleistocene karstic event (Szentpétery et al. 2006).

Nordstrandite occurrences

In the Aggtelek-Rudabánya-Mountains nordstrandite occurs in the karstic doline conglomerates. The clasts of the conglomerate are in red, clayed matrix, sometimes the texture is grain supported. The carbonate clasts are slightly angular and rounded, the diameter of which varies between 2

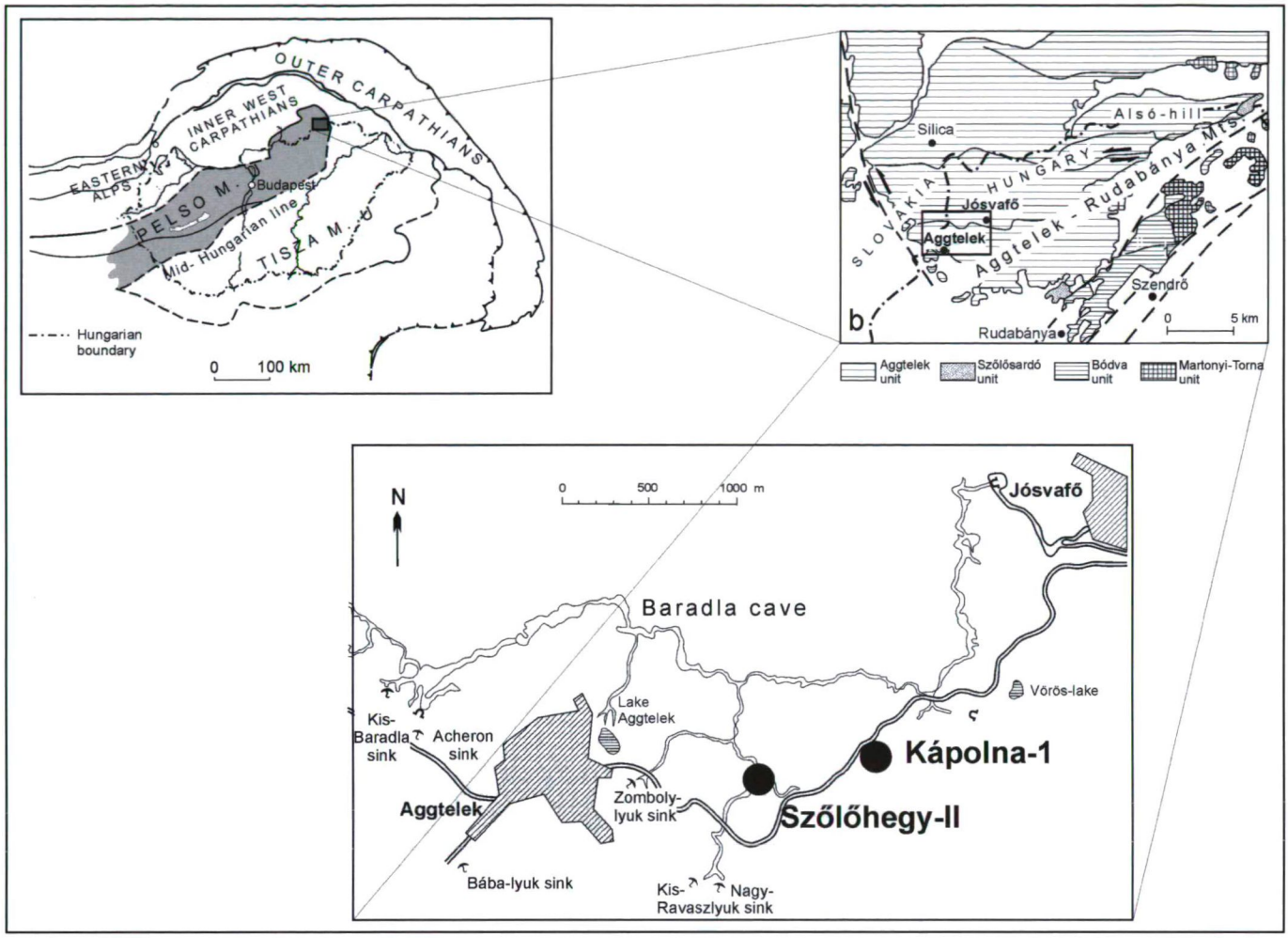

Fig. 2. Sites of nordstrandite occurrences from Aggtelek-Rudabánya-Mountains.

mm and 3 cm. On the edge of the biggest clasts stylolith can be seen, along which dark red clay concentrates. The same dark red clay fills the fractures and fissures, dissecting the matrix of the conglomerate (Fig. 3).

Nordstrandite was first detected by X-ray investigation from the insoluble residue of the red clayed matrix of the carbonate conglomerate deposited in the karstic doline of the Middle Triassic platform limestone. Two samples yielded nordstrandite: Szőlőhegy–II/a (21%) and Kápolna–1 (7%). The present of nordstrandite was confirmed by electron microprobe analyses carried on at Eötvös Loránd University, Department of Petrology and Geochemistry.

METHODS

The X-ray diffraction analyses were done by Philips PW 1710 diffractometer under the following conditions: Cu anti-cathode, 40 kV and 30 mA tube-current, graphite monochromator, goniometer speed 2 °2θ/minute. The mineral composition was calculated on the basis of the relative intensity rates of the reflections characteristic to the minerals, applying the literature or experimental corundum factors on minerals.

The thermoanalytical investigation was executed using a Derivatograph-PC, a computer controlled simultaneous TG, DTG, DTA apparatus. The tests were carried out in ceramic (corundum) crucible, up to 1000 °C. The temperature of the furnace was regulated by a linear heating program at a rate of 10 °C/min. The analytical conditions: air atmosphere, mass of sample about 100 mg, reference material Al_2O_3.

Chemical analysis were preformed on several small crystals by electron microprobe analysis (Department of

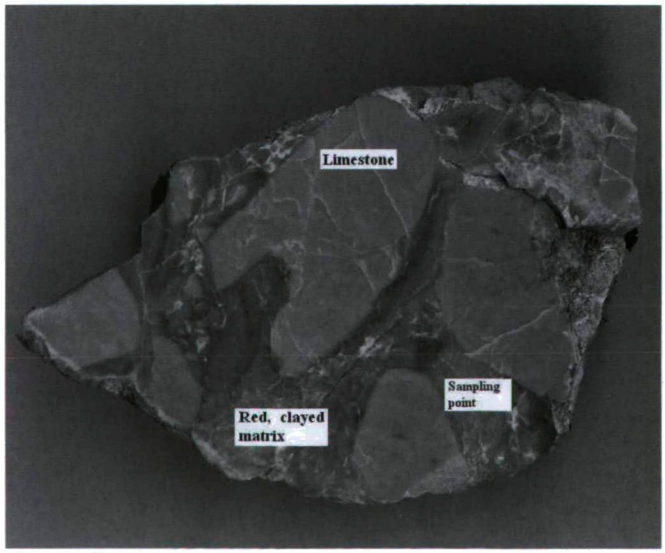

Fig. 3. Carbonatic clasts in red clayed matrix (Field of view is 6 cm wide).

Petrology and Geochemistry of University of Eötvös Lorand), using an AMRAY 1830I/T6 instrument, operated in energy dispersive (EDS) mode (EDAX PV 9800) at 20 kV, with 1-2 nA sample current.

X-RAY DIFFRACTION DATA

Samples of nordstrandite were separated from the conglomerate. The calcite contant was eliminated by dilute acetic acid (20%). The finer clayed matrix was removed from the acid insoluble residues by wet sieving with distilled water. The mineralogical composition (%) of the insoluble residues is presented below (Table 2).

Table 2. The mineralogical composition (%) of the insoluble residues of the nordstrandite-bearing samples.

Minerals	Sample Szőlőhegy-II/a	Sample Kápolna-1
Montmorillonite	2	4
Kaolinite	29	43
Muscovite	13	15
Quartz	5	5
K-feldspars	-	1
Plagioclase	3	3
Dolomite	5	-
Siderite	1	-
Boehmite	1	-
Nordstrandite	21	7
Al-goethite	1	2
Hematite	8	9
Anatase	2	2
Rutile	1	-
Bassanite	2	2
Amorphous	6	7

The X-ray powder diffraction data for the separated insoluble residues are given in Table 3. along with the data for nordstrandite, and other minerals. The X-ray diffractogram of the residual rest in the range of 8 – 26 °2 Θ is shown in Figure 4. Table 4 represents the most important X-ray data for the distinction of different crystalline modifications of $Al(OH)_3$.

On Fig. 5 may be seen the characteristic reflections of nordstrandite (4,790 Å), gibbsite (4,849 Å) and bayerite (4,710 Å) in the investigated sample. Although the 4.794 Å peak of doyleite is situated near the 4.790 Å peak of nordstrandite, but other peaks of the doyleite can not be identified (4.076 Å, 3.096 Å, 2.421 Å, 2.361 Å, 2.325 Å).

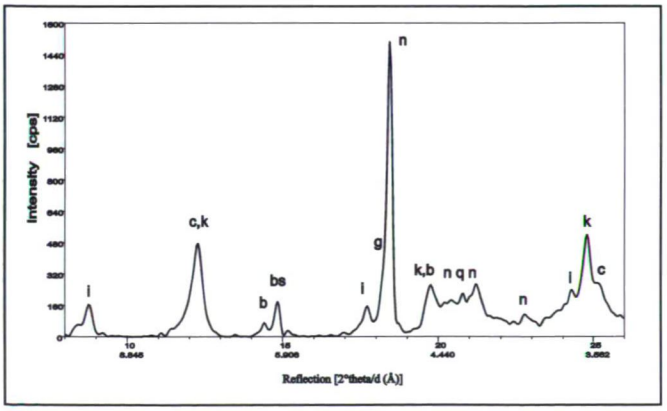

Fig. 4. The X-ray diffractogram of the residual rest in range of 8-26 °2Θ.

Table 3. The X-ray powder diffraction data for the separated insoluble residues.

Szőlőhegy-II/a		Nordstrandite JCPDS 24-0006					Other minerals
d Å	I_{rel}	d Å	I_{rel}	h	k	l	
9.952	10						Muscovite
7.146	31						Kaolinite
6.109	5						Boehmite
5.924	12						Bassanite
4.974	10						Muscovite
4.780	100	4.790	100	0	1	0	
4.467	18						Muscovite. Kaolinite
4.370	12						Kaolinite
4.324	13	4.320	25	0	0	1	
4.250	15	4.210	18	1	0	-1	Quartz
4.193	15						Kaolinite
4.164	18	4.160	12	1	0	0	
3.883	8	3.890	12	1	1	0	
3.841	6						Kaolinite
3.773	7						Kaolinite
3.643	17	3.610	8	1	1	-1	
3.573	36						Kaolinite
3.528	19						Anatase
3.433	7	3.430	6	0	1	1	
3.377	11						Kaolinite
3.340	49						Quartz
3.246	11						Rutile
3.197	11						Plagioclase
3.177	10						Kaolinite
2.965	13						Muscovite
2.884	18						Muscovite. Dolomite
2.797	6						Muscovite
2.699	14						Hematite
2.564	15						Muscovite. Kaolinite
2.514	18						Hematite
2.496	13						Kaolinite
		2.480	12	1	2	0	
2.453	10	2.455	8	1	0	1	
2.388	14	2.393	25	0	2	0	
2.345	16						Kaolinite
		2.333	6	1	2	-1	
2.297	3						Kaolinite
2.283	6						Quartz
		2.271	30	1	1	-2	
2.260	6						Kaolinite
2.202	6						Hematite. Kaolinite
2.189	9						Rutile
2.032	14						Sample holder
2.015	8	2.016	25	1	2	1	
1.994	9						Muscovite. Kaolinite
1.977	7						Muscovite. Kaolinite
		1.945	6	2	2	0	
1.903	5	1.902	20	-2	1	1	
1.783	5	1.784	14	1	2	0	
1.711	5						Muscovite
1.695	7						Muscovite. hematite
1.669	7						Kaolinite
1.600	2	1.598	6	2	3	-1	
1.545	4	1.547	6	3	2	-2	
1.542	5						Quartz
1.503	6						Muscovite
1.490	7						Kaolinite. hematite
1.453	8						Hematite. rutile

Table 4. Crystalline modifications of $Al(OH)_3$

Name	Bayerite	Doyleite	Gibbsite			Nordstrandite
JCPDS Card	20-0011	38-0376	07-0324	29-0041	33-0018	24-0006

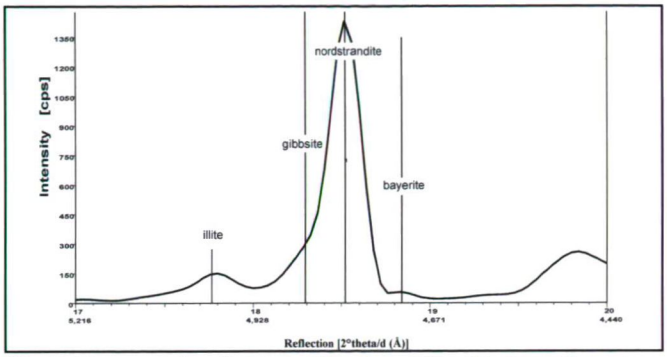

Fig. 5. Characteristic reflections of nordstrandite, gibbsite and bayerite.

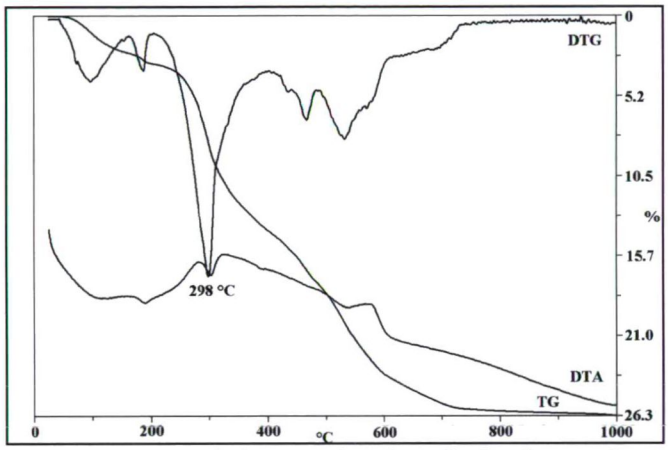

Fig. 6. Thermoanalytical curves of nordstrandite-bearing sample.

THERMAL BEHAVIOUR

Thermal reaction(s) of nordstrandite are very similar to the natural gibbsite (dehydroxylation at about 280 °C). Thermal decomposition appears to proceed as follows:

$$Al(OH)_3 \rightarrow \gamma\text{-}Al_2O_3 + H_2O$$
$$\text{than} \rightarrow \theta\text{-}Al_2O_3 \rightarrow \alpha\text{-}Al_2O_3$$
(Ivanova et al. 1974, Sato 1986, 1987)

Hathaway and Schlanger (1962) mentioned that the D.T.A. of nordstrandite is of limited diagnostic value. Mackenzie (1970) gives this dehydroxylation reaction between 320-330 °C. Van Alker et al. (1956) presented two distinct endothermic reactions, at 110 °C and other stronger at 270 °C. The low temperature water escape at about 100 °C of our sample may be also the reaction of the small amount of bassanite or montmorillonite present in the rock (Fig. 6).

SCANNING-ELECTRONMICROSCOPE AND MICROPROBE

The scanning-electronmicroscope shows the euhedral nordstrandite crystals to be elongated and prismatic (20-40 μm). These appear as individual or radial crystal aggregates in voids (fissures or cavities) in Triassic karst limestone terra rossa (Fig. 7).

GENESIS

The nordstrandite is crystallised at high pH value (7,5-9) (Van Nordstrand et al. 1956). It is not stable on a longer

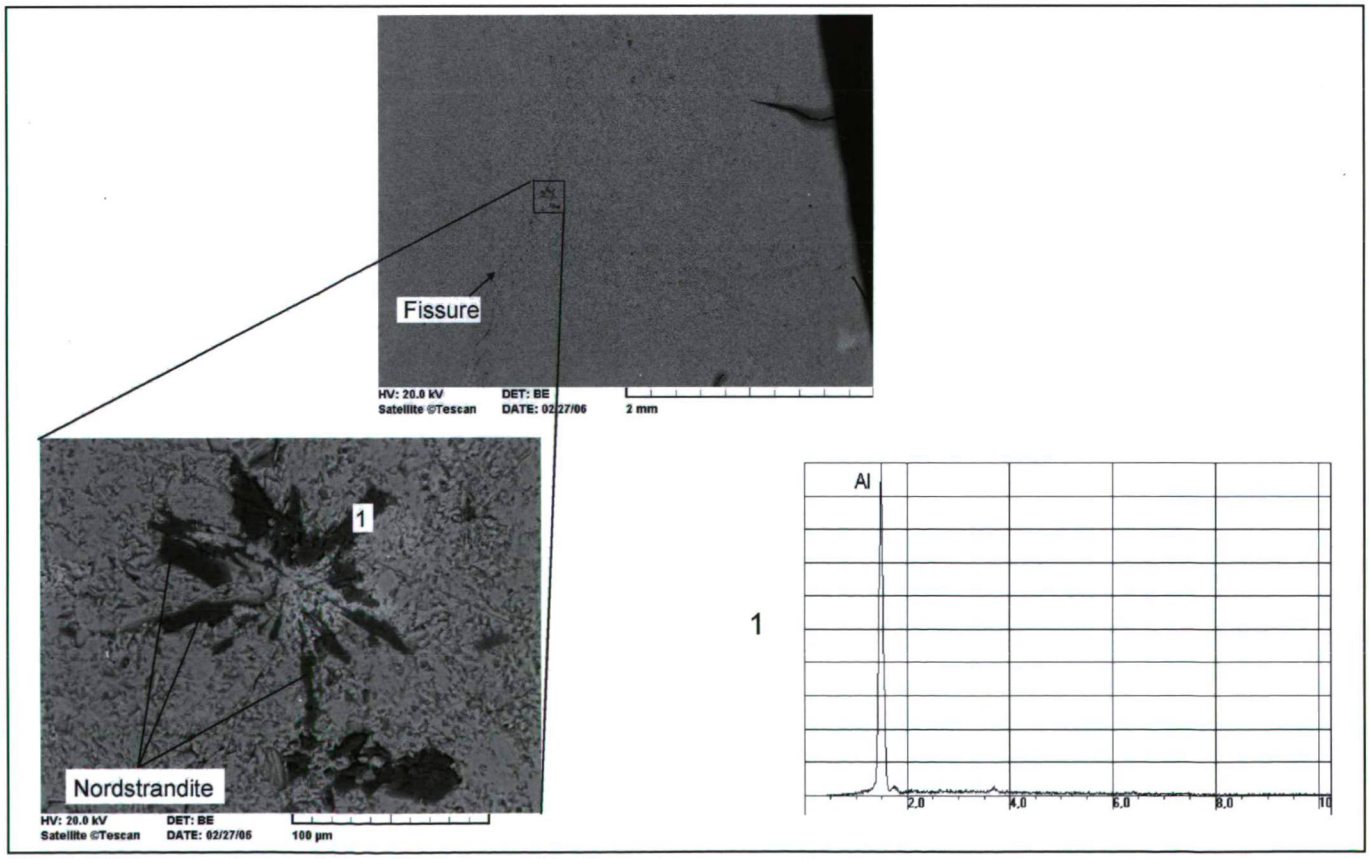

Fig. 7. SEM photomicrographs and EDS spectra (1) of nordstrandite crystals.

time. Its appearance is not likely in deposites older than Miocene, because due to pressure and longer time period it recrysallises into gibbsite. It appears most frequently in karst bauxites, in laterites only by alkaline pH. It can be found frequently in terra rossa deposites formed on carbonatic rocks. In addition to this nordstrandite occurs in cavities of nepheline syenite and in bauxites formed on phonolite (Table 1).

In our case the nordstrandite precipitated from amorphous $Al(OH)_3$ gels, from the alkaline phreatic solutions, infiltrating along the fissures of the clayed matrix of conglomerates accumulated in dolines of Triassic limestones. The huge amount of nordstrandite (sample Szőlőhegy-II/a) refers to in situ precipitation. Taking into consideration the geological history of the area (Szentpétery et al. 2006) nordstrandite was formed during Late Miocene-Pleistocene. Because of many of its properties, in particular the X-ray diffraction pattern, are similar to gibbsite, nordstrandite is probably an unrecognized constituent in many other similar terra rossa occurrences.

ACKNOWLEDGEMENTS

This work was financed by the National Scientific Research Found (OTKA) project number T 037747.

REFERENCES

ALBERT, J., MÁTRAI, J. (1970): Processes taking place in the firing of brick clays. Acta Chim. Hung., **65**, 2, 207–232.

ALBERT, J., NÁRAY-SZABÓ, I., PÉTER, É. (1973): Die mineralische Zusammensetzung und geologische, chemische und technologische Charakterisierung der Ziegeltone. IXth Congr. Carp.-Balk. Geol. Assoc., Budapest, 1969, **4**, 285–296.

CHAO, G. Y., BAKER, J. (1982): Nordstrandite from Mont St-Hilaire, Quebec. Can. Min., **20**, 77–85.

DANI, N., FORMOSO, M. L. L., DECARREAU, A., MEUNIER, A. (2001): Nordstrandite in bauxite derived from phonolite, Lages, Santa Catarina, Brazil. Clays & Clay Minerals, **49/ 3**, 216–226.

FÜLÖP, J., BREZSNYÁNSZKY, K., HAAS, J. (1987): The new map of basin basement of Hungary. Acta Geol. Hung., **30**, 3–20.

GOLDBERY, R., LOUGHNAN, F. C. (1970): Dawsonite and nordstrandite in the Permian Berry Formation of the Sydney Basin, New South Wales. Am. Min., **55**, 477–490.

HAAS, J. (ED), BÉRCZINÉ MAKK, A., BUDAI, T., HARANGI, SZ., HIPS, K., JÓZSA, S., KONRÁD, GY., KOVÁCS, S., LESS, GY., PELIKÁN, P., PENTELÉNYI, L., PIROS, O., RÁLISCHNÉ FELGENHAUER, E., TÖRÖK, Á., VELLEDITS, F. (2005): Magyarország geológiája. Triász (Geology of Hungary. Triassic). Eötvös Univ. Press, Budapest. (in Hungarian)

HATHAWAY, J. C., SCHLANGER, S. O. (1962): Nordstrandite ($Al_2O_3 \cdot 3H_2O$) from Guam. Am. Min., **50**, 1029–1037.

IVANOVA, V. P., KASATOV, B. K., KRASAVINA, T. N., ROZINOVA, E. L. (1974): Termičeskij analiz mineralov i gornyh porod. Nedra, Leningrad, 399. (in Russian)

JAMET, R., TRICHET, J., MILLOT, G. (1991): Conditions d'apparition de la nosrdstrandite dans les sols de la Polynésie francaise. C. R. Acad. Sci. Paris, **312**, II: 1655–1660. (in French)

KOCH, S. (1985): Magyarország ásványai. (The Minerals of Hungary). Akad. Kiadó, Budapest, 562. (in Hungarian)

KOVÁCS, S., SZEDERKÉNYI, T., HAAS, J., BUDA, GY., CSÁSZÁR, G., NAGYMAROSY, A. (2000): Tectonostratigraphic terranes in the pre-Neogene basement of the Hungarian part of the Pannonian area. Acta Geol. Hung., **43**, 225–328.

KOZUR, H., MOCK, R. (1973): Die Bedeutung der Trias-Conodonten für die Stratigraphie und Tektonik der Trias in den Westkarpaten. – Geol. Pal. Mitt., Innsbruck, **3/2**, 1–14. (in German)

KULIKOVA, G. V., TSEKHOVOLSKAYA, D. I., SHITOV, V. A. (1974): First find of nordstrandite in the USSR. Dokl. Akad. Nauk SSSR, Earth Sci. Sect., **217**, 1, Min., 190–193. (in Russian)

MACKENZIE, R. C. (1970): Differential Thermal Analysis. Volume 1: Fundamental Aspects. Acad. Press, London, New York, 775.

MARIČ, L. (1968): Nordstrandite and gibbsite in the terra rossa of Dinarides karst. Geol. Vjesn., **21**, 281–291. (in Croatian)

MILTON, C., DWORNIK, E. J., FINKELMANN, R. B. (1975): Nordstrandite, $Al(OH)_3$, from the Green River Formation in Rio Blanco County, Colorado. Am. Min., **60**. 285–291.

NÁRAY-SZABÓ, I., PÉTER, É. (1967): Nachweis von Nordstrandit und Bayerit in ungarischen Ziegeltonen. Acta Geol. Hung., **11/ 4**, 375–377. (in German)

PAPÉE, D., TERTIAN, R., BIAÍS, R. (1958): Recherches sur la constitution des gels et des hydrates crystallines d'alumin. Bull. Soc. Chim. France, **81**, 1301–1311. (in French)

PETERSEN, O. V., JOHNSEN, O., LEONARDSEN, E. S. (1976): Nordstrandite from Narssâssuk, Greenland. Min. Rec., **7/ 2**, 78–82.

RODGERS, K. A., GREGORY, M. R., BARTON, R. (1991): Bayerite, nordstrandite, gibbsite, brucite, and pseudoboehmite in discharged caustic waste from Campbell Island, Southwest Pacific. Clays & Clay Minerals, **39/1**, 103–107.

SABINA, A. P. (1977): New occurrences of minerals in parts of Ontario. Geol. Surv. Canada, Paper 77–1A, 335–339.

SATO, T. (1986): Thermal transformation of aluminium hydroxides to aluminas. Shizuoka Daigaku Kogakubu, Kenkyu Hokoku, (Rep. Fac. Eng., Shizuoka Univ.), **37**, 9–16. (in Japanese)

SATO, T. (1987): Thermal decomposition of aluminium hydroxides. J. Thermal Anal., **32/1**, 61–70.

SZAKÁLL, S., GATTER, I. (1993): Magyarországi ásványfajok. (Mineral Species of Hungary). Fair System Kft, Miskolc, 211. (in Hungarian)

SZAKÁLL, S., GATTER, I., SZENDREI, G. (2005): A Magyarországi Ásványfajok. (The Mineral Species of Hungary). Kőország Kiadó, Budapest, 427. (in Hungarian)

SZENTPÉTERY, I., LESS, GY. (eds), Kovács, S., Grill, J., Róth, L., Gyuricza, Gy., Sásdi, L., Piros, O., Réti, Zs., Elsholtz, L., Árkai, P., Nagy, E.†, Borka, Zs., Harnos, J., Zelenka, T. (2006): Az Aggtelek-Rudabányai-hegység földtana (Geology of the Aggtelek-Rudabánya Hills). Geol. Inst. Hungary, Budapest. (in Hungarian)

VAN NORDSTRAND, R. A., HETTINGER, W. P., KEITH, C. D. (1956): A new aluminium trihydrate. Nature, **177**, 713-714.

VICZIÁN, I. (1999): A nordstrandit és a bayerit magyarországi előfordulásának revíziója (Revision of occurrences of nordstrandite and bayerite from Hungary). Manuscript, Geol. Inst. Hungary, Budapest. (in Hungarian)

VON ALKER, A., GOLOB, P., POSTL, W. (1981): Hydrotalkit, Nordstrandit und Motukoreait vom Stradner Kogel, südlich Gleichenberg, Steiermark. Mitt._BL. Abt. Miner. Landesmuseum Joanneum, Graz, **49**, 279–291. (in German)

WALL, J. R. D., WOLFENDEN, E. B., BEARD, E. H., DEANS, T. (1962): Nordstrandite in soil from West Sarawak, Borneo. Nature, **196**, 264–265.

Received:October 26, 2008; accepted: December 19, 2008

*Acta Mineralogica-Petrographica, Szeged 2008, Vol. **48**, pp. 49-53.*

ACTA Mineralogica Petrographica

PYRITE GENERATIONS FROM THE PERMIAN/TRIASSIC BOUNDARY SECTION, BÁLVÁNY, BÜKK MTS., HUNGARY

NORBERT ZAJZON[1], ISTVÁN VETŐ[2]

[1]Institute of Mineralogy and Geology, University of Miskolc; H-3515, Miskolc, Egyetemváros, Hungary.
[2]H-1026, Budapest, Balogh Ádám u. 18/c.
e-mail: nzajzon@uni-miskolc.hu, vetoie@gmail.com

ABSTRACT

Three pyrite generations were described in the Bálvány Composite Section based on morphology, WDX and $\delta^{34}S$ data. Among them the 0.1–0.2 mm size, isotopically light euhedral pyrite is early diagenetic. This generation was found in the whole section. The "boundary shale" is characterised by microbial pyrite framboids, which formed on the surface, or close to the surface of the sediment around the redox boundary with the presence of dysoxic bottom-water. This, and the laminated structure of the sediment prove anoxic conditions in the whole sediment. Most probably there was dysoxic bottom water. The third generation is also euhedral, but has a larger grain size (1–2 mm). Based on $\delta^{34}S$ data and sphalerite inclusions, this generation is of late diagenetic or hydrothermal origin. This type occurs only in the shale and the top of the underlying limestone. The sulphides of the section are almost totally oxidised.

Key words: $\delta^{34}S$, pyrite, Bálvány-hill, Permian – Triassic boundary.

INTRODUCTION

Related to a multidisciplinary research project (Haas et al. 2004, Haas et al. 2007), we studied the pyrite content and its sulphur isotope composition of the Bálvány Composite Section. This carbonate-dominated section contains the continuous Permian – Triassic boundary.

The sulphur isotope composition of authigenic sulphides (predominantly pyrite) can provide useful data about the environment of the sulphide formation (connection of the pore- and the sea-water, oxygen content of the bottom water). There are three general sources of sulphur in a carbonatic sediment. The sulphides, the sulfates and the so called carbonate associated sulfates (CAS). In the same rock usually the sulphides contain isotopically light sulphur and the sulphates contain isotopically heavy sulphur because of the fractionation. Kaiho et al., (2006) studied the sulphur isotopes at the Bálvány and Meishan (S-China). They made selective sulphur extraction in the Bálvány-section. They separated the CAS and the sulphide sulphur. The CAS was varied between +10.2 – +26.6 ‰ $\delta^{34}S$. They observe fluctuations from which the biggest is in the boundary shale. They conclude this signal profile is simultaneous in both sections and also in Siusi (Italy). This shift to lighter isotope values can be the result of increased sulphide formation. They give four different hypotheses for the extra sulphur: 1: release of H_2S from the euxinic ocean water due to abrupt warming by volcanic CO_2 or impact shock wave; 2: volcanism penetrated huge sulphide ore deposit; 3: extraterrestrial impact into sulphide rich sediment or ore; 4: release of mante origin sulphur by impact of huge asteroid (>70 km).

Gorjan et al. (2007) investigate sulphate and sulphide $\delta^{34}S$ and pyrite morphology (this only at Bulla) in the Bulla section (Italy) and the Bálvány section. They use the same samples from Bálvány as Kaiho et al. (2006). Their sulphide $\delta^{34}S$ values in the Bálvány section are 10–15 ‰ more negative then the sulphate $\delta^{34}S$ (Kaiho et al. 2006). They do not distinguished among the different pyrite fractions and not separated them, thus their result could be questionable (see this study), but their observation about dysoxic/euxin condition in the seawater at the P/Tr boundary is likely correct. Shen et al. (2007) report pyrite framboids from the Meishan section (S-China) with narrow size distribution and average diameter of 4.6–8.7 μm. It coincides with the mass extinction event. They think this is the sign of dysoxia, which was a global scale marine event during the Permian–Triassic transition. Jiang et al. (2006) publishes two different pyrite generations (none of them is framboidal) from the same section. One of them has a bacterial origin which formed in the shallow burial zone. It's $\delta^{34}S$ value varies between -15 – - 40 ‰. The second appears at the top of the upper Permian Changxing Formation, and has volcanic origin with much higher $\delta^{34}S$ value. The highest is +2.2 ‰ $\delta^{34}S$. This pyrite forms distorted and elongated cubes and interlocking crystal forms of pentagon-dodekahedron.

LOCATION, GEOLOGICAL SETTING

The section is located close to the top of the Bálvány Hill in the Bükk Mountains (about 120 km NE of Budapest). This composite section is exposed in two outcrops within a distance of a few hundred meters from each other. The outcrop containing the lower part of the section is situated on the northern slope of the hill and is called "Bálvány North". The upper part of the section is cropping out at the eastern side of the hill and is referred to as "Bálvány East". The section contains the top of the black, thick bedded Nagyvisnyó Limestone Formation and the lower part of the Gerennavár Limestone Formation.

The upper Permian, thick bedded, inner ramp facies Nagyvisnyó Limestone Formation is rich in fossils. It is followed by a thin bedded, fossile-poor limestone, belonging to the lowermost part of the Gerennavár Limestone Formation. Between the two limestones there is an about one

meter thick shale, which forms the uppermost part of the Nagyvisnyó Formation. This layer can be interpreted as boundary shale between the Permian and Triassic layers. It contains numerous relics of upper Permian bivalve and brachiopod fauna (Csontos Kis and Pelikán 1990, Hips and Pelikán 2002, Haas et al. 2004, Posenato et al. 2004, 2005). Conodont data (Haas et al. 2004, 2007) also support the upper Permian age for the shale. The next 8.5 m thick limestone contains only a few ostracods and primitive arlandias. After 17 m of mudstone limestone, a brownish grey, thick bedded limestone starts which is a typical rock type for the Gerennavár Formation. This limestone is more than 100 m thick, dominantly ooidic, sometimes bioclastic with grainstone texture. These facies indicate continuation of sediment deposition in shallow marine environment after the ecological crisis.

Materials and Methods

We collected 34 samples from the Bálvány sections for mineralogical studies (9 samples from the limestone part, 13 from the shale of the Nagyvisnyó Formation, and 12 samples from the Gerennavár Formation).

500 g of crushed samples was weighted for micro-mineralogical studies. First the carbonate component was dissolved, with 10 v/v% hydrochloric acid, then the residue was disintegrated with ultrasound and washed out in a 0.25 mm sieve. The coarser fraction was ground in agate mortar (except large single pyrite crystals). This carbonate-free residue was washed until neutral pH. Using a 0.063 mm sieve the 0.25–0.063 mm fraction was separated from the finer material. Heavy mineral separation was done by settling in bromoform (density 2.78 g/cm^3). From the heavy-fraction, the pyrite grains were separated under a stereomicroscope.

Sulphur isotope measurements

Three samples contained unaltered pyrite of which we tried to measure the sulphur isotope composition. These samples are from the eastern section: the "boundary shale" (BK 3) and just below (BK 2) and above the "boundary shale" (BK 4). The BK 2 pyrite sample composed of small euhedral crystals. The sulphur content of the BK 3 "pyrite" sample was too low to perform isotope measurement, because of oxidation. The BK 4 sample contained both euhedral pyrite types, which could be separated under stereomicroscope, thus we were able to determine the sulphur isotope composition separately.

The digestion of the samples and the precipitation of sulphur as $BaSO_4$ were done in a laboratory of the Geological Institute of Hungary. The digestion was done by a mixture of Na_2CO_3 and KNO_3. After filtering the solution, all the sulphur content was precipitated as $BaSO_4$ by $BaCl_2$. This process extracts all the sulphur (sulphide, sulphate) content of the sample.

The sulphur isotope ratio was determined in the barium-sulphate using the method of Halas et al. (1982), at the Nuclear Research Institute of the Hungarian Academy of Science, Debrecen. NBS-127 barite standard was used as reference material. The measurements were done in a high-precision McKinney-Nier type stable isotope mass-spectrometer. For further technical details see Hertelendi et al. (1986). The $\delta^{34}S$ data are reported as ‰ relative to the Vienna Canyon Diablo Troilite (V-CDT) standard.

Results

Description of the heavy fraction

The >63 µm heavy mineral fraction dominantly build up by limonitised rock fragments and limonitised, hematitised pyrite and marcasite crystals. The >63 µm heavy mineral residue is generaly 0.25 g (between 0.006–2.009 g). More than 99 % of the sulphides is oxidized. Only two samples (BK 2 and BK 4), both from the Nagyvisnyó Formation of the "Bálvány East" section contained enough unaltered pyrite for $\delta^{34}S$ measurements. These samples are from the eastern section just below and above the "boundary shale". The BK 4 sample contained two pyrite types, which could be separated under stereomicroscope.

Detrital pyrite and sphalerite are also found in the section. Detrital pyrite occurs as inclusions in almandine, dravite and ferrotschermakite and as accessory mineral in amphibolite. Sphalerite is found in individual, 200 µm size grains in the shale and above the shale.

Morphology

All the samples contained subordinate singenetic and/or postgenetic pyrite or Fe-oxihydroxides after pyrite. The phases were divided into three main morphology groups: euhedral pyrite, framboidal pyrite (Fig. 1), and subordinate amount of infilling of fossils (Fig. 2). The euhedral pyrite was subdivided to two groups according to their size.

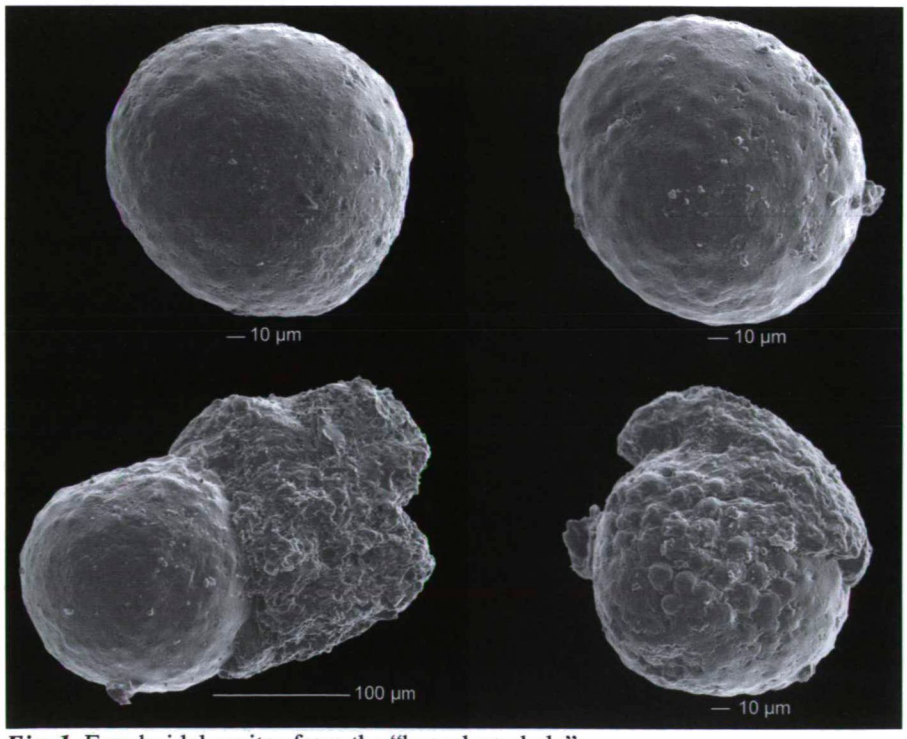

Fig. 1. Framboidal pyrites from the "boundary shale".

The euhedral pyrite with relatively small crystals (0.1–0.2 mm) (Fig. 3) are typical for the section. The euhedral pyrite with relatively large crystals (1–2 mm) (Fig. 4) occurs only in few samples around the „boundary shale". Framboidal pyrite is characteristic only for samples from the „boundary shale" and nearby samples below and above that. In these samples the framboids are abundant.

Euhedral pyrite with large crystals:

Many combinations appear from simple hexaeder to more complex forms. Characteristic growth-lines are also visible. The corners and the edges are sharp, unrounded. The surfaces of the crystals are usually oxidized. According to WDX measurements the Zn and Cu content are under the detection limit. In polished surfaces small sphalerite inclusions were visible in the crystals.

Framboidal pyrite:

The sizes of the framboids are between 100–150 µm. The morphological properties allowed us to easily separate the framboids from other spherule-looking grains under stereomicroscope. Also the polished, condrum-like inner structure was significant (Fig. 5). All the spheres are oxidized without any sulphur content remaining. The composition of the framboids was measured by WDX on polished surfaces. The chemical compositions are listed in Table 1.

Sulphur isotope data

The sulphur content and isotope data are listed in Table 2. The BK 2 and the BK 4 (small euhedral crystals) samples have similar $\delta^{34}S$ values: –15.8 ‰ and –17.7 ‰. The large crystals of sample BK 4 have a significantly different value: +7.8 ‰.

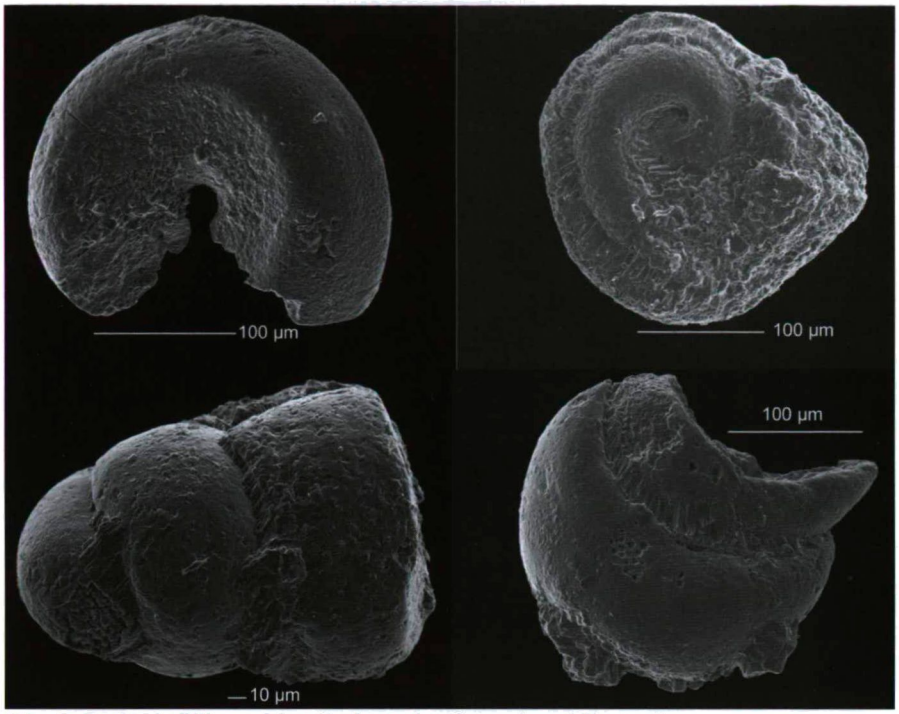

Fig. 2. Pyrite infilling of fossils from the Nagyvisnyó Formation.

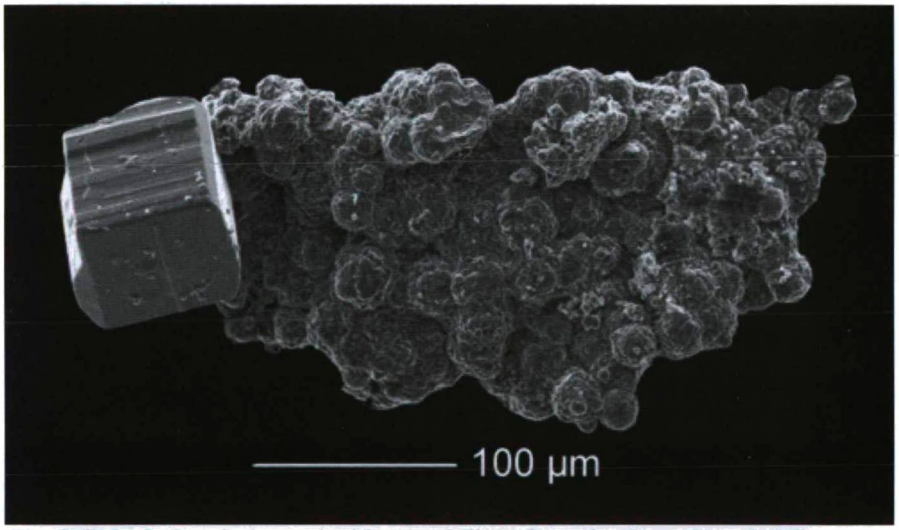

Fig. 3. Euhedral pyrite crystal with growth lines from the "boundary shale".

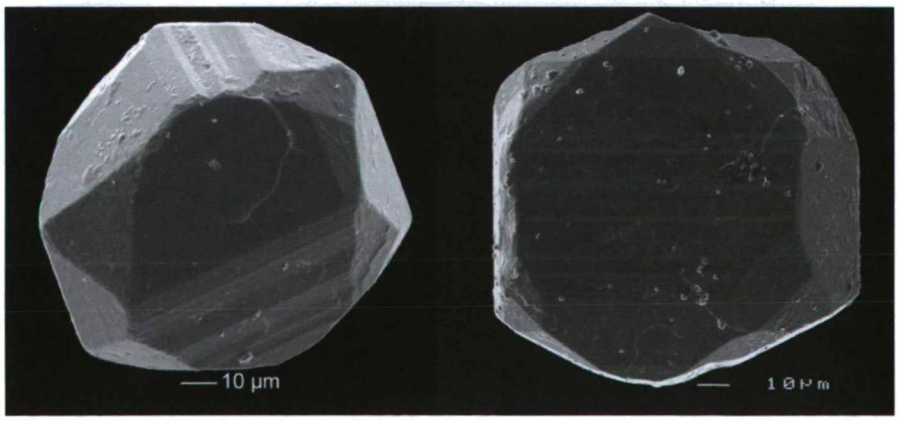

Fig. 4. Euhedral pyrite crystals with growth lines from the Nagyvisnyó Formation.

DISCUSSION

Based on the -16 and -18 ‰ values, the small euhedral pyrite was formed in the sediment. If there would be anoxic environment in the water column, the $\delta^{34}S$ value has to be more negative for the pyrite which could be formed on the sediment surface. It can not be formed in the water column because of their size. Based on this assumption the sea-water was not anoxic. The formation of pyrite framboids is around the redox boundary, because it needs partly oxidised sulphur (Wilkin and Barnes 1997). This formation happens in the topmost layers of the sediment with the

presence of dysoxic bottom-water. Framboids can syngenetically form in the water column, if the redox boundary is in the water, or they can form diagenetically in the sediment. They can be easily distinguished from each other, because the syngenetic framboids are smaller (<6 μm) and have narrow size distribution. The size of them is limited, because the dense particles rapidly sink out of the water column. The diagenetic framboids are much bigger then them (Wilkin et al. 1997, Wignall et al. 2005). This size difference is important especially in weathered samples, as we have at the Bálvány-section, because the oxidation can change the geochemical composition of the sample, but the pseudomorphs after the framboids can easily be examined (Wignall et al. 2005). Thus the bottom water most probably was dysoxic. The not anoxic sea-water is also supported by the presence of megafauna. In contrast to this, the "boundary shale" and the overlying beds are laminated. The presence of fossils together with the lamination is controversial. The fossils could have suffered short transportation. The lack of bioturbation could be the result of the mass-extinction or the boundary of the anoxia was at the sediment surface or very close to that. These questions require more work to understand them.

The $\delta^{34}S$ of the large euhedral pyrite is +7.8 ‰, which is 26 ‰ higher than the small crystals. It means this type of pyrite generation can not be early diagenetic. It has to be formed in a system which was closed from the seawater. Most probably this generation was formed by a later hydrothermal event, but based on the $\delta^{34}S$ value, late diagenetic origin can not be excluded. Presence of sphalerite inclusions agrees with both interpretations.

At the Ursula Creek (British-Columbia, Canada) a continuous Permian – Triassic deep water section is known. Here a continuous decrease can be seen in the oxygen fugacity of the bottom-water during the Changshingian, marked by the lack of bioturbation, concentration of authigenic uranium minerals and formation of framboidal pyrite. This resulted anoxia at the end-Changshingian – early-Triassic (Wignall and Newton 2003).

In the Gartnerkofel (S-Caravancas) section and the Gartnerkofel-1 drill core around the Permian – Triassic boundary large amount of pyrite was formed. The pyrite is partly framboidal and partly euhedral (small hexaeders). The oxidation of the pyrite was done in two steps: during the Cretaceous and the Holocene. The sizes of the framboids are between 20–100 μm. The -18 – -27 ‰ $\delta^{34}S$ values of the framboidal pyrite support its bacterial origin. The pyrite is syngenetic–diagenetic, and was formed in reductive environment (Attrep et al. 1991, Holser et al. 1991). This "two step oxidation" could be the case in the Bálvány section also, because a Cretaceous metamorphism is proved there. More data has to be collected to prove this comparison.

Many similarities can be found among the Bálvány section and the other sections around the world: significant mass-extinction below the biostratigraphical boundary, followed by low oxygen fugacity and pyrite formation, the presence of the "boundary shale" and the similar facies of the limestones. Based on these data some peculiarities can be found in the whole Paleothetys, but local processes strongly influenced or overprinted them.

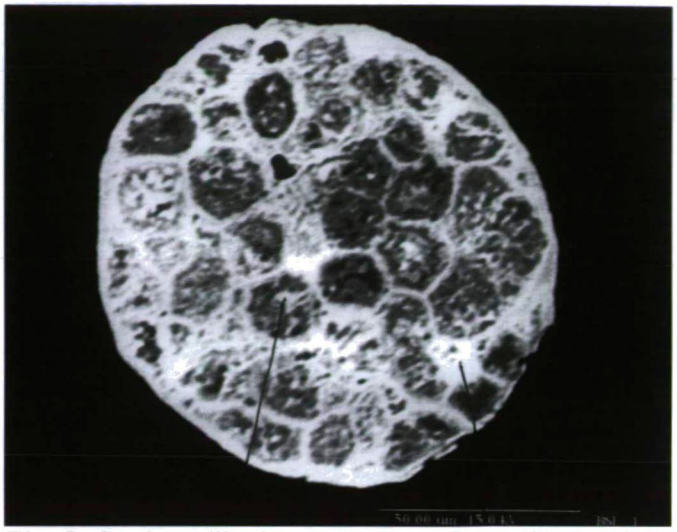

Fig. 5. Condrum like inner structure of a pyrite framboid from the "boundary shale" (backscattered electron image).

Table 1. WDX data of the framboidal pyrite. Elements under detection limit: Na, K, Mn, Ti, Cr, Ni (and S by EDX).

Analysis	Grain	SiO_2	Fe_2O_3	MgO	Al_2O_3	CaO	Summ.
123	79	2.81	75.41	0.54	0.82	0.32	79.91
124	79	3.06	79.61	0.47	0.98	0.47	84.59
125	80	1.96	77.96	0.31	0.13	0.24	80.59
126	80	4.27	75.31	0.67	2.24	0.50	82.99
127	81	4.92	73.22	0.36	1.57	0.54	80.61

Table 2. Sulphur content and $\delta^{34}S$ ‰ of the pyrite separates from the Bálvány section.

Sample	S %	$\delta^{34}S$ ‰
BK 2 (small crystals)	5.82	-15.8
BK 4 (small crystals)	9.60	-17.7
BK 4 (large crystals)	53.30	+7.8
BK 3 (small crystals)	0.08	non measurable

Conclusions

The small euhedral pyrite was formed in the sediment, with -16 and -18 ‰ $\delta^{34}S$ values.

The formation of pyrite framboids happened in the topmost layers of the sediment is around the redox boundary with the presence of dysoxic bottom-water. This, and the laminated structure of the sediment prove anoxic conditions in the whole sediment. Most probably there was dysoxic bottom water. The not anoxic sea-water is also supported by the presence of megafauna.

The large euhedral pyrite has 26 ‰ $\delta^{34}S$, thus this type of pyrite generation can not be early diagenetic. Most probably this generation was formed by a later hydrothermal event, or has late diagenetic origin. Presence of sphalerite inclusions agrees with both interpretations.

"Two step oxidation" (Cretaceous and Holocene) of the pyrite could be the case in the Bálvány section as it mentioned in the Gartnelkofel sections.

ACKNOWLEDGEMENTS

We acknowledge the financial support of the Hungarian Scientific Research Fund (OTKA) grant 7966. The authors are also grateful István Futó for sulphur isotope measurement.

REFERENCES

ATTREP, M.,. JR., ORTH, C. J., QUINTANA, L. R. (1991): The Permian–Triassic of the Gartnerkofel-1 Core (Carnic Alps, Austria): Geochemistry of Common and Trace Elements II – INAA and RNAA. Abhandlungen der Geologischen Bundesanstalt, **45**, 123–137.

CSONTOSNÉ KIS, K., PELIKÁN P. (1990): Bükk, Nagyvisnyó, Bálvány-észak földtani alapszelvény. Magyarország Geológiai Alapszelvényei, 136. Magyar Állami Földtani Intézet, Budapest: 6.

HAAS, J., HIPS, K., PELIKÁN, P., ZAJZON, N., GÖTZ, A., TARDY-FILÁCZ, E. (2004): Facies analysis of marine Permian/Triassic boundary sections in Hungary. Acta Geologica Hungarica, **47/4**, 297–340.

HAAS, J., DEMÉNY, A., HIPS, K., ZAJZON, N., WEISZBURG, T. G., SUDAR, M., PÁLFY, J. (2007): Environmental changes in the Permian–Triassic boundary interval recorded on a Western–Tethyan ramp in the Bükk-Mts., Hungary. Global and Planetary Change, **55**, 155–176.

HALAS, S., SHAKUR, A., KROUSE, H. R. (1982): Modified method of SO_2 extraction from sulphates for isotopic analysis using $NaPO_3$. Isotopenpraxis Bd. **18** II (12), 433–435.

HERTELENDI, E., GÁL, J., PAÁL, A., FEKETE, S., GIURGIU, M., GÁL, I., KERTÉSZ, ZS., NAGY, S. (1986): Stable isotope mass spectrometer. In: Stiehle, G. (ed): Proc. 4th Working Meet., Isotopes in Nature, Lepzig, 323–334.

HIPS, K., PELIKÁN, P. (2002): Lower Triassic shallow marine succession in the Bükk Mountains, NE Hungary. Geologica Carpathica, **53/6**, 351–367.

HOLSER, W. T., SCHÖNLAUB, H. P., BOECKELMANN, K., MAGARITZ, M. (1991): The Permian–Triassic of the Gartnerkofel-1 Core (Carnic Alps, Austria): Synthesis and Conclusions. Abhandlungen der Geologischen Bundesanstalt, **45**, 213–232.

JIANG, Y-F., TANG, Y-G., CHOU, C-L. (2006): Research on Genesis of Pyrite near the Permian–Triassic Boundary in Meishan, Zhejiang, China. Journal of China University of Mining and Technology (English Edition), **16/4**, 457–460.

KAIHO, K., KAJIWARA, Y., CHEN, Z-Q., GORJAN, P. (2006): A sulphur isotope event at the end of the Permian. Chemical Geology, **235**, 33–47.

POSENATO, R. PELIKÁN, P., HIPS, K. (2004). Uppermost Permian bivalves and brachiopods from the Bükk Mountains (Bálvány-North section, Northern Hungary). 32nd International Geological Congress, Firenze, Abstract volume, 966.

POSENATO, R., PELIKÁN, P., HIPS, K. (2005): Bivalves and brachiopods near the Permian–Triassic boundary from the Bükk Mountains (Bálvány-North section, Northern Hungary). Rivista Italiana di Paleontologia e Stratigrafia, **111**, 217–234.

SHEN, W., LIN, Y., XU, L., LI, J., WU, Y., SUN, Y. (2007): Pyrite framboids in the Permian–Triassic boundary section at Meishan, China: Evidence for dysoxic deposition. Palaeogeography, Palaeoclimatology, Palaeoecology, **253**, 323–331.

WIGNALL, P. B., NEWTON, R. (2003): Contrasting deep-water records from the Upper Permian and Lower Triassic of South Tibet and British Columbia: Evidence for a diachronous mass extinction. Palaios, **18/2**, 153–167.

WIGNALL, P. B., NEWTON, R., BROOKFIELD, M. E. (2005): Pyrite framboid evidence for oxygen-poor deposition during the Permian–Triassic crisis in Kashmir. Palaeogeography, Palaeoclimatology, Palaeoecology, **216**, 183–188.

WILKIN, R. T., BARNES, H. L. (1997): Formation processes of framboidal pyrite. Geochimica Cosmochimica Acta, **60**, 3897–3912.

WILKIN, R. T., ARTHUR, M. A., DEAN, W. E. (1997): History of water-column anoxia in the Black Sea indicated by pyrite framboid size distributions. Earth and Planetary Science Letters, **148**, 517–525.

Received: May 12, 2008; accepted: July 30, 2008

*Acta Mineralogica-Petrographica, Szeged 2008, Vol. **48**, pp. 55-57.*

ACTA Mineralogica Petrographica

FOLD SYSTEMS IN THE „MÓRÁGY FORMATION", MECSEK MOUNTAINS, SOUTH-TRANSDANUBIAN REGION, HUNGARY

ERNŐ MAUL

H-7140 Bátaszék, Kossuth L. u. 18., Hungary

ABSTRACT

In the quarries of Mórágy and Bátaapáti four fold systems have been determined. It was also possible to determine the possible orogenic phases.

Editorial note (Tibor Szederkényi):

Concerning investigations carried out for the radioactive waste disposal in the Eastern Mecsek Mountains, new tectonic evaluations were made mainly in the area of the Mórágy Hill. These interpretations became widely accepted by now. However, based on field observations by other researchers, ideas different from these were formulated. The author – who is the doyen of Hungarian geology – have dealt among others more than sixty years with this topic. He has numerous statements, which are in contrast with the new interpretations. There might be some doubts concerning his opinion on the tectonic character and development of the crystalline mass of Mórágy Hill, nevertheless, these conclusions deserve a debate. Our periodical is willing to provide a framework for these discussions.

Key words: Mórágy Formation, fold systems.

INTRODUCTION

In 1940 count Géza Teleki- in his paper- supposes, Mecsek Granite being folded by a system of NNW-SSE direction. In April 1943- on a geological excursion- Assistant Professor Sándor Vitális-in the quarries of Mórágy and Kismórágy- demonstrated granite rocks being multiple folded (Fig. 1-2).

DESCRIPTION OF FOLD SYSTEMS

According to author's research work during the last four years- there were four fold systems in the Mecsek Mountains and the Granite Region- as follows:

Axial plane 105-285°: Vergency toward 195° Austrian orogenic phrase.

Axial plane 15-195°: Vergency toward 105° Subhercynian orogenic phrase.

Axial plane 60- 240°: Vergency toward 150° .Early Laramian

Axial plane 150-330°: Symmetric folds- commonly no vergency. Late Laramian pfase. In the Mecsek Mountains No.1. and No.3. are common, (more than 99%) No.2. and No.4. are very rare

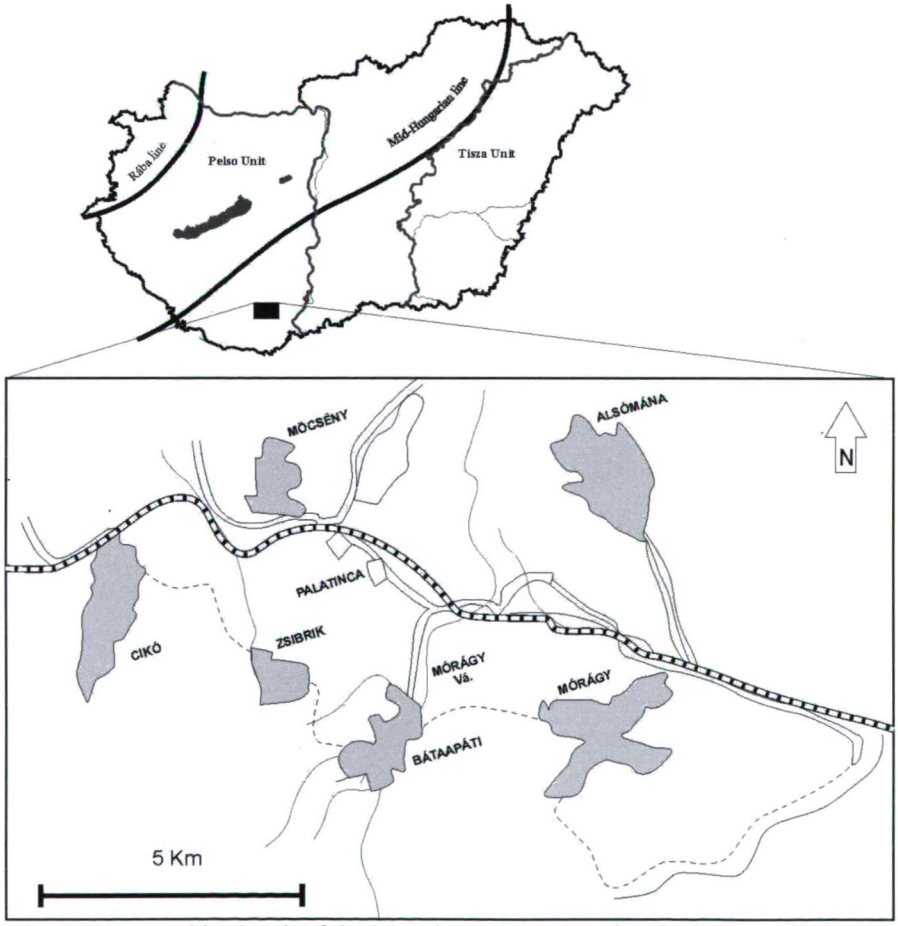

Fig. 1. Topographic sketch of the investigated quarries after Szabados (1995), with modifications.

In the two examined quarries, the ratio among the four systems is as follows:

1: 20 %
2: 6.3 %
3: 33.3 %
4: 40 %

The 40% of system number 4 proves evidence to count Géza Teleki's assumption of a NNW-SSE system.

It is notewonthy that the lineation of bostonite slabs and phenocrysts of sanidine is parallel to the main shear planes- on the limbs of folds and on the fracture cleaveges. Parallel lineation could be obtained near these shear surfaces within a distance of 10-15 cm. Beyond this distance crystals and rock fragments are placed irregularly.

Conclusion

Four fold systems have been determined in the two quarries. System number 4 which occurs rarely in the Mecsek Mountains- is found here to reach a value of 40%- which proves count Géza Teleki's statement about the folding of granitic rocks.

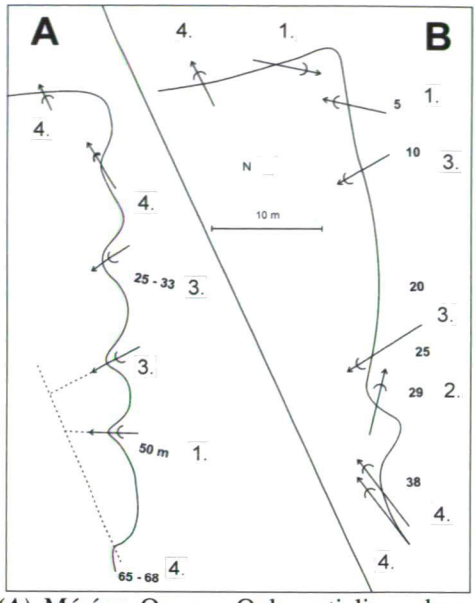

Fig. 2. ***(A)*** Mórágy Quarry. Only anticlines demonstrated. Arrows show direction and plunge of folds. ***(B)*** Bátaapáti Quarry. Only anticlines demonstrated. Arrows indicate direction and plunge of folds. Ground –level contours from E. Dudko.

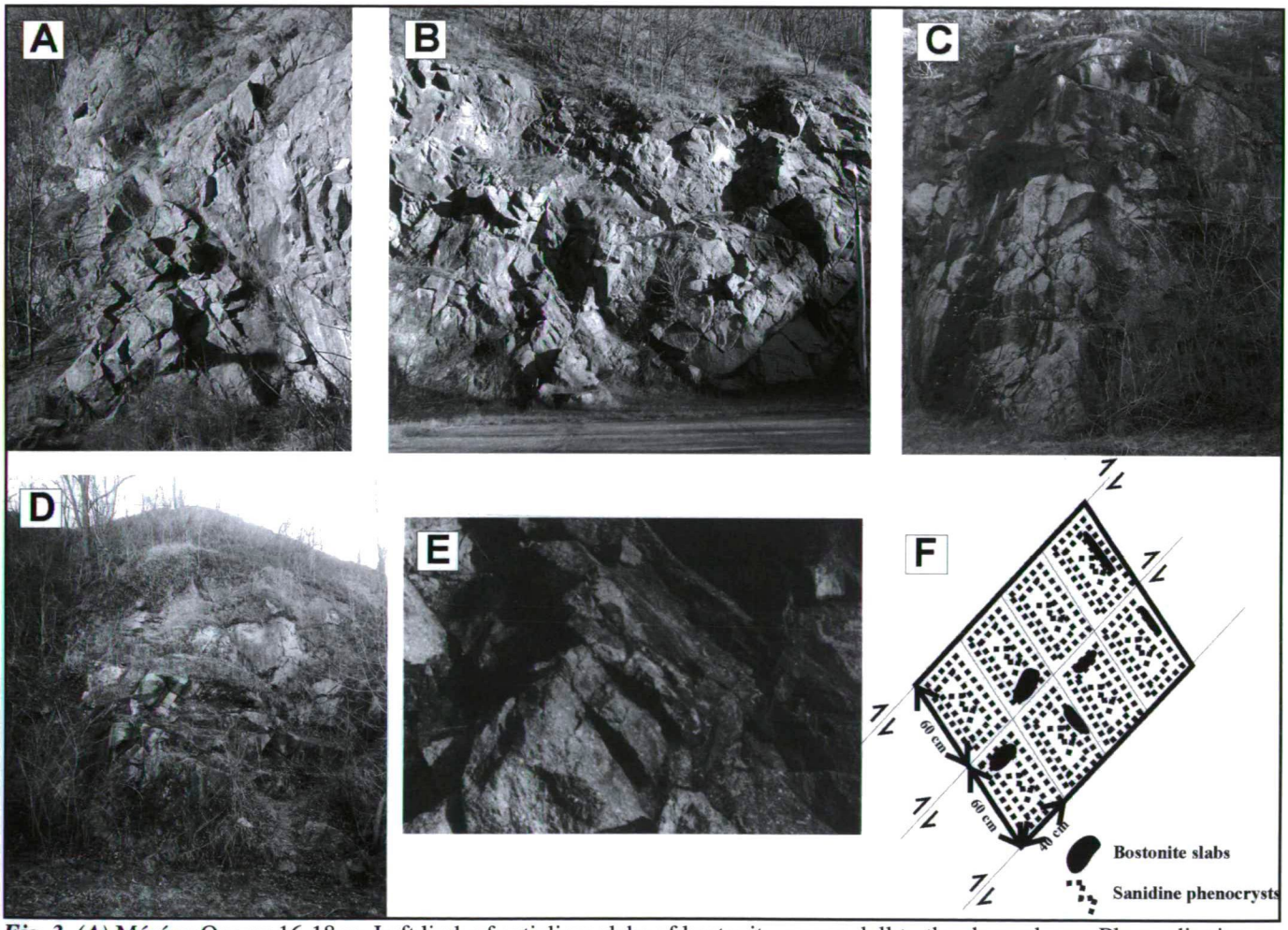

Fig. 3. ***(A)*** Mórágy Quarry 16-18 m. Left limb of anticline; slabs of bostonite are paralell to the shear planes. Planes dipping to the right are fracture cleavages. ***(B)*** Mórágy Quarry 25-33m. ***(C)*** Mórágy Quarry 50 m. ***(D)*** Mórágy Quarry 84-86m. ***(E)*** Mórágy Quarry 25-33m. Bostonite slabs and sanidine phenochrysts parallel to main shear planes. ***(F)*** Sketch illustrating lineation in folds. Left limb.

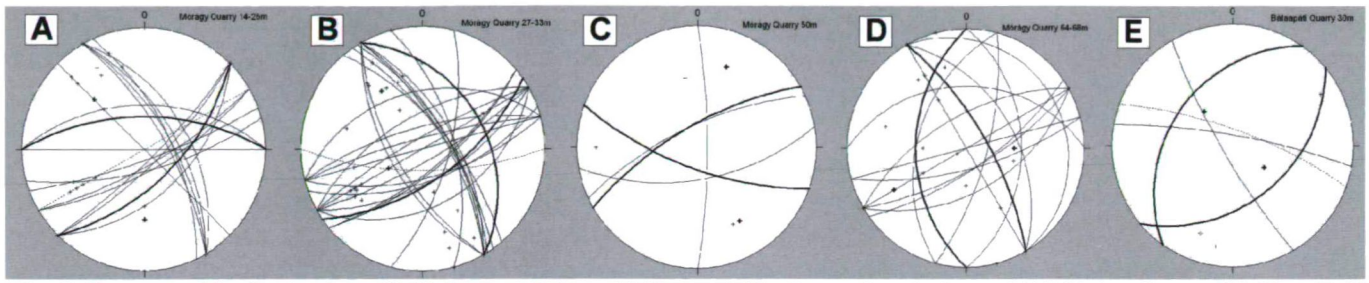

Fig. 5. Stereographics Projection of Mórágy and Bátaapáti Quarry folds. Lower hemisphere. ***(A)*** Mórágy Quarry 14-25m. Fold system No.3. ***(B)*** Mórágy Quarry. 27-33m. Fold system No.3. ***(C)*** Mórágy Quarry 50m. System No.1. Axis dislocated by system No.4. (at 64-68m). ***(D)*** Mórágy Quarry 64m. Fold system No.4. ***(E)*** Bátaapáti Quarry. Probably system No.2. dislocated by No.3. and No.4. systems.

REFERENCES

DUDKO, A. (2003): A Magyarhoni Földtani Társulat vándorgyűlése. Bátaapáti szept. 11-13. (in Hungarian)

FÜLÖP, J. (1994) Magyarország geológiája, Paleozoikum. Akadémiai Kiadó 306–317. (in Hungarian)

JANTSKY, B. (1950): A mecseki kristályos alaphegység földtani viszonyai. MÁFI Évi jelentés 1950. évről, 65–77. (in Hungarian)

JANTSKY, B. (1979): A mecseki gránitosodott kristályos alaphegység földtana. MÁFI Évkönyv 60, 30, 147, 150.

KOCSI, Z. (1995): A Mórágyi rögben található alsó kréta korú bosztonitok térbeli elhelyezkedése és petrográfiája. Manuscript. JATE Szeged. (in Hungarian)

MAROS, GY., PALOTÁS, K. (1999): Fracturing of the Mórágy Granite in Outtcrops and the Üveghuta Core Drill 1999/ II. Annual Report of the Geological Institute of Hungary.

SZABADOS, CS. (1995): Petrographical Study of Subvolcanic Rocks Surrounding of Mórágy and Ófalu. Acta Min Petr. 129–142.

SZEDERKÉNYI, T. (1996): Metamorphic Formations and Their Correlation int he Hungarian Part of Tisia Megaunit. (Tisia Composite Terrane.) Acta Min. Petr. 143–160.

TELEKI, G. (1941): Adatok a dunántúli paleozoikum tektonikájához. Földtani Közlöny **7/7-12**. 205-212; 295-296. (in Hungarian)

Received: August 8, 2008; accepted: September 17, 2008

INSTRUCTIONS FOR AUTHORS

General

Acta Mineralogica-Petrographica (AMP) publishes articles (papers longer than 4 printed pages but shorter than 16 pages, induding figures and tables), notes (not longer than 4 pages, including figures and tables), and short communications (book reviews, short scientific notices, current research projects, comments on formerly published papers, and necrologies of 1 printed page) dealing with crystallography, mineralogy, ore deposits, petrology, volcanology, geochemistry and other applied topics related to the environment and archaeometry. Articles longer thanthe given extent can be published only with the prior agreement of the editorial board. Occasionally, in the form of supplement issues AMP publishes materials of conferences, or other events of scientific interest.

The journal accepts papers that represent new and original scientific results, which have not appeared elsewhere before, and are not in press either.

All articles and notes submitted to AMP are reviewed by two referees (short communications will be reviewed only by one referee) and are normally published in the order of acceptance, however, higher priority may be given to Hungarian researches and results coming from the Alpine-Carpathian-Dinaric region. Of course, the editorial board does accept papers dealing with other regions as well, let they be compiled either by Hungarian or foreign authors.

The manuscripts (prepared in harmony of the instructions below) must be submitted to the Editorial office in triplicate. All pages must carry the author's name, and must be numbered. At this stage (revision), original illustrations and photographs are not required, though, quality copies are needed. It is favourable, if printable manuscriptsare sent on CD, as well. In these cases the use of Microsoft Word or any other IBM compatible editing programmes is suggested.

Language

The language of AMP is English.

Preparation of the Manuscript

Title

The title has to be short and informative. No subtitles if possible. If the main title is too long, an additional shortened title is needed for the running head.

Author

The front page has to carry (under the main title) the full name(s) (forename, surname), affiliation(s), current address(es), e-mail address(es) of the author(s).

Abstract and keywords

The abstract is required to be brief (max. 250 words), and has to highlight the aims and the results of the article. The abstracts of notes are alike (but max. 120 words). As far as possible, citations have to be avoided. In the near future the abstracts are going to be distributed in digital form, as well.

The abstract has to be followed by 4 to 10 keywords.

Text and citations

The format of the manuscripts is required to be: double-spacing (same for the abstract), text only on one side of the page, size 12 Times New Roman fonts. Margin width is 2.5 cm, except the left margin, which has to be 3.5 cm wide. Underlines and highlights ought not be used. Please avoid the use of foot and end notes. Accents of Romanian, Slovakian, Czech, Croatian etc. characters must be marked on the manuscript clearly.

When compiling the paper an Introduction – Geological setting – Materials and Methods – Results – Conlclusions structure is suggested.

The form of citations is: the author's surname followed by the date of publication e.g. (Szederkényi 1996). In case of two authors: (Rosso and Bodnar 1995) If there are more than two authors, after the first name the co-authors must be denoted as "et al.", e.g. (Roser et al. 1980). Citations are divided by "," e.g. (Rosso and Bodnar 1995, Szederkényi 1996)

References

The reference list can only consist of published papers, M.Sc., Ph.D. and D.Sc. theses, and papers in press.

Only works cited previously in the text can be put in the reference list.

Examples:

ADRIANO, D.C. (1986): Trace elements in the terrestrial environment, Springer-Verlag, New York, 219–262.

BAKKER, R. J. (2002): http://www.unileoben.ac.at/~buero62/minpet/Ronald/Programs/Computer.html. accessed: June 15, 2003.

CSEH NÉMETH, J. (1975): A recski mélyszinti színesfémérc előfordulás és annak teleptani, ércföldtani képe (Deep-seated basemetal ore occurrence of Recsk: geological pattern of ore accumulation). Földtani Közlöny, **105**, 692–708. (in Hungarian)

LE MAITRE, R. W. (ed.) (1989): A Classification of Igneous Rocks and Glossary of Terms. Blackwell, Oxford, 192.

PÁL-MOLNÁR, E. (1998): Geology and petrology of the Ditró Syenite Massif with special respect to formation of hornblendites and diorites. PhD. thesis, University of Szeged, Szeged, Hungary.

ROSSO, K. M., BODNAR, R. J. (1995): Microthermometric and Raman spectroscopic detection limits of CO_2 in fluid inclusions and the Raman spectroscopic characterization of CO_2. Geochimica et Cosmochimica Acta, **59**, 3961–3975.

SZEDERKÉNYI, T. (1996): Metamorphic formations and their correlation in the Hungarian part of Tisia Megaunit (Tisia Megaunit Terrane). Acta Mineralogica-Petrographica, **37**, 143–160.

ZIEGLER, A. M., SCOTESE, C. R., BARETT, S. F. (1983): Mesosoic and Cenozoic paleogeographic maps. In Borsche, P., Sundermann, J. (eds.): Tidal Friction and the Earth's Rotation, II. Springer Verlag, New York, 240–252.

The full titles of journals ought to be given. In case more works of the same author are published in the same year, then these has to be differentiated by using a, b, etc. after the date.

Figures and Tables

Finally, each figure, map, photograph, drawing, table has to be attached in three copies, they must be numbered and carry the name of the author on their reverse. All the illustrations ought to be printed on separate sheets, captions as well if possible. Foldout tables and maps are not accepted. In case an illustration is not presented in digital form then one of the copies has to be submitted as glossy photographic print suitable for direct reproduction. Photographs must be clear and sharp. Coloured figure, map or photograph can only be published at the expense of the author(s).

The width of figures and tables can be 56, 87, 118, or 180 mm. The maximum height is 240 mm (with caption).

All figures, maps, photographs and tables are placed in the text, hence, it is favourable if in case of whole page illustrations enough space is left on the bottom for inserting captions. In the final form the size of the fonts on the illustrations must be at least 1,5 mm, their outline must be 0,1 mm wide. Digital documents should be submitted in JPG-format. The resolution of line-drawings must be 400 dpi, while that of photographs must be 600 dpi. The use of Corel Draw for preparing figures is highly appreciated, and in this case please submit the .CDR file, as well. In terms of tables follow the style seen in this volume and use as less formatting as possible. Tables are asked to be prepared either by Microsoft Word or Excel.

Proofs and Offprints

After revision the author(s) receive only the page-proof. The accepted and revised manuscripts need to be returned to the Editors on CD or as an e-mail attachment. Proofreading must be limited to the correction of typographical errors. If an illustration cannot be presented in digital form, it must be submitted as a high quality camera-ready print.

The author(s) will receive 25 free offprints. On payment of the full price, further offprints can be ordered when the corrected proofs are sent back.

Manuscripts for publication in the AMP should be submitted to:

Dr. Elemér Pál-Molnár
e-mail: palm@geo.u-szeged.hu
Phone: 00-36-62-544-683, Fax: 00-36-62-426-479
Department of Mineralogy, Geochemistry and Petrology
University of Szeged
P. O. Box 651
H-6701 Szeged, Hungary

Published in 450 copies/issue (300 in Hungary, 150 abroad).
Distributed by the Department of Mineralogy, Geochemistry and Petrology, University of Szeged, Hungary.
Price of subscription to volume 48, 2008 (including postage):
HUF 10000 in Hungary, EUR 50 in all other countries.

established in 1922

ACTA MINERALOGICA-PETROGRAPHICA

VOLUME 48 2008

HU ISSN 0365-8066

CONTENTS:

Printed in Hungary by Páskum Nyomda, H-7103 Szekszárd, P.O. Box 627